BMJ Open is committed to open peer review. As part of this commitment we make the peer review history of every article we publish publicly available.

When an article is published we post the peer reviewers' comments and the authors' responses online. We also post the versions of the paper that were used during peer review. These are the versions that the peer review comments apply to.

The versions of the paper that follow are the versions that were submitted during the peer review process. They are not the versions of record or the final published versions. They should not be cited or distributed as the published version of this manuscript.

BMJ Open is an open access journal and the full, final, typeset and author-corrected version of record of the manuscript is available on our site with no access controls, subscription charges or pay-per-view fees (http://bmjopen.bmj.com).

If you have any questions on BMJ Open's open peer review process please email info.bmjopen@bmj.com

Assessment of myocardial ischemia in borderline coronary artery lesions based on optical pumped magnetometer magnetocardiography

Journal:	*BMJ Open*
Manuscript ID	bmjopen-2024-086433
Article Type:	Original research
Date Submitted by the Author:	16-Mar-2024
Complete List of Authors:	yang, shuwen; Capital Medical University, Department of Cardiology Feng, Lanxin; Capital Medical University, Department of Cardiology Zhang, Mingduo; Capital Medical University Affiliated Anzhen Hospital Zhang , Min; Department of Cardiology, Beijing Anzhen Hospital, Capital Medical University Ma, Zhao; Capital Medical University, Department of Cardiology Zhang, Huan; Capital Medical University, Department of Cardiology Zhang, YaZhe; Capital Medical University, Department of Cardiac Surgery Liu, Linqi; Capital Medical University, Department of Cardiology Zhou, Shu; Capital Medical University, Department of Cardiology Zhao, Xin; Capital Medical University, Department of Cardiology Yang, Xue Yao; Capital Medical University Affiliated Anzhen Hospital He, Jiqiang; Beijing An Zhen Hospital, Capital Medical University, Cardiology Ren, Yanlong; Capital Medical University Affiliated Anzhen Hospital Luo, Yawei; Capital Medical University Affiliated Anzhen Hospital Xu, Feng; Capital Medical University Affiliated Anzhen Hospital Tu, Chenchen; Capital Medical University, Department of Cardiology song, xiantao; Capital Medical University, Department of Cardiology Zhang, Hong-Jia; Beijing Chaoyang Hospital, Department of Cardiac Surgery; Capital Medical University School of Basic Medical Sciences, Department of Physiology and Pathophysiology
Keywords:	Diagnostic Imaging, Ischaemic heart disease < CARDIOLOGY, Clinical Trial

I, the Submitting Author has the right to grant and does grant on behalf of all authors of the Work (as defined in the below author licence), an exclusive licence and/or a non-exclusive licence for contributions from authors who are: i) UK Crown employees; ii) where BMJ has agreed a CC-BY licence shall apply, and/or iii) in accordance with the terms applicable for US Federal Government officers or employees acting as part of their official duties; on a worldwide, perpetual, irrevocable, royalty-free basis to BMJ Publishing Group Ltd ("BMJ") its licensees and where the relevant Journal is co-owned by BMJ to the co-owners of the Journal, to publish the Work in this journal and any other BMJ products and to exploit all rights, as set out in our licence.

The Submitting Author accepts and understands that any supply made under these terms is made by BMJ to the Submitting Author unless you are acting as an employee on behalf of your employer or a postgraduate student of an affiliated institution which is paying any applicable article publishing charge ("APC") for Open Access articles. Where the Submitting Author wishes to make the Work available on an Open Access basis (and intends to pay the relevant APC), the terms of reuse of such Open Access shall be governed by a Creative Commons licence – details of these licences and which Creative Commons licence will apply to this Work are set out in our licence referred to above.

Other than as permitted in any relevant BMJ Author's Self Archiving Policies, I confirm this Work has not been accepted for publication elsewhere, is not being considered for publication elsewhere and does not duplicate material already published. I confirm all authors consent to publication of this Work and authorise the granting of this licence.

Assessment of myocardial ischemia in borderline coronary artery lesions based on optical pumped magnetometer magnetocardiography

Shuwen Yang1#, Lanxin Feng 1#, Mingduo Zhang1, Min Zhang1, Zhao Ma1, Huan Zhang1, Yazhe Zhang2, Linqi Liu1, Shu Zhou1, Xin Zhao1, Xueyao Yang1, Jiqiang He1, Yanlong Ren1, Yawei Luo1, Feng Xu1, Chenchen Tu1*, Xiantao Song1*, Hongjia Zhang2

#These authors contributed equally to this work.

* These corresponding authors contributed equally to this work.

1Department of Cardiology, Beijing Anzhen Hospital, Capital Medical University, 100029, Beijing, China

2Department of Cardiac Surgery, Beijing Anzhen Hospital, Capital Medical University, 100029, Beijing, China

Corresponding Author:

The first corresponding author：Dr ChenChen Tu

Department of Cardiology, Anzhen Hospital, Capital Medical University, 2 Anzhen Road, Chaoyang District, 100020, Beijing, China E-mail: tcc2033@163.com

Dr Xiantao Song

Department of Cardiology, Anzhen Hospital, Capital Medical University, 2 Anzhen Road, Chaoyang District, 100020, Beijing, China E-mail: song0929@mail.ccmu.edu.cn

Disclosures: The authors have nothing to disclose.

Abstract

Aims: Despite clinical guideline recommendations for its use, the uptake of fractional flow reserve (FFR) in borderline coronary artery lesions remains low. As a noninvasive and safe test for myocardial ischemia, the validity of optical pumped magnetometer magnetocardiography (OPM-MCG) versus invasive FFR has not been fully established. **Methods and Results:** A total of 141 stable patients with borderline coronary artery lesions were prospectively enrolled from June 30 to November 30, 2023. All of them underwent sequential OPM-MCG before invasive coronary angiography and FFR. Six parameters were included in the final diagnostic model: MAg_{max}-TT, CAg_{max}-TT, δAg_{sum}-C, δPs_{sum}-PP, δAr_{sum}-N and $RtoAr_{max}$-PN. 500 bootstrap replications showed that the area under the receiver operating characteristic curve 95% confidence interval of the diagnostic model was 0.841 (0.804-0.844), with sensitivity of 76.5%, specificity of 91.8%, positive predictive value of 89.7%, negative predictive value of 80.7%. 1000 bootstrap replications showed that the model was well-calibrated. There is a net clinical benefit of using the MCG ischemia diagnostic model for borderline coronary lesions if the threshold probability of patients is greater than 12%. **Conclusion:** A nomogram based on 6 OPM parameters was built to assess myocardial ischemia in borderline coronary artery lesions and can reduce unnecessary invasive examination.

Keywords: borderline coronary artery lesions； optical pumped magnetometer magnetocardiography； fractional flow reserve； myocardial ischemia

Introduction

Borderline coronary lesions have stenosis ranging from 40% to 90% as seen in invasive coronary angiography. The FAME study [1] found that over 80% of lesions fell into this category, with only 35% of stenoses between 50-70% being hemodynamically significant. Predicting relevance was most accurate when estimating coronary artery diameter over 90%. The ongoing debate stems from the 2021 ACC/AHA/SCAI Guidelines for Coronary Artery Revascularization [2] indicating uncertainty regarding the advantages of coronary interventions in patients with nonischemic borderline lesions.

T Fractional flow reserve (FFR) guided intervention in patients with borderline coronary artery lesions (40-90% stenosis) has become a recommended treatment strategy in the 2018 ESC Interventional Guidelines [3]. The 2021 ACC/AHA/SCAI Guidelines for Coronary Artery Revascularization also have clear recommendations for borderline lesions: FFR and instantaneous wave-free ratio (iFR) are used to assess the need for percutaneous coronary intervention (PCI) in patients without evidence of ischemia but with angina and other equivalent symptoms (Class I); PCI is not recommended for stable patients with FFR >0.8 or iFR >0.89 (Class III). FFR is considered the benchmark for detecting ischemia in such situations. However, its widespread adoption in coronary catheter laboratories is hindered by its time-consuming nature, consumption of resources, and potential adverse effects associated with adenosine application.

Optical pumped magnetometer magnetocardiography (OPM-MCG) measures tiny magnetic fields (10^{-15} Tesla) from the heart using atomic magnetometer technology, without radiation. It's quick, contactless, and suitable for diverse populations. Clinical studies have shown that MCG is better than electrocardiogram (ECG) at detecting early myocardial ischemia [4,5,6] and has similar diagnostic effectiveness as SPECT for coronary artery disease (CAD) [7,8]. MCG is precise in diagnosing non-ST-segment elevation myocardial infarction, even in individuals who do not exhibit typical angina. [9,10]. However, the use of MCG for assessing myocardial ischemia in borderline coronary artery lesions still needs to be established.

Hence, this study aims to investigate the accuracy of OPM-MCG in diagnosing myocardial ischemia in patients with borderline coronary lesions, with invasive FFR examination serving as the reference standard.

Method

Study population

This study was a prospective, single-center, observational, cohort study which was reviewed by the Ethics Committee of Beijing Anzhen Hospital, Capital Medical University, and registered with the China Clinical Trial Registry (ChiCTR2300072382). All participants signed an informed consent. The methods described in this article follow the STARD 2015 guidelines.

Participants aged 18-80 with typical angina symptoms (CCS class II or higher) or 40-90% stenosis on CCTA were scheduled for hospitalization for invasive coronary angiography (ICA). Exclusion criteria included: 1) Coronary artery stenosis outside of 40%-90% range on ICA; 2) Acute myocardial infarction; 3) Previous myocardial infarction; 4) Complex arrhythmias; 5) Bundle-branch block; 6) Pacemakers, metallic implants in trunk; 7) Claustrophobia.

Sample size was calculated by PASS 2021 software. This study was a prospective cohort study, and the area under the ROC curve was used for sample size calculation, taking the significance level (α) as 0.025 and the degree of certainty (1-β) as 0.90,combining the results of the literature review of related studies as well as the statistics of the small sample in the previous period, and calculating according to the FFR-positive (ischemic)/FFR-negative (non-ischemic)=2:3. The sample size was calculated as 138.

Between June 30 and November 30, 2023, patients who satisfied the inclusion criteria were consecutively enrolled, resulting in a total of 163 participants being recruited for this study. 141 patients with borderline coronary lesions underwent OPM-MCG and FFR assessments after excluding 22 patients for different reasons (Figure 1). In this study, the cardiologists were not aware of the MCG results at the time of the FFR examination, and the MCG parameters were determined before the FFR examination.

MCG imaging

MCG recordings were conducted using a 36-channel OPM-MCG system with atomic magnetometers (Miracle MCG, Beijing X-MAGTECH Technologies Ltd.). The sensitivity of the magnetometers is below 30fT/Hz1/2, and the residual magnetic field is kept below 5nT. Each subject had a 90-second continuous recording at 36 locations (6×6 grid) above the chest using an arrayed sensor grid. Once MCG data collection is complete, the software automatically generates precise magnetic field and current density maps and outputs their parameters (see Supplemental text for additional detail). The parameters and cut-off values of MCG that indicate myocardial ischemia are presently undefined, thus the current study is exploratory in its approach.

ICA and FFR procedures

Coronary angiography and FFR measurements were performed on the vessels according to the 2021 ACC/AHA/SCAI Guidelines for Coronary Artery Revascularization and Expert consensus on the clinical pathway for FFR measurement in China. After administration of nitroglycerin, a pressure monitoring guidewire was advanced through the stenosis. Hyperemia was attained by administration of intravenous adenosine (140μg/kg/min). The FFR pressure wire was positioned a minimum of 20 mm distal to the stenosis in vessel segments ≥2 mm. The presence of an FFR ≤0.80 was considered a positive indicator of functional ischemia in patients and was defined as the FFR-positive group.

Statistical Analysis

Data analysis was performed with SPSS 26.0 and R 4.3.2 (http //www.R-project.org/). Counting data were presented as numbers and percentages, while normally distributed measurement data were shown as mean ± standard deviation. Continuous variables that were not normally distributed were presented using median and quartile values. Statistical significance was determined for all analyses with a P-value less than 0.05.

Development and internal validation of the diagnostic model

We used logistic regression and LASSO regression to select the most predictive variables from 65 pre-selected potential candidate variables obtained based on OPM-MCG (see Supplementary Text for definitions and pre-selection of candidate variables). The optimal model was determined through cross-validation. We considered the number and reasonableness and evaluated the parameters for the regression model and used multivariate logistic regression with the backward method to incorporate predictor variables. The model's predictive performance was assessed using the enhanced bootstrap method and clinical benefit was evaluated using decision curve analysis. The MCG-FFR nomogram was used to report scores for assessing myocardial ischemia with OPM-MCG parameters.

Result

Clinical characteristics

The study included 141 patients, mostly male (77.3%) with an average age of 60.64 ± 9.70 years. After MCG scans, all patients underwent ICA and FFR examination, with 48.2% having positive FFR

(FFR ≤ 0.8). A total of 157 vessels were examined, with 47.1% having FFR ≤ 0.8. Interval between MCG and FFR less than 30 days, median 2 days. Most patients had FFR measurements primarily done on the LAD. See Table 1 for patient clinical characteristics.

Selection of parameters and development of the diagnostic model

Fifty variables that were statistically significant ($P < 0.1$) in univariable logistic regression were included in the LASSO regression (Table 2 and Figure 2 in supplemental text), and eight variables were selected based on the reasonableness of the parameters selected to reduce the model overfitting and covariance through LASSO regression. By using the backward approach, six parameters were included in the final diagnostic model: MAg_{max}-TT, CAg_{max}-TT, δAg_{sum}-C, δPs_{sum}-PP, δAr_{sum}-N and $RtoAr_{max}$-PN. The model area under the receiver operating characteristic curve (AUC) obtained from multivariate logistic regression analysis was 0.87, with sensitivity of 76.5%, specificity of 91.8%, positive predictive value of 89.7%, negative predictive value of 80.7%. The nomogram (Figure 2) provides a graphical overview of the diagnostic model using multivariate logistic regression analysis (Table 3 in supplemental text).

Internal validation and net benefit of the model

The model performance for the diagnosis of myocardial ischemia in borderline coronary artery lesions of the OPM-MCG was evaluated by bootstrap replications.500 bootstrap replications showed that the model AUC and a 95% confidence interval (CI) of 0.87 (0.809-0.932) (Figure 3). 1000 bootstrap replications showed that the model was well-calibrated. The mean absolute error was 0.032 (Figure 3). The decision curve analysis (DCA) for the diagnostic model showed that if the threshold probability of patients is greater than 12% (Figure 3), screening strategies based on the OPM-MCG diagnostic model resulted in superior net benefit than screen-none or screen-all strategies.

Discussion

The feasibility of diagnosing myocardial ischemia in patients with borderline lesions using OPM-MCG was shown in our study, when compared to invasive FFR. The collective diagnostic potential of MCG parameters in detecting myocardial ischemia in borderline coronary artery lesions resulted in an AUC of 0.87 (95% CI 0.809 to 0.932), comparable to a prior investigation conducted by Park JW et al [11] which found that ST-segment fluctuation scores had an AUC of 0.84. This study stands out as the sole comparison between MCG and FFR for CAD utilizing a '64-channel axial gradiometer system.' In the study by Park JW and colleagues, patients could only detect myocardial ischemia under stress conditions, and the examination required a specialized shielded room. In contrast, OPM-MCG does not require liquid helium cooling or a dedicated shielded room. It can accurately diagnose myocardial ischemia caused by borderline coronary artery lesions even when the patient is at rest, presenting a contrast to the previous study.

CAD is presently characterized by an epicardial vascular lesion with a stenosis exceeding 50% in the ICA. Frequently, this description acts as a reference for heart muscle revascularization. Moreover, FFR can be used to evaluate the existence of myocardial ischemia, with a threshold of 0.8. Numerous studies [12,13] have consistently demonstrated that FFR-guided stenting leads to superior immediate outcomes and long-term prognosis. Therefore， FFR carries a Class 1a recommendation for guiding revascularization in angiographically borderline coronary stenoses in patients with stable angina. However, as illustrated in the Figure 4, the coronary stenosis identified in ICA may not precisely align with the invasive FFR results. This observation is in line with the conclusions drawn in the 2019 ESC Guidelines for Chronic Coronary Syndromes [14,15], emphasizing that the accuracy of determining CAD solely based on angiographic stenosis was as low as 64% when compared to flow reserve fraction. The positive mismatch rate, where lesions with less than 50% stenosis may demonstrate an FFR ≤ 0.8, was 19%, while the negative mismatch rate, where lesions with over 50% stenosis may result in an FFR value > 0.8, reached up to one-third. However, due to factors such as time consumption, costs, patient-related discomfort, contraindications, and a lack of reimbursement, the current rate of FFR utilization in catheterization laboratories in China is less than 6% [**Error! Bookmark not defined.**]. OPM-MCG allows ischemia assessment in patients with borderline coronary lesions prior to ICA and has a good concordance with invasive FFR.As a result, OPM-MCG can provide a basis for precise diagnostic and treatment strategies in patients with borderline coronary lesions before ICA, reducing unnecessary invasive testing.

The current non-invasive methods with high accuracy for myocardial ischemia assessment are SPECT, positron emission tomography/CT (PET/CT) and cardiac magnetic resonance imaging (CMR). However, due to the use of radioactive substances, tedious operation, high price, long examination time and waiting time for appointments, CMR (13.5%) and SPECT (12.9%) are not widely practiced [16]. In a prospective study done by Roel S. et al. [17] 2022, which included 189 patients in a head-to-head comparison, it was found that using FFR as the gold standard, the sensitivity of SPECT, PET/CT, and CMR was only 67%, 81%, and 66%, and the specificity was only 61%, 65%, and 62%. The diagnostic accuracy of PET/CT (75%) was not statistically different from that of SPECT (65%, P=0.03) and MRI (64%, P=0.052). In recent years, CT-derived fractional flow reserve (CT-FFR) has gradually developed into a new noninvasive test for detecting myocardial ischemia. The results of a multicenter study showed that the sensitivity of CT-FFR in diagnosing coronary myocardial ischemia was 89%, the specificity was 91%, and the diagnosis was in good concordance with FFR [18]. However, CT-FFR still has obvious limitations. Good image quality is essential for CT-FFR, but in this research, 13.9% of instances (58 out of 418) were unable to calculate CT-FFR due to inadequate image quality and the intricate nature of the coronary artery system. Additionally, CT-FFR cannot currently assess microvascular lesions (<2 mm in diameter) and diffuse lesions [19].

Similar to previous studies [20,21], a positive MCG scan was demonstrated by one or more abnormalities in the TT segment, including changes in TT segment parameters and changes in image dipoles (non-dipole phenomena and angular deflection of currents or magnetic fields). Different MCG parameters and combinations of parameters can provide more incremental information on cardiovascular disease. MCG is capable of accurately diagnosing myocardial ischemia resulting from epicardial coronary artery disease as well as effectively detecting myocardial ischemia caused by coronary microvascular dysfunction (CMD). The accuracy of MCG identification of CMD is 94.8% (±6.4%), sensitivity of 100% (±0.0%), and specificity of 93.3% (±8.2%) [22]. In our study, we also found a small number of FFR-negative patients with positive MCG scans as described above [23], and considered the possibility of CMD. In the future, we will summarize the characteristic images of patients with CMD and further explore the incremental information provided by the MCGs for these patients.

OPM-MCG tackles the pain points of SQUID-based MCG and facilitates its promotion in the clinic. MCG is mainly divided into two types: superconducting SQUID-based MCG and OPM-MCG. Although the SQUID-based MCG was developed earlier, it requires liquid helium refrigeration to realize low-temperature superconductivity and the construction of a large magnetic shielding room, which limits its large-scale popularization and use. The OPM-MCG can operate at room temperature without liquid helium cooling [24]. Moreover, the MCG is equipped with a lightweight magnetic shielding system, which enables it to realize high-sensitivity magnetic measurements while significantly reducing equipment maintenance costs and providing more flexible application scenarios.

MCG has been proved to be in good concordance with FFR in the preoperative assessment of myocardial ischemia in patients with borderline coronary artery lesions, and more clinical information can be provided to patients with cardiovascular disease through more studies in the future. MCG is expected to be used for the preoperative assessment of lesion-specific ischemia in patients with borderline coronary arteries, and to reduce the number of unnecessary invasive coronary arteriography examinations. This will effectively reduce the pressure on national healthcare expenditures and reduce the burden on patients with cardiovascular diseases.

Limitation

The study is a single-center registry study with some limitations. There is a need for a multicenter, prospective study involving a larger patient population. There are many types of MCG, and the current method of analyzing the cardiac magnetic field for the Miracle MCG was not compared head-to-head with other equipment. This study was not further externally validated, and in the future we will further refine and explore the feasibility of myocardial ischemia by MCG parameters.

Conclusion

MCG shows good sensitivity, specificity, and diagnostic accuracy in identifying significant coronary artery disease when compared to FFR. More extensive future research is necessary to confirm the effectiveness of MCG as a non-invasive approach for diagnosing and assessing the ischemic condition of borderline coronary artery blockages. Therefore, MCG can provide the evidence for a precise diagnostic strategy for patients with borderline coronary lesions before ICA, reducing unnecessary invasive examination.

Ethics approval and consent to participate

This study was performed in accordance with the principles of the Declaration of Helsinki. This study was approved by the ethics committee of Beijing Anzhen Hospital, Capital Medical University (KS2023008). Written informed consent was required for participation in the study.

Competing interests

The authors declare that they have no conflicts of interest.

Funding

This study was supported by Sponsored by Capital's Funds for Health Improvement and Research (2024-2-2066), Beijing Nova Program (20220484222), 'Deng Feng' Training Program (DFL20220603), Beijing Hospitals Authority 'sailing' Program (YGLX202323) and Project of The Beijing Lab for Cardiovascular Precision Medicine (PXM2018_014226_000013).

Author contribution

Xiantao Song, Chenchen Tu and Hongjia Zhang helped to conceive the topic and revised the article. Shuwen Yang and Lanxin Feng wrote the manuscript. and finished the statistics, Mingduo Zhang, Min Zhang, Jiqiang He, Yanlong Ren, Yawei Luo and Feng Xu contributed to the data collection. Zhao Ma, Huan Zhang, Yazhe Zhang, Linqi Liu, Shu Zhou, Xin Zhao, and Xueyao Yang helped with data analysis.

All authors read and approved the final manuscript .

Acknowledgments

The authors thank Zhechun Zeng, Ming Ding, and Bin Cai for their help in data analysis, and Xin Chen, Jinfan Tian, and Yulong Xue for their help in data collection.

Patient and Public Involvement

Patients make more people aware of the clinical role of the MCG and how it is examined by forwarding news stories and sharing information about clinical studies with others

Abbreviations

AUC= area under the receiver operating characteristic curve

CCTA= coronary computed tomography angiography

CI= confidence intervals

FFR= fractional flow reserve

ICA= invasive coronary angiography

NPV= negative predictive value

OPM-MCG= optical pumped magnetometer magnetocardiography

OR= Odds ratio

PPV= positive predictive value

ROC= receiver-operating characteristic

Availability of data and materials

The data that support the findings of this study are available on request from the corresponding author, Xiantao Song， upon reasonable request.

Reference

[1] van Nunen LX, Zimmermann FM, Tonino PA, et al. Fractional flow reserve versus angiography for guidance of PCI in patients with multivessel coronary artery disease (FAME): 5-year follow-up of a randomised controlled trial. Lancet. 2015;386(10006):1853-1860.

[2] Writing Committee Members, Lawton JS, Tamis-Holland JE, Bates ER, et al. 2021 ACC/AHA/SCAI Guideline for Coronary Artery Revascularization: Executive Summary: A Report of the American College of Cardiology/American Heart Association Joint Committee on Clinical Practice Guidelines [published correction appears in J Am Coll Cardiol. 2022 Apr 19;79(15):1547]. J Am Coll Cardiol. 2022;79(2):197-215.

[3]Neumann FJ, Sousa-Uva M, Ahlsson A, et al. 2018 ESC/EACTS Guidelines on myocardial revascularization [published correction appears in Eur Heart J. 2019 Oct 1;40(37):3096]. Eur Heart J. 2019;40(2):87-165.

[4] Nomura M, Nakaya Y, Fujino K, et al. Magnetocardiographic studies of ventricular repolarization in old inferior myocardial infarction. Eur Heart J. 1989;10(1):8-15.

[5] Hänninen H, Takala P, Mäkijärvi M, et al. Recording locations in multichannel magnetocardiography and body surface potential mapping sensitive for regional exercise-induced myocardial ischemia. Basic Res Cardiol. 2001;96(4):405-414.

[6] Kanzaki H, Nakatani S, Kandori A, et al. A new screening method to diagnose coronary artery disease using multichannel magnetocardiogram and simple exercise. Basic Res Cardiol. 2003;98(2):124-132.

[7] Nakai K, Izumoto H, Kawazoe K, et al. Three-dimensional recovery time dispersion map by 64-channel magnetocardiography may demonstrate the location of a myocardial injury and heterogeneity of

repolarization. Int J Cardiovasc Imaging. 2006;22(3-4):573-580. doi:10.1007/s10554-005-9019-x.

[8] Tolstrup, Kirsten, Donatella Brisinda, Am Meloni, et al. Comparison of resting magnetocardiography with stress single photon emission computed tomography in patients with stable and unstable angina. J Am Coll Cardiol 2006;47(4 Suppl 1):176A. Abstract 930-247.

[9] Lim HK, Kwon H, Chung N, et al. Usefulness of magnetocardiogram to detect unstable angina pectoris and non-ST elevation myocardial infarction. Am J Cardiol. 2009;103(4):448-454.

[10] Shin ES, Lam YY, Her AY, et al. Incremental diagnostic value of combined quantitative and qualitative parameters of MCG to detect coronary artery disease. Int J Cardiol. 2017;228:948-952.

[11] Park JW, Shin ES, Ann SH, et al. Validation of magnetocardiography versus fractional flow reserve for detection of coronary artery disease. Clin Hemorheol Microcirc. 2015;59(3):267-281.

[12] Xaplanteris P, Fournier S, Pijls NHJ, et al. Five-Year Outcomes with PCI Guided by Fractional Flow Reserve. N Engl J Med. 2018;379(3):250-259.

[13] Zimmermann FM, Ferrara A, Johnson NP, et al. Deferral vs. performance of percutaneous coronary intervention of functionally non-significant coronary stenosis: 15-year follow-up of the DEFER trial. Eur Heart J. 2015;36(45):3182-3188.

[14] Knuuti J, Wijns W, Saraste A, et al. 2019 ESC Guidelines for the diagnosis and management of chronic coronary syndromes [published correction appears in Eur Heart J. 2020 Nov 21;41(44):4242]. Eur Heart J. 2020;41(3):407-477.

[15] Derimay F, Finet G and Rioufol G. Coronary artery stenosis prediction does not mean coronary artery stenosis obstruction. Eur Heart J. 2021;42(42):4401.

[16] Working Group of Cardiovascular Imaging of National Center for Medical Quality Control of Cardiovascular Diseases Survey of the Application Status of Cardiovascular Imaging Modalities and Medical Quality Report in China [J]. Chin circ J ,2020,35(7):625-633.

[17] Driessen RS, van Diemen PA, Raijmakers PG, et al. Functional stress imaging to predict abnormal coronary fractional flow reserve: the PACIFIC 2 study. Eur Heart J. 2022;43(33):3118-3128.

[18] Tang CX, Liu CY, Lu MJ, et al. CT FFR for Ischemia-Specific CAD With a New Computational Fluid Dynamics Algorithm: A Chinese Multicenter Study. JACC Cardiovasc Imaging. 2020;13(4):980-990.

[19] Li Y, Yu M, Dai X, et al. Detection of Hemodynamically Significant Coronary Stenosis: CT Myocardial Perfusion versus Machine Learning CT Fractional Flow Reserve. Radiology. 2019;293(2):305-314.

[20] Rong Tao, Shulin Zhang, Xiao Huang, et al. Magnetocardiography-Based Ischemic Heart Disease Detection and Localization Using Machine Learning Methods. IEEE Trans Biomed Eng. 2019;66(6):1658-1667.

[21]Xu F, Tu CC, Yang SW, et al. Clinical value of helium-free magnetocardiography in diagnosis of coronary heart disease [J]. Chin. J. gen. pract. 2023,22(11):1159-1166.

[22] Rong Tao, Shulin Zhang, Xiao Huang, et al. Magnetocardiography-Based Ischemic Heart Disease Detection and Localization Using Machine Learning Methods. IEEE Trans Biomed Eng. 2019;66(6):1658-1667.

[23] Yang SW, Zhang H, Liu LQ, et al. Characteristic changes of magnetocardiogram in patients with coronary microcirculation dysfunction: a report of two cases [J]. Chin. J. gen. pract. 2023,22(7):740-744.

[24] Tu CC, Ding M, Cai B, et al. magnetocardiography based on atomic magnetometer technology[J]. Beijing Biomed. eng. 2023,42(3):298-304.

Table 1 Clinical characteristics (n = 141)

Characteristics	Total(n=141)
Age (yrs)	60.64±9.70
Male, n (%)	109(77.3)
BMI [a] (Kg/m^2)	26.15±3.36
Diabetes, n (%)	47(33.3)
Hypercholesterolemia, n (%)	65(46.1)
Hypertension, n (%)	82(58.2)
Stroke, n (%)	9(6.4)
Smoke, n (%)	43(30.5)
Systolic blood pressure, mmHg	128.69±15.54
Diastolic blood pressure, mmHg	75.15±10.79
Heart rate	73.81±10.38
Medication， n(%)	
Aspirin	129(91.5)
Statin	137(97.2)
ACEI/ARB [b]	45(35.6)
SGLT2 [c] inhibitors	22(16.7)
Nicorandil	23(16.3)
Admission lab results	
Low-density lipoprotein cholesterol (mmol/L)	1.82±0.69

hs Tnl(pg/ml)	3.5(2.5,5.8)
Brain natriuretic peptide (pg/ml)	29.00(14.75,48.25)
Blood glucose (mmol/L)	5.52(4.82,7.33)
HbA1c [d](%)	6.25(5.7,7.1)
ICA [e] and FFR [f] characteristics	
1-vessel disease	50(35.5)
2-vessel disease	43(30.5)
3-vessel disease	48(34.0)
Number of patients with FFR≤0.8	68(48.2)
Number of vessels with FFR	157
Number of vessels with FFR≤0.8	74(47.1)
Left anterior descending artery with FFR	97(68.8)
Left circumflex artery with FFR	25(17.7)
Right coronary artery with FFR	35(24.8)
Interval between MCG and FFR	2(1,7)

Values are n (%) or mean ± SD.;

a. BMI= Body Mass Index; b. ACEI= angiotensin converting enzyme inhibitor; ARB = angiotensin receptor blocker; c. SGLT2 inhibitors = sodium-glucose cotransporter-2 inhibitors; d. HbA1c= glycated hemoglobin; e. ICA = invasive coronary angiography; f. FFR = fractional flow reserve.

Figure legend

Figure 1. Flowchart of the study design.

Figure legend : CCTA= coronary computed tomography angiography; MCG=magnetocardiography; ICA= invasive coronary angiography; FFR=fractional flow reserve; PCI= percutaneous coronary intervention.

Figure 2. Nomogram of the diagnostic model.

Figure legend: The nomogram graphically demonstrates the diagnostic model of OPM-MCG. Points for MAg_{max}-TT, CAg_{max}-TT, δAg_{sum}-C, δPs_{sum}-PP, δAr_{sum}-N and $RtoAr_{max}$-PN can be obtained using a point caliper and then summed to obtain a total score that can be obtained using a point caliper and then summed to obtain a total score that can be measured with diagnosing myocardial ischemia in patients with borderline coronary lesions.

Figure 3 Accuracy and internal validation of the diagnostic model.

Figure legend: (A) ROC curves and 95% confidence intervals. After 500 bootstrap replications, the area under the curve and 95% confidence interval for receiver operating characteristic is 0.87 (0.809-0.932).(B) Calibration curve for the diagnostic model. Calibration curve for the borderline lesion ischemia diagnostic model was established by comparing the observed and predicted probability of a positive FFR in patients with borderline lesions of the coronary arteries. The smaller the distance of the scatter from the dashed line, the better the calibration. (C) Decision curve analysis (DCA) for diagnostic models of ischemia in borderline coronary lesions. None: net benefit when it is assumed that no patients with critical lesions of the coronary arteries would have the outcome (FFR-positive). All: net benefit when all patients with critical coronary lesions are assumed to have an outcome (FFR-positive). model: net benefit of managing critical coronary lesions with a diagnosis of myocardial ischemia based on the diagnostic model estimate. The strategy with the highest net benefit at any given threshold is the preferred strategy.

Figure 4 Normal, FFR-positive and FFR-negative MCG scan and ICA Images.

Figure legend: MCG scan showed no evidence of ischemia or obstructive coronary artery disease, as demonstrated by the lack of significant current deviations within the myocardium and absence of angle shift between the positive red pole and negative blue pole between T wave onset (T-onset) and T wave peak (T-peak) ; (B) The MCG scan of a patient in their 70s showed magnetic field angular deflection , abnormal magnetic field distribution of the positive and multipolarisation of negative poles , suggesting significant myocardial ischemia, and the ECG showed no significant abnormality. The ICA showed two lesions: 60% stenosis of the D1, 50% stenosis of the R-PDA ,. The FFRs were 0.77 for the R-PDA;(C) MCG scan of a patient in their 60s showed no myocardial ischemia, ECG showed no significant abnormalities, echocardiography showed widening of the ascending aorta and aortic sinus. ICA showed 75% stenosis of the LAD, 60% stenosis of the RCA, FFR value of the LAD was 0.88. MCG= magnetocardiography; FFR= fractional flow reserve ; ICA= invasive coronary angiography; D1= Diagonal branches ; R-PDA : Posterior descending artery ; LAD= Left Anterior descending artery; RCA= right coronary artery.

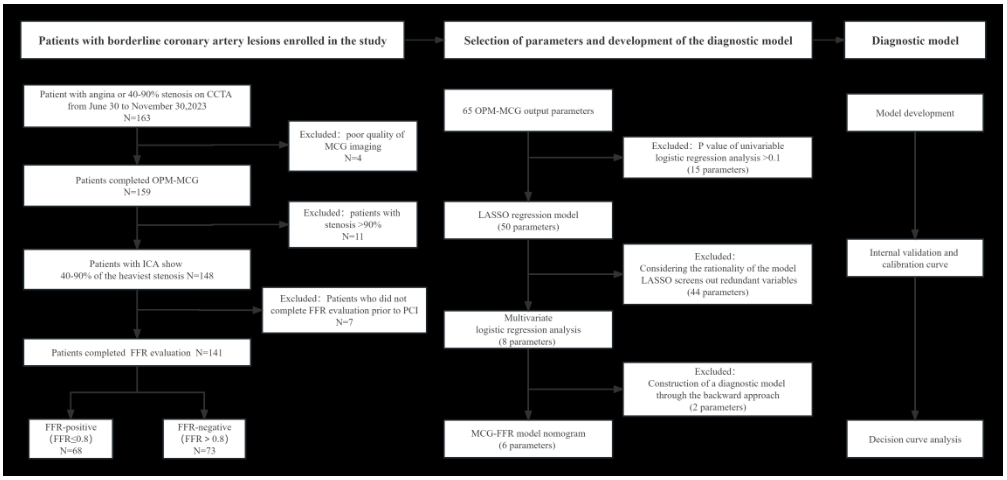

Figure 1. Flowchart of the study design.
Figure legend : CCTA= coronary computed tomography angiography; MCG=magnetocardiography; ICA= invasive coronary angiography; FFR=fractional flow reserve; PCI= percutaneous coronary intervention.

1139x537mm (96 x 96 DPI)

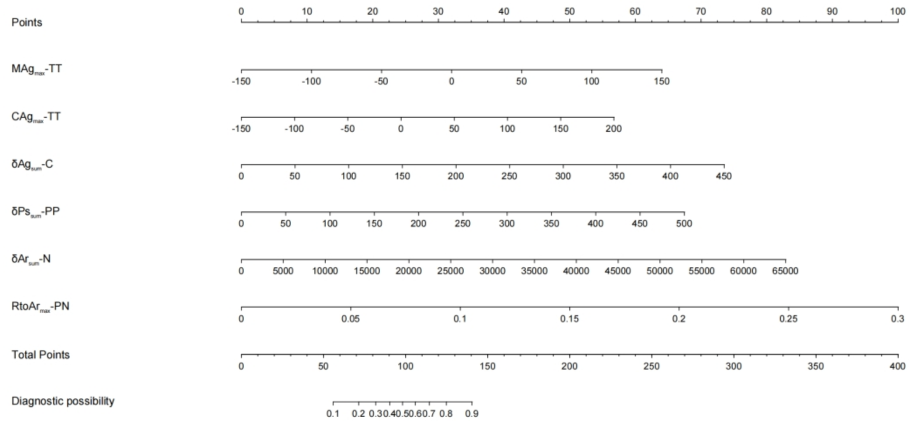

Figure 2. Nomogram of the diagnostic model.

Figure legend: The nomogram graphically demonstrates the diagnostic model of OPM-MCG. Points for MAgmax-TT, CAgmax-TT, δAgsum-C, δPssum-PP, δArsum-N and RtoArmax-PN can be obtained using a point caliper and then summed to obtain a total score that can be obtained using a point caliper and then summed to obtain a total score that can be measured with diagnosing myocardial ischemia in patients with borderline coronary lesions.

381x203mm (160 x 160 DPI)

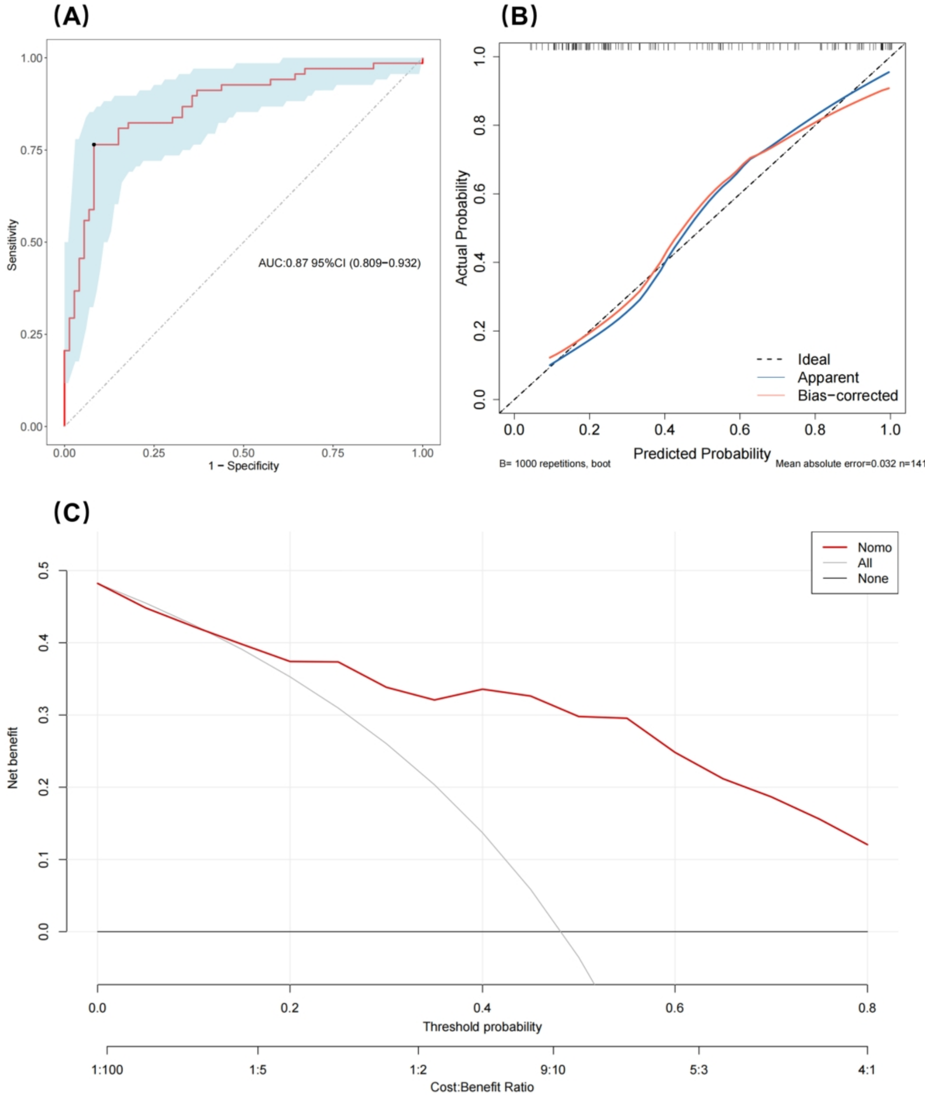

Figure 3 Accuracy and internal validation of the diagnostic model.
Figure legend: (A) ROC curves and 95% confidence intervals. After 500 bootstrap replications, the area under the curve and 95% confidence interval for receiver operating characteristic is 0.87 (0.809-0.932).(B) Calibration curve for the diagnostic model. Calibration curve for the borderline lesion ischemia diagnostic model was established by comparing the observed and predicted probability of a positive FFR in patients with borderline lesions of the coronary arteries. The smaller the distance of the scatter from the dashed line, the better the calibration. (C) Decision curve analysis (DCA) for diagnostic models of ischemia in borderline coronary lesions. None: net benefit when it is assumed that no patients with critical lesions of the coronary arteries would have the outcome (FFR-positive). All: net benefit when all patients with critical coronary lesions are assumed to have an outcome (FFR-positive). model: net benefit of managing critical coronary lesions with a diagnosis of myocardial ischemia based on the diagnostic model estimate. The strategy with the highest net benefit at any given threshold is the preferred strategy.

590x677mm (120 x 120 DPI)

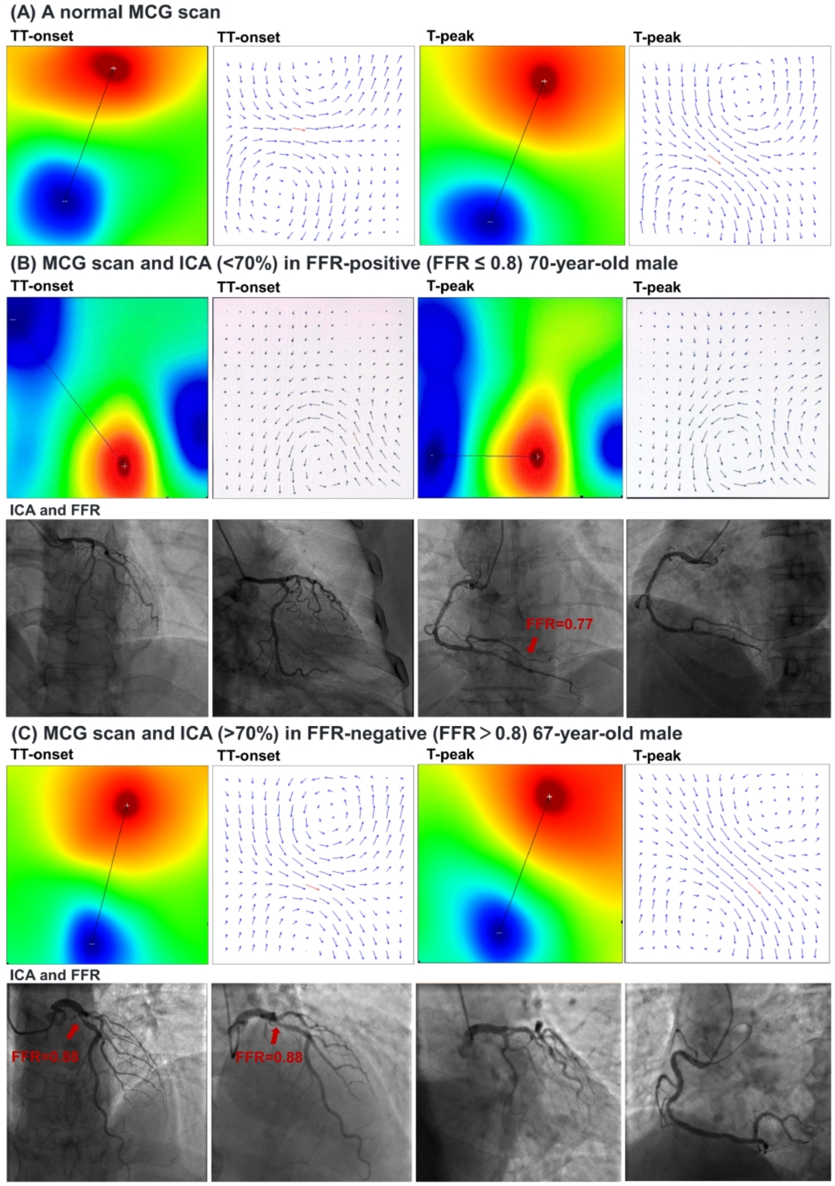

Figure 4 Normal, FFR-positive and FFR-negative MCG scan and ICA Images.
Figure legend: MCG scan showed no evidence of ischemia or obstructive coronary artery disease, as demonstrated by the lack of significant current deviations within the myocardium and absence of angle shift between the positive red pole and negative blue pole between T wave onset (T-onset) and T wave peak (T-peak) ; (B) The MCG scan of a patient in their 70s showed magnetic field angular deflection , abnormal magnetic field distribution of the positive and multipolarisation of negative poles , suggesting significant myocardial ischemia, and the ECG showed no significant abnormality. The ICA showed two lesions: 60% stenosis of the D1, 50% stenosis of the R-PDA ,. The FFRs were 0.77 for the R-PDA;(C) MCG scan of a patient in their 60s showed no myocardial ischemia, ECG showed no significant abnormalities, echocardiography showed widening of the ascending aorta and aortic sinus. ICA showed 75% stenosis of the LAD, 60% stenosis of the RCA, FFR value of the LAD was 0.88.
MCG= magnetocardiography; FFR= fractional flow reserve ; ICA= invasive coronary angiography; D1= Diagonal branches ; R-PDA : Posterior descending artery ; LAD= Left Anterior descending artery; RCA= right coronary artery.

628x898mm (140 x 140 DPI)

Supplementary Material

Assessment of myocardial ischemia in borderline coronary artery lesions based on optical pumped magnetometer magnetocardiography

Shuwen Yang1#, Lanxin Feng 1#, Zhao Ma1, Huan Zhang1, Yazhe Zhang2, Linqi Liu1, Shu Zhou1, Xin Zhao1, Xueyao Yang1, Mingduo Zhang1, Min Zhang1, Jiqiang He1, Yanlong Ren1, Yawei Luo1, Feng Xu1, Xiantao Song1*, Chenchen Tu1*, Hongjia Zhang2

#These authors contributed equally to this work.

1Department of Cardiology, Beijing Anzhen Hospital, Capital Medical University, 100029, Beijing, China

2Department of Cardiac Surgery, Beijing Anzhen Hospital, Capital Medical University, 100029, Beijing, China

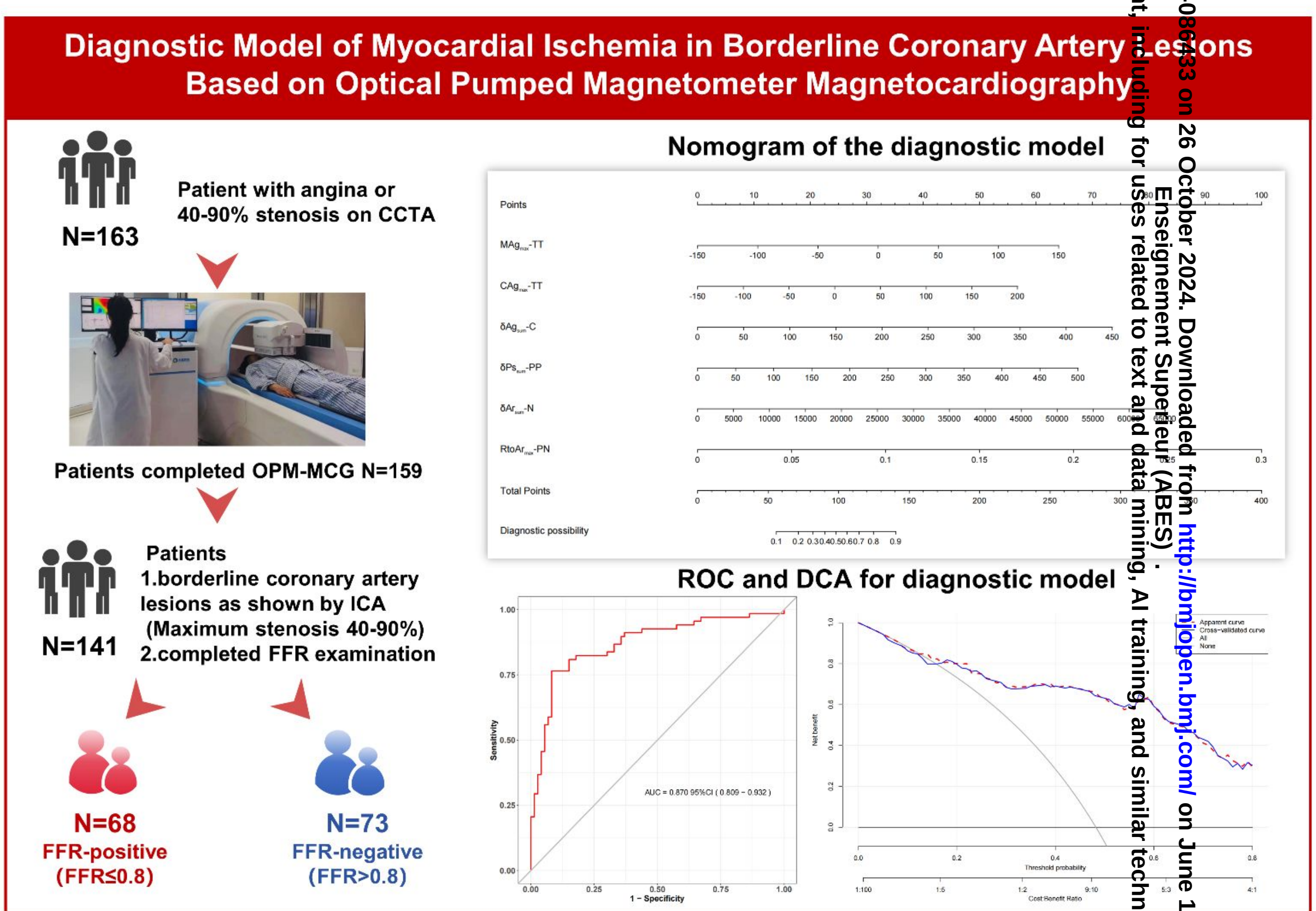

Figure 1 Graphical Abstracts: Diagnostic Model of Myocardial Ischemia in Borderline Coronary Artery Lesions Based on Optical Pumped Magnetometer Magnetocardiography

CCTA= coronary computed tomography angiography; MCG=magnetocardiography; ICA= invasive coronary angiography; FFR=fractional flow reserve; PCI= percutaneous coronary intervention.

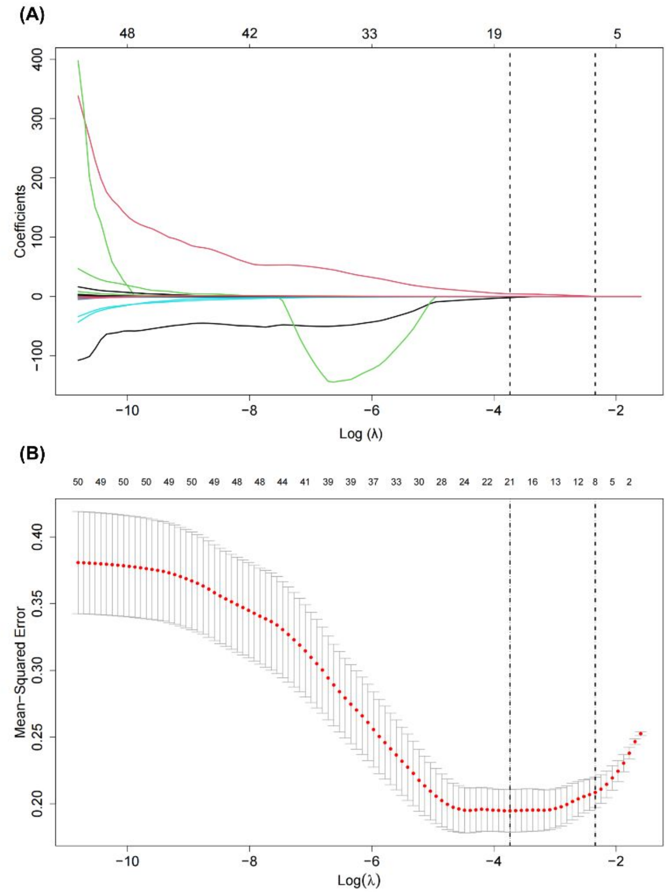

Figure 2 Least absolute shrinkage and selection operator (LASSO) regression

Figure legend :(A) LASSO model coefficient profiles of the 50 candidate parameters. As log λ increases, the regression coefficients continue to converge, and there are fewer parameters with non-zero regression coefficients.

(B) Tuning parameter selection by cross-validation in the LASSO model. The solid vertical lines represent the partial likelihood deviance standard error (SE). The red dotted line indicates the cross-validation curve. The vertical dashed lines are drawn at the optimal values on the basis of the minimum criteria and 1-SE criteria. Considering the reasonableness of the variables included in this model, with the λ value of 0.02380779 was chosen.

Table 1 OPM-MCG Parameters and Definitions

Parameters	Definition
δ Ag_{max}-M	The maximum value of changes in magnetic field angle at intervals of a certain time τ within TT segment
δ Ag_{min}-M	The minimum value of changes in magnetic field angle at intervals of a certain time τ within TT segment
δ Ag_{std}-M	The standard deviation of changes in magnetic field angle at intervals of a certain time τ within TT segment
δ Ag_{sum}-M	The sum of changes in magnetic field angle at intervals of a certain time τ within TT segment
δ Dt_{max}-PN	The maximum value of changes in magnetic pole distance at intervals of a certain time τ within TT segment
δ Dt_{min}-PN	The minimum value of changes in magnetic pole distance at intervals of a certain time τ within TT segment
δ Dt_{std}-PN	The standard deviation of changes in magnetic pole distance at intervals of a certain time τ within TT segment
δ Dt_{sum}-PN	The sum of changes in magnetic pole distance at intervals of a certain time τ within TT segment
δ Ag_{max}-C	The maximum value of changes in current angle at intervals of a certain time τ within TT segment
δ Ag_{min}-C	The minimum value of changes in current angle at intervals of a certain time τ within TT segment
δ Ag_{std}-C	The standard deviation of changes in current angle at intervals of a certain time τ within TT segment
δ Ag_{sum}-C	The sum of changes in current angle at intervals of a certain time τ within TT segment
δ Ps_{max}-C	The maximum value of changes in the position of the current angle at intervals of a certain time τ within TT segment
δ Ps_{std}-C	The standard deviation of changes in the position of the current angle at intervals of a certain time τ within TT segment
δ Ps_{sum}-C	The sum of changes in the position of the current angle at intervals of a certain time τ within TT segment
δ Ar_{max}-NP	The maximum value of changes in negative pole point area at intervals of a certain time τ within TT segment
δ Ar_{min}-NP	The minimum value of changes in negative pole point area at intervals of a certain time τ within TT segment
δ Ar_{std}-NP	The standard deviation of changes in negative pole point area at intervals of a certain time τ within TT segment
δ Ar_{sum}-NP	The sum of changes in negative pole point area at intervals of a certain time τ within TT segment
δ Ar_{bp}-NP	The change in negative pole point area between T-begin and T-peak
Ar_{max}-NP	The maximum value of the negative pole point area at intervals of a certain time τ within TT segment
Ar_{min}-NP	The minimum value of the negative pole point area at intervals of a certain time τ within TT segment
δ Ps_{max}-NP	The maximum value of changes in the position of the negative pole point at intervals of a certain time τ within TT segment
δ Ps_{std}-NP	The standard deviation of changes in the negative of the positive pole point at intervals of a certain time τ within TT segment
δ Ps_{sum}-NP	The sum of changes in the position of the negative pole point at intervals of a certain time τ within TT segment
δ Ar_{max}-N	The maximum value of changes in negative pole area at intervals of a certain time τ within TT segment

Parameters	Definition
$\delta\ Ag_{max}$-M	The maximum value of changes in magnetic field angle at intervals of a certain time τ within TT segment
$\delta\ Ar_{min}$-N	The minimum value of changes in negative pole area at intervals of a certain time τ within TT segment
$\delta\ Ar_{std}$-N	The standard deviation of changes in negative pole area at intervals of a certain time τ within TT segment
$\delta\ Ar_{sum}$-N	The sum of changes in negative pole area at intervals of a certain time τ within TT segment
$\delta\ Ar_{bp}$-N	The change in nagative pole area between T-begin and T-peak
Ar_{max}-N	The maximum value of the negative pole area at intervals of a certain time τ within TT segment
Ar_{min}-N	The minimum value of the negative pole area at intervals of a certain time τ within TT segment
$\delta\ ArRto_{max}$-PN	The maximum value of changes in the ratio of positive and negative pole area at intervals of a certain time τ within TT segment
$\delta\ ArRto_{min}$-PN	The minimum value of changes in the ratio of positive and negative pole area at intervals of a certain time τ within TT segment
$\delta\ ArRto_{std}$-PN	The standard deviation of changes in the ratio of positive and negative pole area at intervals of a certain time τ within TT segment
$\delta\ ArRto_{sum}$-PN	The sum of changes in the ratio of positive and negative pole area at intervals of a certain time τ within TT segment
$\delta\ Ar_{max}$-PP	The maximum value of changes in positive pole point area at intervals of a certain time τ within TT segment
$\delta\ Ar_{min}$-PP	The minimum value of changes in positive pole point area at intervals of a certain time τ within TT segment
$\delta\ Ar_{std}$-PP	The standard deviation of changes in positive pole point area at intervals of a certain time τ within TT segment
$\delta\ Ar_{sum}$-PP	The sum of changes in positive pole point area at intervals of a certain time τ within TT segment
$\delta\ Ar_{bp}$-PP	The change in positive pole point area between T-begin and T-peak
Ar_{max}-PP	The maximum value of the positive pole point area at intervals of a certain time τ within TT segment
Ar_{min}-PP	The minimum value of the positive pole point area at intervals of a certain time τ within TT segment
$\delta\ Ps_{max}$-PP	The maximum value of changes in the position of the positive pole point at intervals of a certain time τ within TT segment
$\delta\ Ps_{std}$-PP	The standard deviation of changes in the position of the positive pole point at intervals of a certain time τ within TT segment
$\delta\ Ps_{sum}$-PP	The sum of changes in the position of the positive pole point at intervals of a certain time τ within TT segment
$\delta\ Ar_{max}$-P	The maximum value of changes in positive pole area at intervals of a certain time τ within TT segment
$\delta\ Ar_{min}$-P	The minimum value of changes in positive pole area at intervals of a certain time τ within TT segment
$\delta\ Ar_{std}$-P	The standard deviation of changes in positive pole area at intervals of a certain time τ within TT segment

Parameters	Definition
δ Ag_{max}-M	The maximum value of changes in magnetic field angle at intervals of a certain time τ within TT segment
δ Ar_{sum}-P	The sum of changes in positive pole area at intervals of a certain time τ within TT segment
δ Ar_{bp}-P	The change in positive pole area between T-begin and T-peak
Ar_{ma}x-P	The maximum value of the positive pole area at intervals of a certain time τ within TT segment
Ar_{min}-P	The minimum value of the positive pole area at intervals of a certain time τ within TT segment
MAg_{max}-TT	The maximum magnetic field angle at intervals of a certain time τ within TT segment
CAg_{max}-TT	The maximum current angle at intervals of a certain time τ within TT segment
MAg_{min}-TT	The minimum magnetic field angle at intervals of a certain time τ within TT segment
CAg_{min}-TT	The minimum current angle at intervals of a certain time τ within TT segment
MAg-Rp	The magnetic field angle of the R-peak
RtoAm-R_pT_pN	The ratio of magnetic field amplitude at R-peak and the negative amplitude at T-peak
RtoAm-R_pT_pP	The ratio o magnetic field amplitude at R-peak and the positive amplitude at T-peak
RtoAm-R_pT_p	The ratio of magnetic field amplitudes at R-peak and T-peak
MAg-RpTp	The magnetic field angle between R-peak and T-peak
MAg-Tp	The magnetic field angle of the T-peak
CAg_{max}-Tp	The maximum current angle at T-peak
RtoAm-Tp	The ratio of positive to negative magnetic field amplitude at T-peak
TT	The interval from the beginning of the T-wave to its peak within the cardiac cycle

Dt = Distance, Ps = Position, Ag = Angle, Am = Magnitude, Ar = Area, Rto = Ratio, P = Positive, Positive Pole = PP, Negative = N, NP = Negative Pole, M = Magnetic Field, C = Current, max = Maximum, min = Minimum, sum=Sum of all, std = Standard deviation, δ = Change value, TT= TT segment

Table 2 OPM-MCG parameters of the Participant and univariable logistic regression model

Parameters	ALL N=141	FFR-Positive N=68	FFR-Negative N=73	Hazard Ratio (95%CI)	P value
δ Ag_{max}-M	0.62 (0.44,1.19)	0.77 (0.47,5.76)	0.54 (0.43,0.72)	1.08 (1.01,1.15)	0.002
δ Ag_{min}-M	-0.34 (-0.57,-0.18)	-0.42 (-0.82,-0.28)	-0.26 (-0.42,-0.14)	[illegible] (0.93,1.00)	0.001
δ Ag_{std}-M	0.16 (0.11,0.68)	0.28 (0.14,2.06)	0.14 (0.10,0.20)	[illegible] (1.16,2.19)	<0.001
δ Ag_{sum}-M	10.6 (6.18,26.2)	20.2 (9.88,45.5)	8.28 (4.55,11.8)	[illegible] (1.03,1.10)	<0.001
δ Dt_{max}-PN	2.69 (1.97,4.12)	3.51 (2.16,12.9)	2.22 (1.89,3.16)	[illegible] (1.00,1.03)	<0.001
δ Dt_{min}-PN	-2.20 (-3.27,-1.76)	-2.38 (-4.70,-1.91)	-2.00 (-2.80,-1.63)	[illegible] (0.95,1.00)	0.003
δ Dt_{std}-PN	0.74 (0.55,1.18)	0.82 (0.63,3.45)	0.63 (0.52,0.89)	[illegible] (1.02,1.31)	0.001
δ Dt_{sum}-PN	46.6 (29.1,80.7)	66.6 (42.0,110)	33.3 (25.7,48.6)	[illegible] (1.01,1.04)	<0.001
δ Ag_{max}-C	1.70 (1.21,4.83)	1.79 (1.27,9.10)	1.52 (1.16,2.98)	[illegible] (1.00,1.02)	0.016
δ Ag_{min}-C	-1.24 (-3.81,0.00)	-1.70 (-8.89,-1.01)	-0.91 (-1.75,0.00)	0.98 (0.97,1.00)	<0.001
δ Ag_{std}-C	0.54 (0.36,1.32)	0.80 (0.37,3.16)	0.45 (0.34,0.70)	1.12 (1.01,1.23)	0.003
δ Ag_{sum}-C	15.6 (9.64,38.6)	29.8 (13.5,71.6)	11.9 (7.79,17.5)	1.01 (1.00,1.02)	<0.001
δ Ps_{max}-C	33.0 (1.00,48.8)	33.0 (1.41,125)	31.0 (1.00,34.0)	1.01 (1.00,1.01)	0.008
δ Ps_{std}-C	3.35 (0.24,6.16)	3.57 (0.29,11.7)	3.20 (0.24,4.86)	1.07 (1.01,1.13)	0.016
δ Ps_{sum}-C	39.1 (6.00,86.1)	74.4 (8.31,161)	33.4 (4.00,66.0)	1.01 (1.00,1.01)	<0.001
δ Ar_{max}-NP	136 (74.0,220)	182 (102,314)	105 (59.0,180)	1.00 (1.00,1.00)	<0.001
δ Ar_{min}-NP	-84.00 (-173.00,-54.00)	-99.00 (-187.50,-62.75)	-68.00 (-148.00,-46.00)	1.00 (1.00,1.00)	0.009
δ Ar_{std}-NP	29.6 (20.0,56.7)	31.7 (23.4,70.1)	25.7 (17.1,41.4)	1.00 (1.00,1.01)	0.004
δ Ar_{sum}-NP	2469 (1443,4286)	3369 (2230,5728)	1672 (1277,2987)	1.00 (1.00,1.00)	<0.001
δ Ar_{bp}-NP	944 (18.0,2830)	1168 (152,3066)	626 (-46.00,2383)	1.00 (1.00,1.00)	0.238
Ar_{max}-NP	3873 (3001,5765)	4269 (3260,6056)	3828 (2894,5406)	1.00 (1.00,1.00)	0.160
Ar_{min}-NP	2426 (1639,3326)	2094 (1436,3245)	2614 (2065,3360)	1.00 (1.00,1.00)	0.036
δ Ps_{max}-NP	2.83 (2.24,4.12)	3.00 (2.24,5.28)	2.24 (2.00,3.00)	1.01 (1.00,1.01)	0.005
δ Ps_{std}-NP	0.70 (0.57,1.00)	0.81 (0.65,1.20)	0.66 (0.51,0.85)	1.04 (0.98,1.11)	0.005
δ Ps_{sum}-NP	41.7 (22.2,79.9)	59.8 (39.8,104)	26.4 (20.1,51.1)	1.01 (1.01,1.02)	<0.001
δ Ar_{max}-N	435 (243,750)	539 (269,990)	404 (221,526)	1.00 (1.00,1.00)	0.017

Parameters	ALL N=141	FFR-Positive N=68	FFR-Negative N=73	Hazard Ratio (95%CI)	P value
δ Ar_{min}-N	-170.00 (-369.00,-25.00)	-267.00 (-565.25,-108.75)	-79.00 (-224.00,-15.00)	1.00 (1.00,1.00)	<0.001
δ Ar_{std}-N	125 (80.2,225)	160 (90.5,273)	114 (74.6,158)	1.00 (1.00,1.01)	0.004
δ Ar_{sum}-N	12585 (7372,23204)	19058 (10208,29054)	9520 (6202,15009)	1.00 (1.00,1.00)	<0.001
δ Ar_{bp}-N	10445 (1116,25689)	11528 (588,28595)	8107 (2900,16796)	1.00 (1.00,1.00)	0.840
Ar_{max}-N	53635 (43655,65410)	56546 (44597,77766)	51431 (38201,58878)	1.00 (1.00,1.00)	0.032
Ar_{min}-N	40985 (26175,53701)	39744 (24308,59155)	40985 (29379,49923)	1.00 (1.00,1.00)	0.644
δ $ArRto_{max}$-PN	0.01 (0.00,0.02)	0.01 (0.00,0.03)	0.00 (0.00,0.01)	4.4[illegible]3839e^{10} (5.890000e^{-2},3.426868e^{18})	<0.001
δ $ArRto_{min}$-PN	-0.02 (-0.05,-0.01)	-0.02 (-0.07,-0.01)	-0.02 (-0.04,-0.01)	0.00 (0.00,0.13)	0.134
δ $ArRto_{std}$-PN	0.01 (0.00,0.02)	0.01 (0.00,0.02)	0.01 (0.00,0.01)	3.[illegible]7054e^{16} (1.758000e^{-3},5.740310e^{29})	0.114
δ $ArRto_{sum}$-PN	0.63 (0.32,1.72)	0.85 (0.39,2.36)	0.58 (0.29,0.88)	1.54 (1.15,2.06)	0.014
δ Ar_{max}-PP	195 (126,404)	281 (141,704)	153 (111,286)	1.00 (1.00,1.00)	0.001
δ Ar_{min}-PP	-171.00 (-295.00,-106.00)	-196.00 (-563.75,-109.50)	-153.00 (-226.00,-104.00)	1.00 (1.00,1.00)	0.006
δ Ar_{std}-PP	54.3 (33.7,124)	77.3 (35.5,167)	43.7 (32.1,79.7)	1.01 (1.00,1.01)	0.007
δ Ar_{sum}-PP	4689 (2685,8783)	6608 (3410,14024)	3487 (2556,5786)	1.00 (1.00,1.00)	<0.001
δ Ar_{bp}-PP	1058 (-869.00,5166)	1360 (-872.25,5756)	737 (-869.00,4601)	1.00 (1.00,1.00)	0.872
Ar_{max}-PP	8775 (6335,13548)	9178 (6485,14820)	8775 (6335,12776)	1.00 (1.00,1.00)	0.386
Ar_{min}-PP	5151 (2774,7571)	4626 (2618,6928)	5754 (3719,8258)	1.00 (1.00,1.00)	0.054
δ Ps_{max}-PP	3.16 (2.24,5.00)	3.61 (3.00,100)	3.00 (2.24,3.61)	1.01 (1.00,1.02)	<0.001
δ Ps_{std}-PP	0.82 (0.60,1.15)	0.98 (0.66,8.50)	0.75 (0.57,0.90)	1.12 (1.04,1.20)	<0.001
δ Ps_{sum}-PP	40.4 (23.1,88.6)	73.8 (29.9,195)	32.8 (21.7,54.2)	1.01 (1.01,1.02)	<0.001
δ Ar_{max}-P	244 (90.0,430)	312 (150,692)	172 (70.0,362)	1.00 (1.00,1.00)	0.001
δ Ar_{min}-P	-348.00 (-592.00,-203.00)	-381.00 (-812.00,-188.75)	-311.00 (-497.00,-211.00)	1.00 (1.00,1.00)	0.150
δ Ar_{std}-P	120 (80.2,203)	135 (82.3,267)	109 (75.7,159)	1.00 (1.00,1.00)	0.105
δ Ar_{sum}-P	11899 (6525,19157)	15787 (7938,28576)	9566 (5985,15629)	1.00 (1.00,1.00)	0.002
δ Ar_{bp}-P	-3600.00	-1456.00 (-14861.75,3900)	-4007.00	1.00 (1.00,1.00)	0.533

Parameters	ALL N=141	FFR-Positive N=68	FFR-Negative N=73	Hazard Ratio (95%CI)	P value
	(-12686.00,2509)		(-10962.00,1528)		
Ar_{max}-P	97097 (33699)	95392 (37311)	98685 (30122)	1.00 (1.00,1.00)	0.567
Ar_{min}-P	89822 (63201,104875)	83948 (55748,104204)	92433 (68813,105383)	1.0[illegible] (1.00,1.00)	0.134
MAg_{max}-TT	-62.32 (-70.64,-34.61)	-48.00 (-66.89,15.5)	-67.39 (-72.03,-53.13)	1.0[illegible] (1.01,1.03)	<0.001
CAg_{max}-TT	45.0 (33.3,71.0)	58.2 (39.2,118)	43.1 (32.0,51.1)	1.0[illegible] (1.01,1.03)	<0.001
MAg_{min}-TT	-70.76 (-76.85,-56.92)	-68.28 (-75.62,-41.24)	-71.98 (-77.61,-64.94)	1.0[illegible] (1.00,1.02)	0.050
CAg_{min}-TT	32.8 (5.36,45.9)	34.7 (-10.80,63.8)	32.0 (12.3,44.0)	1.0[illegible] (1.00,1.01)	0.471
MAg-Rp	-61.41 (-71.15,-42.88)	-53.44 (-70.66,-38.24)	-65.92 (-71.78,-50.54)	1.0[illegible] (1.00,1.03)	0.021
RtoAm-R_pT_pN	6.49 (4.32,9.57)	7.35 (4.92,10.4)	5.68 (3.71,8.14)	1.0[illegible] (1.00,1.12)	0.025
RtoAm-R_pT_pP	7.97 (5.88,12.0)	8.66 (6.03,12.9)	7.69 (5.56,11.1)	1.0[illegible] (1.00,1.13)	0.182
RtoAm-R_pT_p	3.64 (2.38,4.70)	4.13 (3.08,5.01)	3.28 (2.36,4.50)	1.22 (1.04,1.43)	0.027
MAg-RpTp	-0.67 (-24.77,19.5)	3.61 (-25.62,33.8)	-2.72 (-22.99,13.2)	1.00 (1.00,1.01)	0.235
MAg-Tp	-64.66 (-71.34,-45.44)	-55.82 (-70.28,-12.79)	-67.91 (-72.69,-53.13)	1.02 (1.01,1.03)	0.002
CAg_{max}-Tp	43.1 (29.4,52.0)	45.0 (27.6,74.7)	42.2 (30.7,46.9)	1.01 (1.00,1.02)	0.039
RtoAm-Tp	0.76 (0.57,1.08)	0.81 (0.52,1.22)	0.75 (0.57,0.98)	1.52 (0.93,2.48)	0.368

Dt = Distance, Ps = Position, Ag = Angle, Am = Magnitude, Ar = Area, Rto = Ratio, P = Positive, Positive Pole = PP, Negative = N, NP = Negative Pole, M = Magnetic Field, C = Current, max = Maximum, min = Minimum, sum=Sum of all, std = Standard deviation, δ = Change value, TT= TT segment

Table 3 Diagnostic model for assessment of myocardial ischemia in borderline coronary artery lesions

Parameters	Diagnostic model			
	B	OR	95%CI	P value
MAgmax-TT	0.011	1.011	(1.000-1.021)	0.029
CAgmax-TT	0.008	1.008	(0.998-1.018)	0.117
δAgsum-C	0.008	1.009	(1.000-1.019)	0.040
δPssum-PP	0.007	1.007	(1.001-1.013)	0.022
δArsum-N	0.001	1.001	(1.000-1.001)	0.002
RtoArmax-PN	17.324	33409.498	(0.694-50738)	0.123

Ps = Position, Ag = Angle, Ar = Area, Rto = Ratio, P = Positive, Positive Pole = PP, Negative = N, M = Magnetic Field, C = Current, max = Maximum, sum=Sum of all, std = Standard deviation, δ = Change value, TT= TT segment

BMJ Open

Assessment of myocardial ischemia in borderline coronary artery lesions based on optical pumped magnetometer magnetocardiography

Journal:	*BMJ Open*
Manuscript ID	bmjopen-2024-086433.R1
Article Type:	Original research
Date Submitted by the Author:	01-Jul-2024
Complete List of Authors:	yang, shuwen; Capital Medical University, Department of Cardiology Feng, Lanxin; Capital Medical University, Department of Cardiology Zhang, Mingduo; Capital Medical University Affiliated Anzhen Hospital Zhang , Min; Department of Cardiology, Beijing Anzhen Hospital, Capital Medical University Ma, Zhao; Capital Medical University, Department of Cardiology Zhang, Huan; Capital Medical University, Department of Cardiology Zhang, YaZhe; Capital Medical University, Department of Cardiac Surgery Liu, Linqi; Capital Medical University, Department of Cardiology Zhou, Shu; Capital Medical University, Department of Cardiology Zhao, Xin; Capital Medical University, Department of Cardiology Yang, Xue Yao; Capital Medical University Affiliated Anzhen Hospital He, Jiqiang; Beijing An Zhen Hospital, Capital Medical University, Cardiology Ren, Yanlong; Capital Medical University Affiliated Anzhen Hospital Luo, Yawei; Capital Medical University Affiliated Anzhen Hospital Xu, Feng; Capital Medical University Affiliated Anzhen Hospital Tu, Chenchen; Capital Medical University, Department of Cardiology song, xiantao; Capital Medical University, Department of Cardiology Zhang, Hong-Jia; Capital Medical University Affiliated Anzhen Hospital,
Primary Subject Heading:	Diagnostics
Secondary Subject Heading:	Diagnostics
Keywords:	Diagnostic Imaging, Ischaemic heart disease < CARDIOLOGY, Clinical Trial

SCHOLARONE™ Manuscripts

I, the Submitting Author has the right to grant and does grant on behalf of all authors of the Work (as defined in the below author licence), an exclusive licence and/or a non-exclusive licence for contributions from authors who are: i) UK Crown employees; ii) where BMJ has agreed a CC-BY licence shall apply, and/or iii) in accordance with the terms applicable for US Federal Government officers or employees acting as part of their official duties; on a worldwide, perpetual, irrevocable, royalty-free basis to BMJ Publishing Group Ltd ("BMJ") its licensees and where the relevant Journal is co-owned by BMJ to the co-owners of the Journal, to publish the Work in this journal and any other BMJ products and to exploit all rights, as set out in our licence.

The Submitting Author accepts and understands that any supply made under these terms is made by BMJ to the Submitting Author unless you are acting as an employee on behalf of your employer or a postgraduate student of an affiliated institution which is paying any applicable article publishing charge ("APC") for Open Access articles. Where the Submitting Author wishes to make the Work available on an Open Access basis (and intends to pay the relevant APC), the terms of reuse of such Open Access shall be governed by a Creative Commons licence – details of these licences and which Creative Commons licence will apply to this Work are set out in our licence referred to above.

Other than as permitted in any relevant BMJ Author's Self Archiving Policies, I confirm this Work has not been accepted for publication elsewhere, is not being considered for publication elsewhere and does not duplicate material already published. I confirm all authors consent to publication of this Work and authorise the granting of this licence.

Assessment of myocardial ischemia in borderline coronary artery lesions based on optical pumped magnetometer magnetocardiography

Shuwen Yang1#, Lanxin Feng 1#, Mingduo Zhang1, Min Zhang1, Zhao Ma1, Huan Zhang1, Yazhe Zhang2, Linqi Liu1, Shu Zhou1, Xin Zhao1, Xueyao Yang1, Jiqiang He1, Yanlong Ren1, Yawei Luo1, Feng Xu1, Chenchen Tu1*, Xiantao Song1*, Hongjia Zhang2

#These authors contributed equally to this work.

* These corresponding authors contributed equally to this work.

1Department of Cardiology, Beijing Anzhen Hospital, Capital Medical University, 100029, Beijing, China

2Department of Cardiac Surgery, Beijing Anzhen Hospital, Capital Medical University, 100029, Beijing, China

Corresponding Author:

The first corresponding author：Dr ChenChen Tu

Department of Cardiology, Anzhen Hospital, Capital Medical University, 2 Anzhen Road, Chaoyang District, 100020, Beijing, China E-mail: tcc2033@163.com

Dr Xiantao Song

Department of Cardiology, Anzhen Hospital, Capital Medical University, 2 Anzhen Road, Chaoyang District, 100020, Beijing, China E-mail: song0929@mail.ccmu.edu.cn

Disclosures: The authors have nothing to disclose.

Abstract

Aims: Despite clinical guideline recommendations for its use, the uptake of fractional flow reserve (FFR) in borderline coronary artery lesions remains low. As a noninvasive and safe test for myocardial ischemia, the validity of optical pumped magnetometer magnetocardiography (OPM-MCG) versus FFR has not been fully established. **Methods and Results:** A total of 141 stable patients with borderline coronary artery lesions were prospectively enrolled from June 30 to November 30, 2023. All of them underwent sequential OPM-MCG before coronary angiography (CAG) and FFR. 6 parameters were included in the final diagnostic model: MAg_{max}-TT, CAg_{max}-TT, δAg_{sum}-C, δPs_{sum}-PP, δAr_{sum}-N and $RtoAr_{max}$-PN. 500 bootstrap replications showed that the area under the receiver operating characteristic curve 95% confidence interval of the diagnostic model was 0.87 (0.809-0.932), with sensitivity of 76.5%, specificity of 91.8%, positive predictive value of 89.7%, negative predictive value of 80.7%. 1000 bootstrap replications showed that the model was well-calibrated. Decision curve analysis showed a net benefit from the predictive model when the threshold probability of an ischemic patient was greater than 12%, suggesting the potential utility of the model in the real world. **Conclusion:** A nomogram based on 6 OPM-MCG parameters was built to assess myocardial ischemia in borderline coronary artery lesions and can reduce unnecessary CAG.

Strengths and limitations of this study

1) This study is the first to demonstrate the importance of OPM-MCG in diagnosing myocardial ischemia in patients with borderline coronary lesions.

2) It creates a diagnostic model and nomogram for clinical use.

3) The conclusions of this study require further validation through multicenter studies.

Keywords: borderline coronary artery lesions； optical pumped magnetometer magnetocardiography； fractional flow reserve； myocardial ischemia

Introduction

Borderline coronary lesions exhibit ranging from 40% to 90% as seen in invasive coronary angiography (CAG). The FAME study [1] found that over 80% of lesions fell into this category, with only 35% of stenoses between 50-70% being hemodynamically significant. Predicting relevance was most accurate when estimating coronary artery diameter over 90%. Therefore, fractional flow reserve (FFR) guided intervention in patients with borderline coronary artery lesions (40-90% stenosis) has become a recommended treatment strategy in the 2018 ESC Interventional Guidelines [2]. The 2021 ACC/AHA/SCAI Guidelines for Coronary Artery Revascularization [3] also have clear recommendations for borderline lesions: FFR and instantaneous wave-free ratio (iFR) are used to assess the need for percutaneous coronary intervention (PCI) in patients without evidence of ischemia but with angina and other equivalent symptoms (Class I); PCI is not recommended for stable patients with FFR >0.8 or iFR >0.89 (Class III). However, its widespread adoption in coronary catheter laboratories is hindered by its time-consuming nature, consumption of resources, and potential adverse effects associated with adenosine application.

Optical pumped magnetometer magnetocardiography (OPM-MCG) measures tiny magnetic fields

(10^-15^ Tesla) from the heart using atomic magnetometer technology, without radiation. It's quick, contactless, and suitable for diverse populations. Clinical studies have shown that MCG is better than electrocardiogram (ECG) at detecting early myocardial ischemia [4,5,6,7] and has similar diagnostic effectiveness as SPECT for coronary artery disease (CAD) [8,9]. MCG is precise in diagnosing non-ST-segment elevation myocardial infarction, even in individuals who do not exhibit typical angina. [10,11]. However, the parameters and cut-off values of OPM-MCG that indicate myocardial ischemia are presently undefined in borderline coronary artery lesion.

Hence, this study aims to investigate the accuracy of OPM-MCG in diagnosing myocardial ischemia in patients with borderline coronary lesions, with invasive FFR examination serving as the reference standard.

Method

Study population

This study was a prospective, single-center, observational, cohort study which was reviewed by the Ethics Committee of Beijing Anzhen Hospital, Capital Medical University, and registered with the China Clinical Trial Registry (ChiCTR2300072382). All participants signed an informed consent. The methods described in this article follow the STARD 2015 guidelines.

Participants aged 18-80 with typical angina symptoms (CCS class II or higher) or 40-90% stenosis on CCTA were scheduled for hospitalization for CAG. Exclusion criteria included: 1) Coronary artery stenosis outside of 40%-90% range on CAG; 2) Acute myocardial infarction; 3) Previous myocardial infarction; 4) Complex arrhythmias; 5) Bundle-branch block; 6) Pacemakers, metallic implants in trunk;

7) Claustrophobia.

This study was based on a prospective cohort design, the sample size of which was calculated by PASS 2021 software using the area under the ROC curve. The significance level (α) was 0.025 and the degree of certainty (1-β) was 0.90, combining the results of the literature review of related studies as well as the statistics of the small sample in the previous period, and calculating according to the FFR-positive (ischemic)/FFR-negative (non-ischemic) =2:3. The sample size was calculated as 138.

A total of 163 patients from June 30th to November 30th, 2023 were consecutively enrolled, and 22 patients were excluded, of which 11 patients with stenosis >90%, 7 patients underwent direct PCI without FFR testing, and 4 patients with poor quality MCG imaging, and Finally 141 patients with borderline coronary lesions underwent MCG and FFR sequentially (Figure 1). In this study, the cardiologists were not aware of the MCG results at the time of the FFR examination, and the MCG parameters were determined before the FFR examination (Supplementary Figure 1-Graphical Abstract).

CAG and FFR procedures

CAG and FFR measurements were performed on the vessels according to the 2021 ACC/AHA/SCAI Guidelines for Coronary Artery Revascularization and Expert consensus on the clinical pathway for FFR measurement in China. After administration of nitroglycerin, a pressure monitoring guidewire was advanced through the stenosis. Hyperemia was attained by administration of intravenous adenosine (140μg/kg/min). The FFR pressure wire was positioned a minimum of 20 mm distal to the stenosis in vessel segments ≥2 mm. The presence of an FFR ≤0.80 was considered a positive indicator of functional ischemia in patients and was defined as the FFR-positive group.

MCG imaging

The MCG recordings were conducted using a 36-channel OPM-MCG system (Miracle MCG), featuring OPM sensors sourced from Beijing X-Mag Technologies Limited's mature commercial product. The OPM sensor is based on spin-exchange relaxation free (SERF) technology, with alkali metal atoms as the core sensitive element. The OPM sensor has a sensitivity below 30 $fT/Hz^{1/2}$, a recording bandwidth of 1 Hz to 40 Hz, a sampling frequency of 200 Hz, and a noise baseline with not higher than 15 fT. The OPM-MCG residual magnetic field is kept below 1.5 nT, and the data acquisition mode is analog signal acquisition (Supplementary Figure 2). Each subject had a 90-second continuous recording at 36 locations (6×6 grid) above the chest using an arrayed sensor grid.

MCG Signal Analysis and Statistical Analysis

After MCG data acquisition, the software automatically post-processes the signals to generate magnetic field and current density maps and output 65 parameters (Supplementary Table 1). The 65 parameters we output characterize the stability of the current dipole in the TT segment (the position from one-third of the T max amplitude (T onset) to T max (T peak)) according to the previous studies of Park et al. and Pena et al. Once OPM-MCG data collection is complete, the software automatically generates precise magnetic field and current density maps and outputs their parameters (see supplementary material for post-processing steps).

Data analysis was performed with SPSS 26.0 and R 4.3.2 (http //www.R-project.org/). Counting data were presented as numbers and percentages, while normally distributed measurement data were shown as mean ± standard deviation. Continuous variables that were not normally distributed were presented using median and quartile values. Statistical significance was determined for all analyses with a P-value less than 0.05. Based on this cohort and the principle of LEAST 10 events per variable (10 EPV), we considered the rationality of the parameters included in the diagnostic model and evaluated the number of parameters. The predictive variables were selected from 65 preselected potential candidates and included in the model by univariate logistic regression, LASSO regression, and multivariate logistic regression with the backward method. The stability of the model was determined by cross-validation. The model's predictive performance was assessed using the enhanced bootstrap method and clinical benefit was evaluated using decision curve analysis. The MCG-FFR nomogram was used to report scores for assessing myocardial ischemia with OPM-MCG parameters.

Patient and Public Involvement

Patients make more people aware of the clinical use of the OPM-MCG and how it is examined by sharing news and information about clinical studies with others.

Result

Clinical characteristics

The study included 141 patients, mostly male (77.3%) with an average age of 60.64 ± 9.70 years. After MCG scans, all patients underwent CAG and FFR examination, with 48.2% having positive FFR (FFR ≤ 0.8). A total of 157 vessels were examined, with 47.1% having FFR ≤ 0.8. Interval between MCG and FFR less than 30 days, median 2 days. Most patients had FFR measurements primarily done on the LAD. See Supplementary Table 2 for patient clinical characteristics.

Selection of parameters and development of the diagnostic model

50 variables that were statistically significant ($P < 0.1$) in univariable logistic regression were included in the LASSO regression (Supplementary Table 3 and Supplementary Figure 3), and 8 variables were selected based on the reasonableness of the parameters selected to reduce the model overfitting and covariance through LASSO regression. By using the backward approach, 6 parameters were included in the final diagnostic model: MAg_{max}-TT, CAg_{max}-TT, δAg_{sum}-C, δPs_{sum}-PP, δAr_{sum}-N and $RtoAr_{max}$-PN (Table 1, Figure 2). The model area under the receiver operating characteristic curve (AUC) obtained from multivariate logistic regression analysis was 0.87, with sensitivity of 76.5%, specificity of 91.8%, positive predictive value of 89.7%, negative predictive value of 80.7%. The nomogram (Figure 3) provides a graphical overview of the diagnostic model using multivariate logistic regression analysis (Supplementary Table 4).

Internal validation and net benefit of the model

The model performance for the diagnosis of myocardial ischemia in borderline coronary artery lesions of the OPM-MCG was evaluated by bootstrap replications.500 bootstrap replications showed that the model AUC and a 95% confidence interval (CI) of 0.87 (0.809-0.932) (Figure 4). 1000 bootstrap replications showed that the model was well-calibrated. The mean absolute error was 0.032 (Figure 4). The decision curve analysis (DCA) for the diagnostic model showed that if the threshold probability of patients is greater than 12% (Figure 4), screening strategies based on the OPM-MCG diagnostic model resulted in superior net benefit than screen-none or screen-all strategies.

Discussion

CAD is presently characterized by an epicardial vascular lesion with a stenosis exceeding 50% in the CAG. Frequently, this description acts as a reference for heart muscle revascularization. Moreover, FFR can be used to evaluate the existence of myocardial ischemia, with a threshold of 0.8. However, as illustrated in the Figure 2, the coronary stenosis identified in CAG may not precisely align with the invasive FFR results. This observation is in line with the conclusions drawn in the 2019 ESC Guidelines for Chronic Coronary Syndromes [12,13], emphasizing that the accuracy of determining CAD solely based on angiographic stenosis was as low as 64% when compared to flow reserve fraction. The positive mismatch rate, where lesions with less than 50% stenosis may demonstrate an FFR ≤ 0.8, was 19%, while the negative mismatch rate, where lesions with over 50% stenosis may result in an FFR value > 0.8, reached up to one-third. Numerous studies [14,15] have consistently demonstrated that FFR-guided stenting leads to superior immediate outcomes and long-term prognosis. Therefore, FFR carries a Class 1a recommendation for guiding revascularization in angiographically borderline coronary stenoses in patients with stable angina. The feasibility of diagnosing myocardial ischemia in patients with borderline lesions using OPM-MCG was shown in our study, when compared to invasive FFR. The collective diagnostic potential of MCG parameters in detecting myocardial ischemia in borderline coronary artery lesions resulted in an AUC of 0.87 (95% CI 0.809 to 0.932). Due to factors such as time consumption, costs, patient-related discomfort, contraindications, and a lack of reimbursement, the current rate of FFR utilization in catheterization laboratories in China is less than 6% [3]. OPM-MCG allows ischemia assessment in patients with borderline coronary lesions prior to CAG and has a good concordance with invasive FFR.

In comparing our MCG results with those reported by Park JW et al. [16], it is clear that FFR, serving as the reference standard, evaluates ischemia through direct measurement of pressure beyond the coronary lesion. In contrast, the six parameters of our OPM-MCG, along with the ST-segment fluctuation scores (AUC=0.835) and Bull's eye analysis (AUC=0.914) employed by Park, offer a non-invasive alternative. According to Park JW et al, the TT segment, defined as the position from one-third of the T max amplitude (T onset) to T max (T peak), is a more effective parameter for analyzing MCG signals due to its superior signal-to-noise ratio in reflecting ventricular repolarization electrical activity [17]. In terms of the selected parameters, consistent with earlier literature [18], we focused on assessing the overall homogeneity of the repolarization process, including spatial structural similarity and smoothing of current changes. Park et al. utilized ST-segment fluctuation scores and Bull's eye analysis to evaluate the uniformity of the repolarization process in relation to current variations and spatial distribution variances for ischemia assessment. In our study, we further characterized the images by incorporating the δAg_{sum}-C, δPs_{sum}-PP, δAr_{sum}-N and $RtoAr_{max}$-PN parameters of the model to analyze changes in currents, pole locations, and areas. Additionally, describing the images using the parameters of the 6 different angular points provided a comprehensive description and response to the images. In terms of practical clinical application, Park JW et al. used a 64-channel axial gradiometer system with greater channel capacity and higher sensitivity for positional discrimination, but required patients to complete two MCG tests in stress and rest states in a shielded room. Conversely, OPM-MCG does not mandate a shielded room and can effectively diagnose myocardial ischemia resulting from coronary artery borderline lesions in the rest state, which improves the generalizability in clinical application.

Non-invasive methods like PET/CT, SPECT and CMR are accurate for assessing myocardial ischemia, but their use is limited due to cost, long wait times and radioactive substances[19]. In a prospective study done by Roel S. et al. [20], which included 189 patients in a head-to-head comparison, it was found that using FFR as the gold standard, the sensitivity of SPECT, PET/CT, and CMR was only 67%, 81%, and 66%, and the specificity was only 61%, 65%, and 62%. The diagnostic accuracy of PET/CT was not statistically different from that of SPECT and CMR. Recently CT-derived fractional flow reserve (CT-FFR) has emerged as a noninvasive test for detecting myocardial ischemia, with a sensitivity of 89% and specificity of 91% according to a multicenter study [21]. The widespread use of CT-FFR has limitations including the need for good image quality and inability to assess microvascular and diffuse lesions [22]. ECG is widely used in the clinic as the fastest and low-cost test. ECG uses a two-dimensional linear approach to record cardiac radial currents to detect ischemia, but it can be affected by body tissues or fluids and has low spatial resolution. MCG detects and measures weak magnetic fields generated by the electrical activity of the heart, and the waveform of the MCG wavefrom is similar to that of the ECG signal. However, MCG is less affected by changes in conductivity and does not suffer from skin electrode contact problems. In addition, MCG is more sensitive to magnetic fields generated by tangential currents that are more affected by myocardial ischemia, and MCG detects eddy currents that are not apparent with ECG [23]. Thus, previous studies have demonstrated that MCG has a higher sensitivity to early myocardial ischemia [24,25]. In most studies of MCG detection of myocardial ischemia, researchers have categorized the analysis of MCG into morphological and quantitative data analyses [26]. Morphological analysis often focuses on amplitude, nondipole phenomena, and current or magnetic field

232 angle. Quantitative data analysis is mostly based on changes in the magnetic field during ventricular
233 repolarization, usually at the end of the ST segment (before the T wave) and/or during the T wave, and
234 partially measured during the QT and QRS segment. These parameters describe the poles, the angles of
235 the magnetic and current fields, and the waveform amplitude by extrema, dynamics, and ratios. Current
236 studies analyzing MCG at rest for the detection of myocardial ischemia use a variety of methods,
237 including dichotomous classification methods based on MCG parameters, quantification of abnormal
238 MCG parameters, creation of composite indices using MCG parameters, and the application of machine-
239 learning methods [27].

240 This is similar to our finding that a positive OPM-MCG scan was demonstrated by one or more
241 abnormalities in the TT segment, including changes in TT segment parameters and changes in image
242 (non-dipole phenomena and angular deflection of currents or magnetic fields). Different MCG
243 parameters and combinations of parameters can provide more incremental information on
244 cardiovascular disease. In addition, studies have shown that MCG is capable of accurately diagnosing
245 myocardial ischemia resulting from epicardial coronary artery disease as well as effectively detecting
246 myocardial ischemia caused by coronary microvascular dysfunction (CMD). The accuracy of MCG
247 identification of CMD is 94.8%, sensitivity of 100%, and specificity of 93.3% [28]. In our study, we also
248 found a small number of FFR-negative patients with positive MCG scans as described above, and
249 considered the possibility of CMD. In the future, we will summarize the characteristic images of patients
250 with CMD and further explore the incremental information provided by the MCGs for these patients.

251 The difference between SQUID-based and OPM-based MCG systems depends on their sensor
252 technology. SQUID-based MCGs were developed earlier and offer high sensitivity. But their reliance

on liquid helium refrigeration for achieving low-temperature superconductivity, as well as the high maintenance costs associated with them, have hindered their widespread adoption and utilization. In contrast, the OPM-MCG operates at room temperature without liquid helium cooling and offers comparable sensitivity, is easier to use and less expensive to operate [29,30]. However, the OPM-MCG also suffers from the problem of being unsuitable for claustrophobic patients. Furthermore, the development of OPM-MCG is late, resulting in a lack of established guidelines for analyzing MCG parameters. As such, we intend to conduct further exploratory studies on OPM-MCG in various clinical settings.

MCG has been proved to be in good concordance with FFR in the preoperative assessment of myocardial ischemia in patients with borderline coronary artery lesions, and more clinical information can be provided to patients with cardiovascular disease through more studies in the future. MCG is expected to be used for the preoperative assessment of lesion-specific ischemia in patients with borderline coronary arteries, and to reduce the number of unnecessary invasive coronary arteriography examinations. This will effectively reduce the pressure on national healthcare expenditures and reduce the burden on patients with cardiovascular diseases.

Limitation

The study is a single-center registry study with some limitations. We are aware that the current diagnostic model may suffer from overfitting and therefore the conclusions of this study await further validation in multicenter studies. In addition, the color coding we are currently using differs from the Rome Biomag Conference in 1981 standard, whereas there are currently multiple types of MCGs globally, and the current methodology for analyzing myocardial ischemia has not been compared head-to-head with other MCG devices.

Conclusion

MCG shows excellent sensitivity, specificity, and diagnostic accuracy in identifying significant coronary artery disease when compared to FFR. MCG can provide the evidence for a precise diagnostic strategy for patients with borderline coronary lesions before CAG, reducing unnecessary invasive examination.

Ethics approval and consent to participate

This study was performed in accordance with the principles of the Declaration of Helsinki. This study was approved by the ethics committee of Beijing Anzhen Hospital, Capital Medical University (KS2023008). Written informed consent was required for participation in the study.

Competing interests

The authors declare that they have no conflicts of interest.

Funding

This study was supported by Sponsored by Beijing Nova Program (20220484222) , Capital's Funds for Health Improvement and Research (2024-2-2066), 'Deng Feng' Training Program (DFL20220603), Beijing Hospitals Authority 'sailing' Program (YGLX202323) and Project of The Beijing Lab for

Cardiovascular Precision Medicine (PXM2018_014226_000013).

Author Contribution Statement

Xiantao Song and Chenchen Tu acted as guarantors. Xiantao Song, Chenchen Tu and Hongjia Zhang helped to conceive the topic and revised the article. Shuwen Yang and Lanxin Feng wrote the manuscript and finished the statistics, Mingduo Zhang, Min Zhang, Jiqiang He, Yanlong Ren, Yawei Luo and Feng Xu contributed to the data collection. Zhao Ma, Huan Zhang, Yazhe Zhang, Linqi Liu, Shu Zhou, Xin Zhao, and Xueyao Yang helped with data analysis. All authors read and approved the final manuscript.

Acknowledgments

The authors thank Zhechun Zeng, Ming Ding, and Bin Cai for their help in data analysis, and Xin Chen, Jinfan Tian, and Yulong Xue for their help in data collection.

Patient and Public Involvement

Patients make more people aware of the clinical role of the MCG and how it is examined by forwarding news stories and sharing information about clinical studies with others

Abbreviations

AUC= area under the receiver operating characteristic curve

CCTA= coronary computed tomography angiography

CI= confidence intervals

FFR= fractional flow reserve

CAG= coronary angiography

NPV= negative predictive value

OPM-MCG= optical pumped magnetometer magnetocardiography

OR= Odds ratio

PPV= positive predictive value

ROC= receiver-operating characteristic

Availability of data and materials

The data that support the findings of this study are available on request from the corresponding author, Xiantao Song， upon reasonable request.

Reference

[1] van Nunen LX, Zimmermann FM, Tonino PA, et al. Fractional flow reserve versus angiography for guidance of PCI in patients with multivessel coronary artery disease (FAME): 5-year follow-up of a randomised controlled trial. Lancet. 2015;386(10006):1853-1860.

[2]Neumann FJ, Sousa-Uva M, Ahlsson A, et al. 2018 ESC/EACTS Guidelines on myocardial revascularization [published correction appears in Eur Heart J. 2019 Oct 1;40(37):3096]. Eur Heart J. 2019;40(2):87-165.

[3] Writing Committee Members, Lawton JS, Tamis-Holland JE, Bates ER, et al. 2021 ACC/AHA/SCAI Guideline for Coronary Artery Revascularization: Executive Summary: A Report of the American College of Cardiology/American Heart Association Joint Committee on Clinical Practice Guidelines [published

correction appears in J Am Coll Cardiol. 2022 Apr 19;79(15):1547]. J Am Coll Cardiol. 2022;79(2):197-215.

[4] Nomura M, Nakaya Y, Fujino K, et al. Magnetocardiographic studies of ventricular repolarization in old inferior myocardial infarction. Eur Heart J. 1989;10(1):8-15.

[5] Brisinda D, Meloni AM, Fenici R. First 36-channel magnetocardiographic study of CAD patients in an unshielded laboratory for interventional and intensive cardiac care. Funct Imaging Model Hear. 2003;LNCS 2674:122-131.

[6] Gapelyuk A, Wessel N, Fischer R, et al. Detection of patients with coronary artery disease using cardiac magnetic field mapping at rest. J Electrocardiol. 2007;40(5):401-407.

[7]Kanzaki H, Nakatani S, Kandori A, et al. A new screening method to diagnose coronary artery disease using multichannel magnetocardiogram and simple exercise. Basic Res Cardiol. 2003;98(2):124-132.

[8] Nakai K, Izumoto H, Kawazoe K, et al. Three-dimensional recovery time dispersion map by 64-channel magnetocardiography may demonstrate the location of a myocardial injury and heterogeneity of repolarization. Int J Cardiovasc Imaging. 2006;22(3-4):573-580. doi:10.1007/s10554-005-9019-x.

[9]Tolstrup, Kirsten, Donatella Brisinda, Am Meloni, et al. Comparison of resting magnetocardiography with stress single photon emission computed tomography in patients with stable and unstable angina. J Am Coll Cardiol 2006;47(4 Suppl 1):176A. Abstract 930-247.

[10] Lim HK, Kwon H, Chung N, et al. Usefulness of magnetocardiogram to detect unstable angina pectoris and non-ST elevation myocardial infarction. Am J Cardiol. 2009;103(4):448-454.

[11] Shin ES, Lam YY, Her AY, et al. Incremental diagnostic value of combined quantitative and qualitative parameters of MCG to detect coronary artery disease. Int J Cardiol. 2017;228:948-952.

[12] Knuuti J, Wijns W, Saraste A, et al. 2019 ESC Guidelines for the diagnosis and management of chronic coronary syndromes [published correction appears in Eur Heart J. 2020 Nov 21;41(44):4242]. Eur Heart J. 2020;41(3):407-477.

[13] Derimay F, Finet G and Rioufol G. Coronary artery stenosis prediction does not mean coronary artery stenosis obstruction. Eur Heart J. 2021;42(42):4401.

[14] Xaplanteris P, Fournier S, Pijls NHJ, et al. Five-Year Outcomes with PCI Guided by Fractional Flow Reserve. N Engl J Med. 2018;379(3):250-259.

[15] Zimmermann FM, Ferrara A, Johnson NP, et al. Deferral vs. performance of percutaneous coronary intervention of functionally non-significant coronary stenosis: 15-year follow-up of the DEFER trial. Eur Heart J. 2015;36(45):3182-3188.

[16] Park JW, Shin ES, Ann SH, et al. Validation of magnetocardiography versus fractional flow reserve for detection of coronary artery disease. Clin Hemorheol Microcirc. 2015;59(3):267-281.

[17]Park J-W, Hill PM, Chung N, Hugenholtz PG, Jung F. Magnetocardiography predicts coronary artery disease in patients with acute chest pain. Ann Noninvasive Electrocardiol. 2005;10(3):312-323.

[18] Chaikovsky I, Hailer B, Sosnytskyy V, et al. Predictive value of the complex magnetocardiographic index in patients with intermediate pretest probability of chronic coronary artery disease: results of a two-center study. Coron Artery Dis. 2014;25(6):474-484.

[19] Working Group of Cardiovascular Imaging of National Center for Medical Quality Control of Cardiovascular Diseases Survey of the Application Status of Cardiovascular Imaging Modalities and Medical Quality Report in China [J]. Chin circ J ,2020,35(7):625-633.

[20] Driessen RS, van Diemen PA, Raijmakers PG, et al. Functional stress imaging to predict abnormal coronary fractional flow reserve: the PACIFIC 2 study. Eur Heart J. 2022;43(33):3118-3128.

[21] Tang CX, Liu CY, Lu MJ, et al. CT FFR for Ischemia-Specific CAD With a New Computational Fluid Dynamics Algorithm: A Chinese Multicenter Study. JACC Cardiovasc Imaging. 2020;13(4):980-990.

[22] Li Y, Yu M, Dai X, et al. Detection of Hemodynamically Significant Coronary Stenosis: CT Myocardial Perfusion versus Machine Learning CT Fractional Flow Reserve. Radiology. 2019;293(2):305-314.

[23]Chaikovsky I, Hailer B, Sosnytskyy V, et al. Predictive value of the complex magnetocardiographic index in patients with intermediate pretest probability of chronic coronary artery disease: results of a two-center study. Coron Artery Dis. 2014;25(6):474-484.

[24]Mace SE, Peacock WF, Stopyra J, et al. American Heart Journal Plus : Cardiology Research and

Practice Accelerated magnetocardiography in the evaluation of patients with suspected cardiac ischemia : The MAGNETO trial. Am Hear J Plus Cardiol Res Pract. 2024;40(February):100372.

[25]Tolstrup K, Madsen BE, Ruiz JA, et al. Non-invasive resting magnetocardiographic imaging for the rapid detection of ischemia in subjects presenting with chest pain. Cardiology.

[26]Camm AJ, Henderson R, Brisinda D, et al. Clinical utility of magnetocardiography in cardiology for the detection of myocardial ischemia. J Electrocardiol. 2019;57:10-17.

[27] Rong Tao, Shulin Zhang, Xiao Huang, et al. Magnetocardiography-Based Ischemic Heart Disease Detection and Localization Using Machine Learning Methods. IEEE Trans Biomed Eng. 2019;66(6):1658-1667.

[28] Rong Tao, Shulin Zhang, Xiao Huang, et al. Magnetocardiography-Based Ischemic Heart Disease Detection and Localization Using Machine Learning Methods. IEEE Trans Biomed Eng. 2019;66(6):1658-1667.

[29]Brisinda D, Fenici P, Fenici R. Clinical magnetocardiography: the unshielded bet—past, present, and future. Front Cardiovasc Med. 2023;10(August):1-24.

[30] Pena ME, Pearson CL, Goulet MP, et al. A 90-second magnetocardiogram using a novel analysis system to assess for coronary artery stenosis in Emergency department observation unit chest pain patients. IJC Hear Vasc. 2020;26(100466):1-7.

Table 1 The definitions of the MCG parameters

MCG Parameters	Definitions
MAgmax-TT	The maximum magnetic field angle at intervals of a certain time τ within TT segment
CAgmax-TT	The maximum current angle at intervals of a certain time τ within TT segment
δAgsum-C	The sum of changes in current angle at intervals of a certain time τ within TT

	segment
δPssum-PP	The sum of changes in the position of the positive pole point at intervals of a certain time τ within TT segment
δArsum-N	The sum of changes in negative pole area at intervals of a certain time τ within TT segment
δRtoArmax	The maximum value of changes in the ratio of positive to negative area at intervals of a certain time τ within TT segment

TT= from T onset to T peak; C= current; PP= positive pole point; P= positive pole; N= negative pole; Ag= angle; Ar= area; Rto= ratio; δ= Change value. τ= one tenth of the time interval between TT segment.

Figure legend

Figure 1. Flowchart of the study design.

Figure legend: CCTA= coronary computed tomography angiography; MCG=magnetocardiography; ICA= invasive coronary angiography; FFR=fractional flow reserve; PCI= percutaneous coronary intervention.

Figure 2 Schematic diagram of OPM-MCG scan.

Figure legend: (A) Schematic diagram of MAg_{max}-TT and CAg_{max}-TT In magnetic field distribution maps and current density maps, the definition rule for angle values is based on the horizontal axis, with counterclockwise angles being negative and clockwise angles being positive. MAg_{max}-TT is the maximum angle between the line connecting the maximum positive and negative magnetic poles and the horizontal axis. in the TT segment. CAg_{max}-TT is the maximum value of the angle between the current vector and the horizontal axis. in the TT segment. (B)Normal OPM-MCG scan The OPM-MCG scan showed no evidence of ischemia or obstructive coronary artery disease, as demonstrated by the lack of significant current deviations within the myocardium and absence of angle shift between the positive red pole and negative blue pole between T wave onset (T-onset) and T wave peak (T-peak) , FFR-positive and FFR-negative OPM-MCG scan and ICA Images. (C) The OPM-MCG scan of a patient in his 70s showed magnetic field angular deflection , abnormal magnetic field distribution of the positive and multipolarisation of negative poles , suggesting significant myocardial ischemia, and the ECG showed no significant abnormality. The ICA showed two lesions: 60% stenosis of the D1, 50% stenosis of the R-PDA ,. The FFRs were 0.77 for the R-PDA. (D) The OPM-MCG scan of a patient in their 60s showed no myocardial ischemia, ECG showed no significant abnormalities, echocardiography showed widening of the ascending aorta and aortic sinus. ICA showed 75% stenosis of the LAD, 60% stenosis of the RCA, FFR value of the LAD was 0.88.

MCG= magnetocardiography; FFR= fractional flow reserve ; ICA= invasive coronary angiography; D1= Diagonal branches ; R-PDA : Posterior descending artery ; LAD= Left Anterior descending artery; RCA= right coronary artery.

Figure 3. Nomogram of the diagnostic model.

Figure legend: The nomogram graphically demonstrates the diagnostic model of OPM-MCG. Points for MAg_{max}-TT, CAg_{max}-TT, δAg_{sum}-C, δPs_{sum}-PP, δAr_{sum}-N and $RtoAr_{max}$-PN can be obtained using a point caliper and then summed to obtain a total score that can be obtained using a point caliper and then summed to obtain a total score that can be measured with diagnosing myocardial ischemia in patients with borderline coronary lesions.

Figure 4 Accuracy and internal validation of the diagnostic model.

Figure legend: (A) ROC curves and 95% confidence intervals. After 500 bootstrap replications, the area under the curve and 95% confidence interval for receiver operating characteristic is 0.87 (0.809-0.932). (B) Calibration curve for the diagnostic model. Calibration curve for the borderline lesion ischemia diagnostic model was established by comparing the observed and predicted probability of a positive FFR in patients with borderline lesions of the coronary arteries. The smaller the distance of the scatter from the dashed line, the better the calibration. (C) Decision curve analysis (DCA) for diagnostic models of ischemia in borderline coronary lesions. None: net benefit when it is assumed that no patients with critical lesions of the coronary arteries would have the outcome (FFR-positive). All: net benefit when all patients with critical coronary lesions are assumed to have an outcome (FFR-positive). model: net benefit of managing critical coronary lesions with a diagnosis of myocardial ischemia based on the diagnostic model estimate. The strategy with the highest net benefit at any given threshold is the preferred strategy.

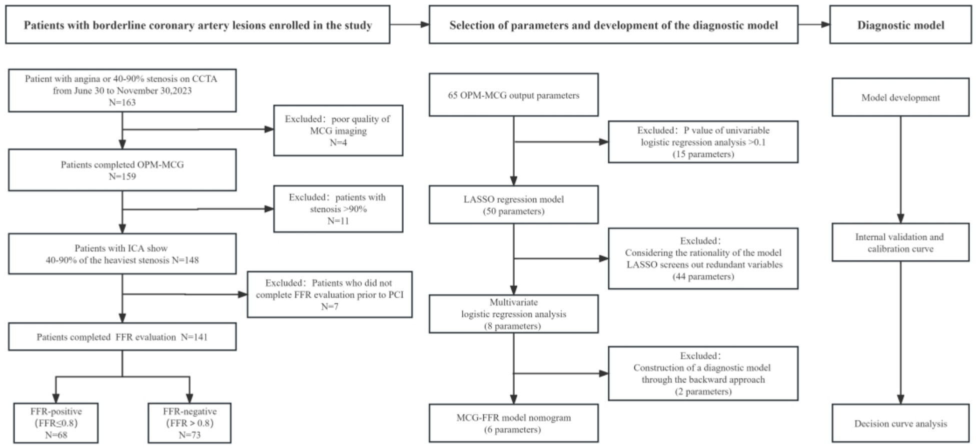

Figure 1. Flowchart of the study design.
Figure legend: CCTA= coronary computed tomography angiography; MCG=magnetocardiography; ICA= invasive coronary angiography; FFR=fractional flow reserve; PCI= percutaneous coronary intervention.

1322x611mm (96 x 96 DPI)

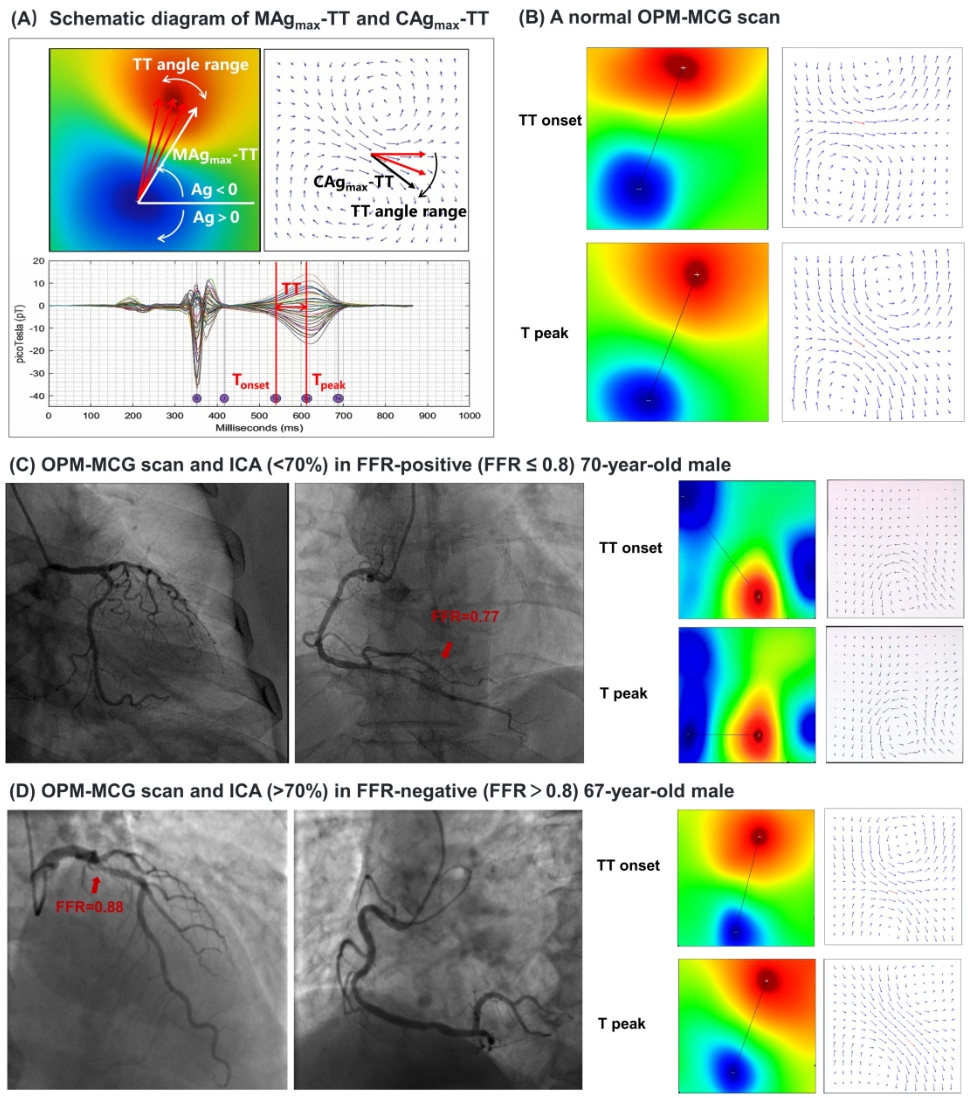

Figure 2 Schematic diagram of OPM-MCG scan

Figure legend: (A) Schematic diagram of MAgmax-TT and CAgmax-TT In magnetic field distribution maps and current density maps, the definition rule for angle values is based on the horizontal axis, with counterclockwise angles being negative and clockwise angles being positive. MAgmax-TT is the maximum angle between the line connecting the maximum positive and negative magnetic poles and the horizontal axis. in the TT segment. CAgmax-TT is the maximum value of the angle between the current vector and the horizontal axis. in the TT segment. (B)Normal OPM-MCG scan The OPM-MCG scan showed no evidence of ischemia or obstructive coronary artery disease, as demonstrated by the lack of significant current deviations within the myocardium and absence of angle shift between the positive red pole and negative blue pole between T wave onset (T-onset) and T wave peak (T-peak) , FFR-positive and FFR-negative OPM-MCG scan and ICA Images. (C) The OPM-MCG scan of a patient in his 70s showed magnetic field angular deflection , abnormal magnetic field distribution of the positive and multipolarisation of negative poles , suggesting significant myocardial ischemia, and the ECG showed no significant abnormality. The ICA showed two lesions: 60% stenosis of the D1, 50% stenosis of the R-PDA ,. The FFRs were 0.77 for the R-PDA. (D) The OPM-MCG scan of a patient in their 60s showed no myocardial ischemia, ECG showed no significant abnormalities, echocardiography showed widening of the ascending aorta and aortic sinus. ICA showed 75% stenosis of the LAD, 60% stenosis of the RCA, FFR value of the LAD was 0.88.

MCG= magnetocardiography; FFR= fractional flow reserve ; ICA= invasive coronary angiography; D1= Diagonal branches ; R-PDA : Posterior descending artery ; LAD= Left Anterior descending artery; RCA= right coronary artery.

1074x1201mm (96 x 96 DPI)

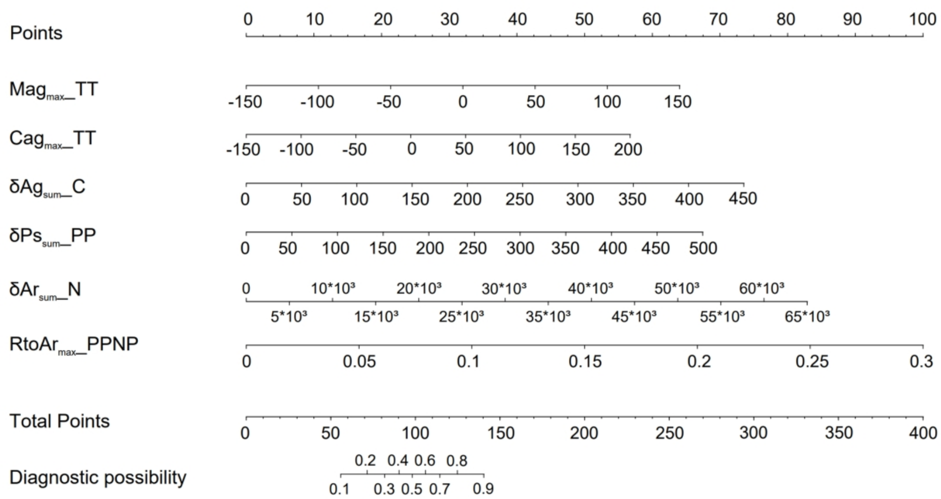

Figure 3. Nomogram of the diagnostic model.

Figure legend: The nomogram graphically demonstrates the diagnostic model of OPM-MCG. Points for MAgmax-TT, CAgmax-TT, δAgsum-C, δPssum-PP, δArsum-N and RtoArmax-PN can be obtained using a point caliper and then summed to obtain a total score that can be obtained using a point caliper and then summed to obtain a total score that can be measured with diagnosing myocardial ischemia in patients with borderline coronary lesions.

1322x711mm (96 x 96 DPI)

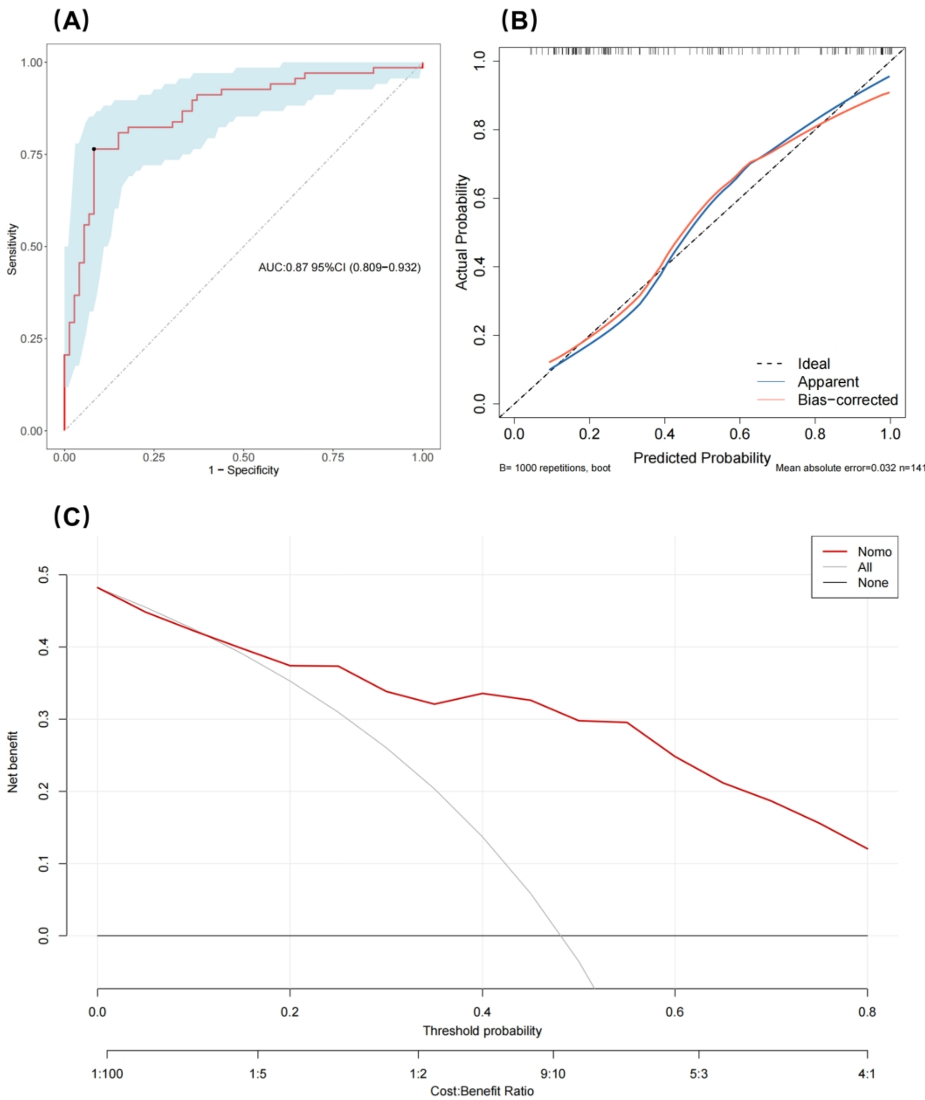

Figure 4 Accuracy and internal validation of the diagnostic model.
Figure legend: (A) ROC curves and 95% confidence intervals. After 500 bootstrap replications, the area under the curve and 95% confidence interval for receiver operating characteristic is 0.87 (0.809-0.932). (B) Calibration curve for the diagnostic model. Calibration curve for the borderline lesion ischemia diagnostic model was established by comparing the observed and predicted probability of a positive FFR in patients with borderline lesions of the coronary arteries. The smaller the distance of the scatter from the dashed line, the better the calibration. (C) Decision curve analysis (DCA) for diagnostic models of ischemia in borderline coronary lesions. None: net benefit when it is assumed that no patients with critical lesions of the coronary arteries would have the outcome (FFR-positive). All: net benefit when all patients with critical coronary lesions are assumed to have an outcome (FFR-positive). model: net benefit of managing critical coronary lesions with a diagnosis of myocardial ischemia based on the diagnostic model estimate. The strategy with the highest net benefit at any given threshold is the preferred strategy.

590x677mm (120 x 120 DPI)

Supplementary Material

Assessment of myocardial ischemia in borderline coronary artery lesions based on optical pumped magnetometer magnetocardiography

Shuwen Yang1#, Lanxin Feng 1#, Zhao Ma1, Huan Zhang1, Yazhe Zhang2, Linqi Liu1, Shu Zhou1, Xin Zhao1, Xueyao Yang1, Mingduo Zhang1, Min Zhang1, Jiqiang He1, Yanlong Ren1, Yawei Luo1, Feng Xu1, Xiantao Song1*, Chenchen Tu1*, Hongjia Zhang1*

#These authors contributed equally to this work.

1Department of Cardiology, Beijing Anzhen Hospital, Capital Medical University, 100029, Beijing, China

2Department of Cardiac Surgery, Beijing Anzhen Hospital, Capital Medical University, 100029, Beijing, China

The post-processing process of MCG signals is as follows. Firstly, a composite gradient magnetometer array is constructed using a separate environmental monitoring channel, and the common mode projection components of the monitoring channel are subtracted from the MCG detection array channels, effectively suppressing environmental magnetic field drift and power frequency interference. Then, notching the 50Hz power frequency and its harmonic components of the data, and performing a 1-40Hz bandpass filter to further remove power-frequency interference and limit the bandpass frequency to the main frequency range of the MCG. Finally, the denoised data is subjected to R-peak detection and recognition, with an average heartbeat cycle of 90 seconds as the length of the slice time, and the identified R-peak point is used as the time alignment point to slice the data and overlay it for average.

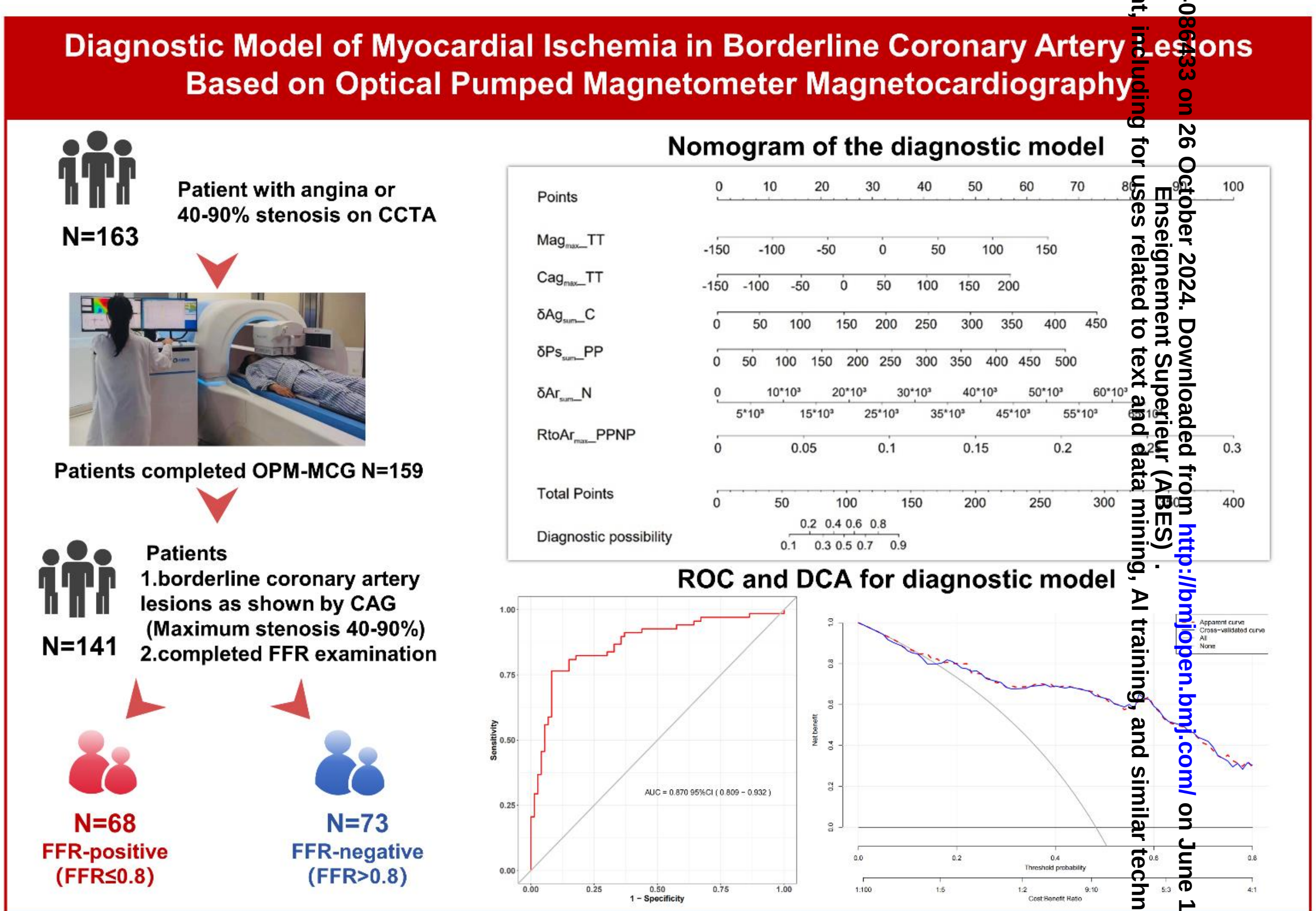

Supplementary Figure 1 Graphical Abstracts: Diagnostic Model of Myocardial Ischemia in Borderline Coronary Artery Lesions Based on Optical Pumped Magnetometer Magnetocardiography

CCTA= coronary computed tomography angiography; MCG=magnetocardiography; CAG= invasive coronary angiography; FFR=fractional flow reserve; PCI= percutaneous coronary intervention.

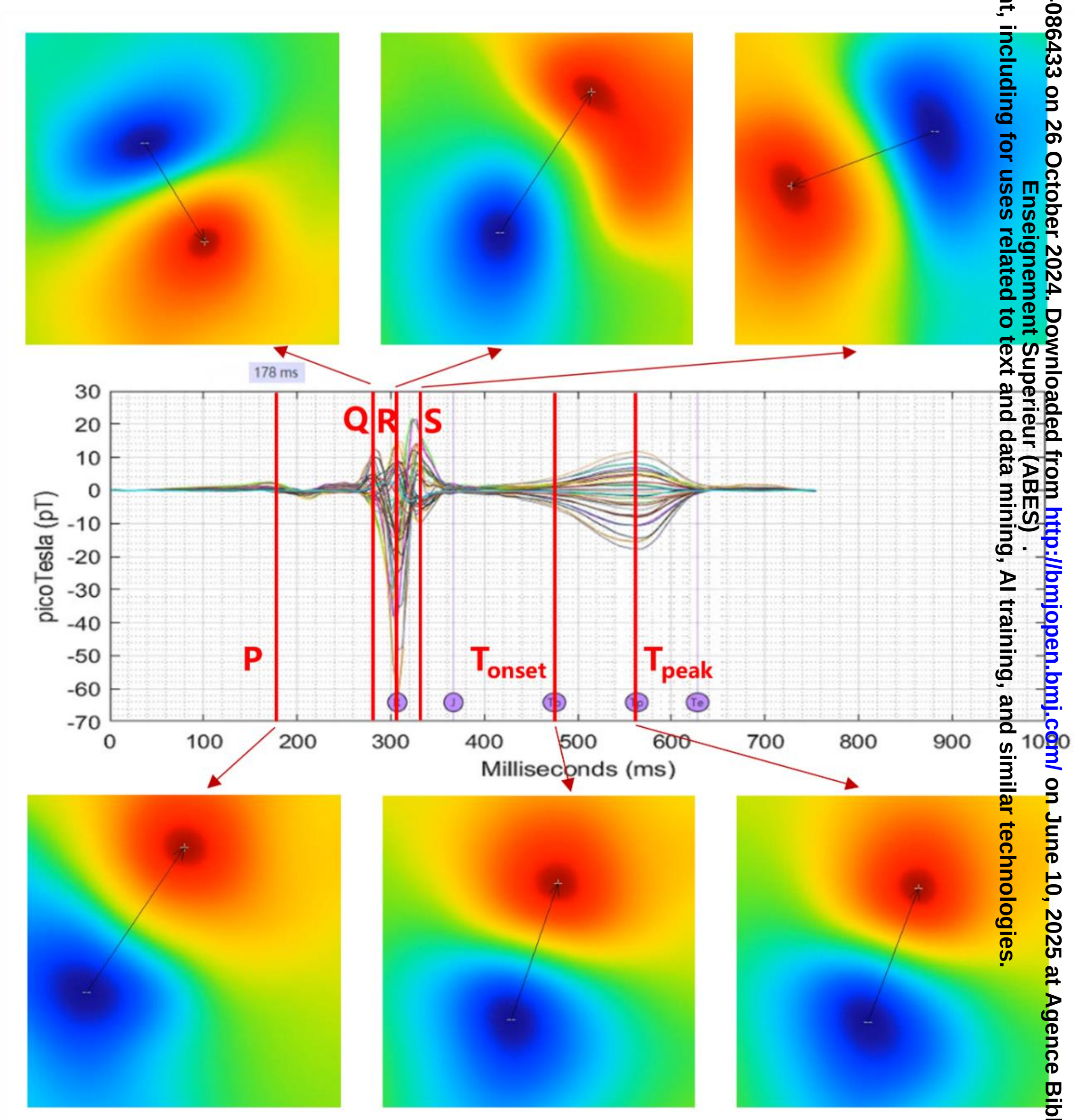

Supplementary Figure 2 The MFD of key points (P, QRS, and T onset and T peak) in the cardiac cycle of healthy individuals

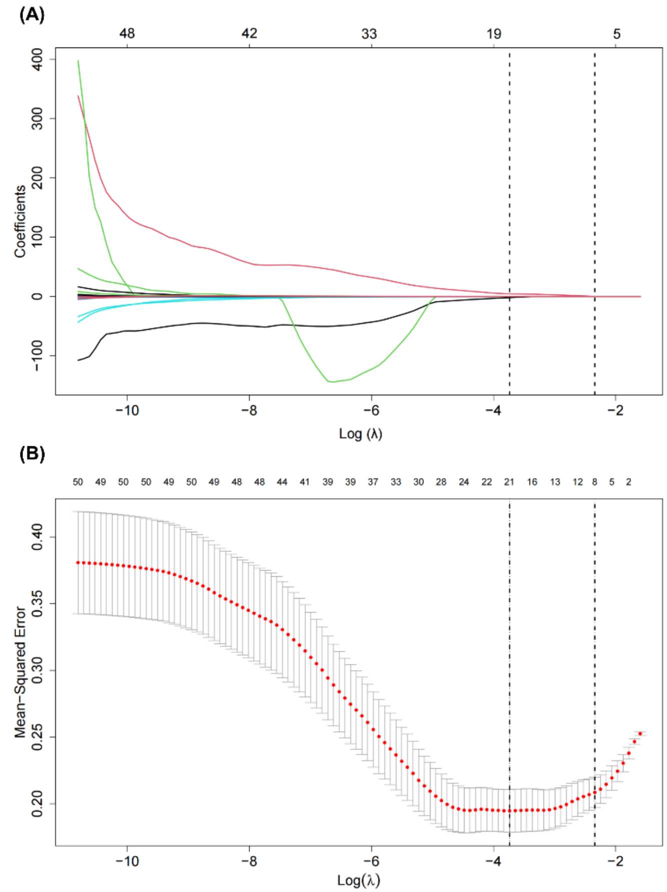

Supplementary Figure 3 Least absolute shrinkage and selection operator (LASSO) regression

Figure legend :(A) LASSO model coefficient profiles of the 50 candidate parameters. As log λ increases, the regression coefficients continue to converge, and there are fewer parameters with non-zero regression coefficients.

(B) Tuning parameter selection by cross-validation in the LASSO model. The solid vertical lines represent the partial likelihood deviance standard error (SE). The red dotted line indicates the cross-validation curve. The vertical dashed lines are drawn at the optimal values on the basis of the minimum criteria and 1-SE criteria. Considering the reasonableness of the variables included in this model, with the λ value of 0.02380779 was chosen.

Supplementary Table 1 OPM-MCG Parameters and Definitions

Parameters	Definition
δ Ag_{max}-M	The maximum value of changes in magnetic field angle at intervals of a certain time τ within TT segment
δ Ag_{min}-M	The minimum value of changes in magnetic field angle at intervals of a certain time τ within TT segment
δ Ag_{std}-M	The standard deviation of changes in magnetic field angle at intervals of a certain time τ within TT segment
δ Ag_{sum}-M	The sum of changes in magnetic field angle at intervals of a certain time τ within TT segment
δ Dt_{max}-PN	The maximum value of changes in magnetic pole distance at intervals of a certain time τ within TT segment
δ Dt_{min}-PN	The minimum value of changes in magnetic pole distance at intervals of a certain time τ within TT segment
δ Dt_{std}-PN	The standard deviation of changes in magnetic pole distance at intervals of a certain time τ within TT segment
δ Dt_{sum}-PN	The sum of changes in magnetic pole distance at intervals of a certain time τ within TT segment
δ Ag_{max}-C	The maximum value of changes in current angle at intervals of a certain time τ within TT segment
δ Ag_{min}-C	The minimum value of changes in current angle at intervals of a certain time τ within TT segment
δ Ag_{std}-C	The standard deviation of changes in current angle at intervals of a certain time τ within TT segment
δ Ag_{sum}-C	The sum of changes in current angle at intervals of a certain time τ within TT segment
δ Ps_{max}-C	The maximum value of changes in the position of the current angle at intervals of a certain time τ within TT segment
δ Ps_{std}-C	The standard deviation of changes in the position of the current angle at intervals of a certain time τ within TT segment
δ Ps_{sum}-C	The sum of changes in the position of the current angle at intervals of a certain time τ within TT segment
δ Ar_{max}-NP	The maximum value of changes in negative pole point area at intervals of a certain time τ within TT segment
δ Ar_{min}-NP	The minimum value of changes in negative pole point area at intervals of a certain time τ within TT segment
δ Ar_{std}-NP	The standard deviation of changes in negative pole point area at intervals of a certain time τ within TT segment
δ Ar_{sum}-NP	The sum of changes in negative pole point area at intervals of a certain time τ within TT segment
δ Ar_{bp}-NP	The change in negative pole point area between T-begin and T-peak
Ar_{max}-NP	The maximum value of the negative pole point area at intervals of a certain time τ within TT segment
Ar_{min}-NP	The minimum value of the negative pole point area at intervals of a certain time τ within TT segment
δ Ps_{max}-NP	The maximum value of changes in the position of the negative pole point at intervals of a certain time τ within TT segment
δ Ps_{std}-NP	The standard deviation of changes in the negative of the positive pole point at intervals of a certain time τ within TT segment
δ Ps_{sum}-NP	The sum of changes in the position of the negative pole point at intervals of a certain time τ within TT segment
δ Ar_{max}-N	The maximum value of changes in negative pole area at intervals of a certain time τ within TT segment
δ Ar_{min}-N	The minimum value of changes in negative pole area at intervals of a certain time τ within TT segment
δ Ar_{std}-N	The standard deviation of changes in negative pole area at intervals of a certain time τ within TT segment

Parameters	Definition
δAg_{max}-M	The maximum value of changes in magnetic field angle at intervals of a certain time τ within TT segment
δAr_{sum}-N	The sum of changes in negative pole area at intervals of a certain time τ within TT segment
δAr_{bp}-N	The change in nagative pole area between T-begin and T-peak
Ar_{max}-N	The maximum value of the negative pole area at intervals of a certain time τ within TT segment
Ar_{min}-N	The minimum value of the negative pole area at intervals of a certain time τ within TT segment
$\delta ArRto_{max}$-PN	The maximum value of changes in the ratio of positive and negative pole area at intervals of a certain time τ within TT segment
$\delta ArRto_{min}$-PN	The minimum value of changes in the ratio of positive and negative pole area at intervals of a certain time τ within TT segment
$\delta ArRto_{std}$-PN	The standard deviation of changes in the ratio of positive and negative pole area at intervals of a certain time τ within TT segment
$\delta ArRto_{sum}$-PN	The sum of changes in the ratio of positive and negative pole area at intervals of a certain time τ within TT segment
δAr_{max}-PP	The maximum value of changes in positive pole point area at intervals of a certain time τ within TT segment
δAr_{min}-PP	The minimum value of changes in positive pole point area at intervals of a certain time τ within TT segment
δAr_{std}-PP	The standard deviation of changes in positive pole point area at intervals of a certain time τ within TT segment
δAr_{sum}-PP	The sum of changes in positive pole point area at intervals of a certain time τ within TT segment
δAr_{bp}-PP	The change in positive pole point area between T-begin and T-peak
Ar_{max}-PP	The maximum value of the positive pole point area at intervals of a certain time τ within TT segment
Ar_{min}-PP	The minimum value of the positive pole point area at intervals of a certain time τ within TT segment
δPs_{max}-PP	The maximum value of changes in the position of the positive pole point at intervals of a certain time τ within TT segment
δPs_{std}-PP	The standard deviation of changes in the position of the positive pole point at intervals of a certain time τ within TT segment
δPs_{sum}-PP	The sum of changes in the position of the positive pole point at intervals of a certain time τ within TT segment
δAr_{max}-P	The maximum value of changes in positive pole area at intervals of a certain time τ within TT segment
δAr_{min}-P	The minimum value of changes in positive pole area at intervals of a certain time τ within TT segment
δAr_{std}-P	The standard deviation of changes in positive pole area at intervals of a certain time τ within TT segment
δAr_{sum}-P	The sum of changes in positive pole area at intervals of a certain time τ within TT segment
δAr_{bp}-P	The change in positive pole area between T-begin and T-peak
Ar_{ma}x-P	The maximum value of the positive pole area at intervals of a certain time τ within TT segment
Ar_{min}-P	The minimum value of the positive pole area at intervals of a certain time τ within TT segment

Parameters	Definition
δ Ag_{max}-M	The maximum value of changes in magnetic field angle at intervals of a certain time τ within TT segment
MAg_{max}-TT	The maximum magnetic field angle at intervals of a certain time τ within TT segment
CAg_{max}-TT	The maximum current angle at intervals of a certain time τ within TT segment
MAg_{min}-TT	The minimum magnetic field angle at intervals of a certain time τ within TT segment
CAg_{min}-TT	The minimum current angle at intervals of a certain time τ within TT segment
MAg-Rp	The magnetic field angle of the R-peak
RtoAm-R_pT_pN	The ratio of magnetic field amplitude at R-peak and the negative amplitude at T-peak
RtoAm-R_pT_pP	The ratio o magnetic field amplitude at R-peak and the positive amplitude at T-peak
RtoAm-R_pT_p	The ratio of magnetic field amplitudes at R-peak and T-peak
MAg-RpTp	The magnetic field angle between R-peak and T-peak
MAg-Tp	The magnetic field angle of the T-peak
CAg_{max}-Tp	The maximum current angle at T-peak
RtoAm-Tp	The ratio of positive to negative magnetic field amplitude at T-peak
TT	The interval from the beginning of the T-wave to its peak within the cardiac cycle

Dt = Distance, Ps = Position, Ag = Angle, Am = Magnitude, Ar = Area, Rto = Ratio, P = Positive, Positive Pole = PP, N = Negative, NP = Negative Pole, M = Magnetic Field, C = Current, max = Maximum, min = Minimum, sum=Sum of all, std = Standard deviation, δ = Change value, TT= TT segment (the position from one-third of the T max amplitude (T onset) to T max (T peak)), R_p=R peak, T_p=T peak

Supplementary Table 2 Clinical characteristics (n = 141)

Characteristics	Total(n=141)
Age (yrs)	60.64±9.70
Male, n (%)	109(77.3)
BMI (Kg/m2)	26.15±3.36
Diabetes, n (%)	47(33.3)
Hypercholesterolemia, n (%)	65(46.1)
Hypertension, n (%)	82(58.2)
Stroke, n (%)	9(6.4)
Smoke, n (%)	43(30.5)
Systolic blood pressure, mmHg	128.69±15.54
Diastolic blood pressure, mmHg	75.15±10.79
Heart rate	73.81±10.38
Medication, n(%)	
Aspirin	129(91.5)
Statin	137(97.2)
ACEI/ARB	45(35.6)
SGLT2 inhibitors	22(16.7)
Nicorandil	23(16.3)
Admission lab results	
Low-density lipoprotein cholesterol (mmol/L)	1.82±0.69
hs Tnl(pg/ml)	3.5(2.5,5.8)
Brain natriuretic peptide (pg/ml)	29.00(14.75,48.25)
Blood glucose (mmol/L)	5.52(4.82,7.33)
HbA1c(%)	6.25(5.7,7.1)
ICA and FFR characteristics	
1-vessel disease	50(35.5)
2-vessel disease	43(30.5)

3-vessel disease	48(34.0)
Number of patients with FFR≤0.8	68(48.2)
Number of vessels with FFR	157
Number of vessels with FFR≤0.8	74(47.1)
Left anterior descending artery with FFR	97(68.8)
Left circumflex artery with FFR	25(17.7)
Right coronary artery with FFR	35(24.8)
Interval between MCG and FFR	2(1,7)

Values are n (%) or mean ± SD

BMI= Body Mass Index, ACEI= angiotensin converting enzyme inhibitor, ARB = angiotensin receptor blocker, SGLT-2 inhibitors = sodium-glucose cotransporter-2 inhibitors, HbA1c= glycated hemoglobin, ICA = invasive coronary angiography, FFR = fractional flow reserve.

Supplementary Table 3 OPM-MCG parameters of the Participant and univariable logistic regression model

Parameters	ALL N=141	FFR-Positive N=68	FFR-Negative N=73	Hazard Ratio (95%CI)	P value
δ Ag_{max}-M	0.62 (0.44,1.19)	0.77 (0.47,5.76)	0.54 (0.43,0.72)	1.08 (1.01,1.15)	0.002
δ Ag_{min}-M	-0.34 (-0.57,-0.18)	-0.42 (-0.82,-0.28)	-0.26 (-0.42,-0.14)	0.96 (0.93,1.00)	0.001
δ Ag_{std}-M	0.16 (0.11,0.68)	0.28 (0.14,2.06)	0.14 (0.10,0.20)	1.59 (1.16,2.19)	<0.001
δ Ag_{sum}-M	10.6 (6.18,26.2)	20.2 (9.88,45.5)	8.28 (4.55,11.8)	1.06 (1.03,1.10)	<0.001
δ Dt_{max}-PN	2.69 (1.97,4.12)	3.51 (2.16,12.9)	2.22 (1.89,3.16)	1.01 (1.00,1.03)	<0.001
δ Dt_{min}-PN	-2.20 (-3.27,-1.76)	-2.38 (-4.70,-1.91)	-2.00 (-2.80,-1.63)	0.97 (0.95,1.00)	0.003
δ Dt_{std}-PN	0.74 (0.55,1.18)	0.82 (0.63,3.45)	0.63 (0.52,0.89)	1.16 (1.02,1.31)	0.001
δ Dt_{sum}-PN	46.6 (29.1,80.7)	66.6 (42.0,110)	33.3 (25.7,48.6)	1.03 (1.01,1.04)	<0.001
δ Ag_{max}-C	1.70 (1.21,4.83)	1.79 (1.27,9.10)	1.52 (1.16,2.98)	1.01 (1.00,1.02)	0.016
δ Ag_{min}-C	-1.24 (-3.81,0.00)	-1.70 (-8.89,-1.01)	-0.91 (-1.75,0.00)	0.98 (0.97,1.00)	<0.001
δ Ag_{std}-C	0.54 (0.36,1.32)	0.80 (0.37,3.16)	0.45 (0.34,0.70)	1.12 (1.01,1.23)	0.003
δ Ag_{sum}-C	15.6 (9.64,38.6)	29.8 (13.5,71.6)	11.9 (7.79,17.5)	1.01 (1.00,1.02)	<0.001
δ Ps_{max}-C	33.0 (1.00,48.8)	33.0 (1.41,125)	31.0 (1.00,34.0)	1.01 (1.00,1.01)	0.008
δ Ps_{std}-C	3.35 (0.24,6.16)	3.57 (0.29,11.7)	3.20 (0.24,4.86)	1.07 (1.01,1.13)	0.016
δ Ps_{sum}-C	39.1 (6.00,86.1)	74.4 (8.31,161)	33.4 (4.00,66.0)	1.01 (1.00,1.01)	<0.001
δ Ar_{max}-NP	136 (74.0,220)	182 (102,314)	105 (59.0,180)	1.00 (1.00,1.00)	<0.001
δ Ar_{min}-NP	-84.00 (-173.00,-54.00)	-99.00 (-187.50,-62.75)	-68.00 (-148.00,-46.00)	1.00 (1.00,1.00)	0.009
δ Ar_{std}-NP	29.6 (20.0,56.7)	31.7 (23.4,70.1)	25.7 (17.1,41.4)	1.00 (1.00,1.01)	0.004
δ Ar_{sum}-NP	2469 (1443,4286)	3369 (2230,5728)	1672 (1277,2987)	1.00 (1.00,1.00)	<0.001
δ Ar_{bp}-NP	944 (18.0,2830)	1168 (152,3066)	626 (-46.00,2383)	1.00 (1.00,1.00)	0.238
Ar_{max}-NP	3873 (3001,5765)	4269 (3260,6056)	3828 (2894,5406)	1.00 (1.00,1.00)	0.160
Ar_{min}-NP	2426 (1639,3326)	2094 (1436,3245)	2614 (2065,3360)	1.00 (1.00,1.00)	0.036
δ Ps_{max}-NP	2.83 (2.24,4.12)	3.00 (2.24,5.28)	2.24 (2.00,3.00)	1.01 (1.00,1.01)	0.005
δ Ps_{std}-NP	0.70 (0.57,1.00)	0.81 (0.65,1.20)	0.66 (0.51,0.85)	1.04 (0.98,1.11)	0.005
δ Ps_{sum}-NP	41.7 (22.2,79.9)	59.8 (39.8,104)	26.4 (20.1,51.1)	1.01 (1.01,1.02)	<0.001
δ Ar_{max}-N	435 (243,750)	539 (269,990)	404 (221,526)	1.00 (1.00,1.00)	0.017

Parameters	ALL N=141	FFR-Positive N=68	FFR-Negative N=73	Hazard Ratio (95%CI)	P value
δ Ar_{min}-N	-170.00 (-369.00,-25.00)	-267.00 (-565.25,-108.75)	-79.00 (-224.00,-15.00)	1.00 (1.00,1.00)	<0.001
δ Ar_{std}-N	125 (80.2,225)	160 (90.5,273)	114 (74.6,158)	1.00 (1.00,1.01)	0.004
δ Ar_{sum}-N	12585 (7372,23204)	19058 (10208,29054)	9520 (6202,15009)	1.00 (1.00,1.00)	<0.001
δ Ar_{bp}-N	10445 (1116,25689)	11528 (588,28595)	8107 (2900,16796)	1.00 (1.00,1.00)	0.840
Ar_{max}-N	53635 (43655,65410)	56546 (44597,77766)	51431 (38201,58878)	1.00 (1.00,1.00)	0.032
Ar_{min}-N	40985 (26175,53701)	39744 (24308,59155)	40985 (29379,49923)	1.00 (1.00,1.00)	0.644
δ $ArRto_{max}$-PN	0.01 (0.00,0.02)	0.01 (0.00,0.03)	0.00 (0.00,0.01)	[illegible]93839e^{10} (5.89[illegible]e^{2},3.426868e^{18})	<0.001
δ $ArRto_{min}$-PN	-0.02 (-0.05,-0.01)	-0.02 (-0.07,-0.01)	-0.02 (-0.04,-0.01)	[illegible] (0.00,0.13)	0.134
δ $ArRto_{std}$-PN	0.01 (0.00,0.02)	0.01 (0.00,0.02)	0.01 (0.00,0.01)	[illegible]77054e^{16} (1.75[illegible]e^{3},5.740310e^{29})	0.114
δ $ArRto_{sum}$-PN	0.63 (0.32,1.72)	0.85 (0.39,2.36)	0.58 (0.29,0.88)	1.54 (1.15,2.06)	0.014
δ Ar_{max}-PP	195 (126,404)	281 (141,704)	153 (111,286)	1.00 (1.00,1.00)	0.001
δ Ar_{min}-PP	-171.00 (-295.00,-106.00)	-196.00 (-563.75,-109.50)	-153.00 (-226.00,-104.00)	1.00 (1.00,1.00)	0.006
δ Ar_{std}-PP	54.3 (33.7,124)	77.3 (35.5,167)	43.7 (32.1,79.7)	1.01 (1.00,1.01)	0.007
δ Ar_{sum}-PP	4689 (2685,8783)	6608 (3410,14024)	3487 (2556,5786)	1.00 (1.00,1.00)	<0.001
δ Ar_{bp}-PP	1058 (-869.00,5166)	1360 (-872.25,5756)	737 (-869.00,4601)	1.00 (1.00,1.00)	0.872
Ar_{max}-PP	8775 (6335,13548)	9178 (6485,14820)	8775 (6335,12776)	1.00 (1.00,1.00)	0.386
Ar_{min}-PP	5151 (2774,7571)	4626 (2618,6928)	5754 (3719,8258)	1.00 (1.00,1.00)	0.054
δ Ps_{max}-PP	3.16 (2.24,5.00)	3.61 (3.00,100)	3.00 (2.24,3.61)	1.01 (1.00,1.02)	<0.001
δ Ps_{std}-PP	0.82 (0.60,1.15)	0.98 (0.66,8.50)	0.75 (0.57,0.90)	1.12 (1.04,1.20)	<0.001
δ Ps_{sum}-PP	40.4 (23.1,88.6)	73.8 (29.9,195)	32.8 (21.7,54.2)	1.01 (1.01,1.02)	<0.001
δ Ar_{max}-P	244 (90.0,430)	312 (150,692)	172 (70.0,362)	1.00 (1.00,1.00)	0.001
δ Ar_{min}-P	-348.00 (-592.00,-203.00)	-381.00 (-812.00,-188.75)	-311.00 (-497.00,-211.00)	1.00 (1.00,1.00)	0.150
δ Ar_{std}-P	120 (80.2,203)	135 (82.3,267)	109 (75.7,159)	1.00 (1.00,1.00)	0.105
δ Ar_{sum}-P	11899 (6525,19157)	15787 (7938,28576)	9566 (5985,15629)	1.00 (1.00,1.00)	0.002

Parameters	ALL N=141	FFR-Positive N=68	FFR-Negative N=73	Hazard Ratio (95%CI)	P value
δ Ar_{bp}-P	-3600.00 (-12686.00,2509)	-1456.00 (-14861.75,3900)	-4007.00 (-10962.00,1528)	1.00 (1.00,1.00)	0.533
Ar_{max}-P	97097 (33699)	95392 (37311)	98685 (30122)	1.00 (1.00,1.00)	0.567
Ar_{min}-P	89822 (63201,104875)	83948 (55748,104204)	92433 (68813,105383)	1.00 (1.00,1.00)	0.134
MAg_{max}-TT	-62.32 (-70.64,-34.61)	-48.00 (-66.89,15.5)	-67.39 (-72.03,-53.13)	1.02 (1.01,1.03)	<0.001
CAg_{max}-TT	45.0 (33.3,71.0)	58.2 (39.2,118)	43.1 (32.0,51.1)	1.02 (1.01,1.03)	<0.001
MAg_{min}-TT	-70.76 (-76.85,-56.92)	-68.28 (-75.62,-41.24)	-71.98 (-77.61,-64.94)	1.01 (1.00,1.02)	0.050
CAg_{min}-TT	32.8 (5.36,45.9)	34.7 (-10.80,63.8)	32.0 (12.3,44.0)	1.00 (1.00,1.01)	0.471
MAg-R_p	-61.41 (-71.15,-42.88)	-53.44 (-70.66,-38.24)	-65.92 (-71.78,-50.54)	1.01 (1.00,1.03)	0.021
RtoAm-R_pT_pN	6.49 (4.32,9.57)	7.35 (4.92,10.4)	5.68 (3.71,8.14)	1.05 (1.00,1.12)	0.025
RtoAm-R_pT_pP	7.97 (5.88,12.0)	8.66 (6.03,12.9)	7.69 (5.56,11.1)	1.06 (1.00,1.13)	0.182
RtoAm-R_pT_p	3.64 (2.38,4.70)	4.13 (3.08,5.01)	3.28 (2.36,4.50)	1.22 (1.04,1.43)	0.027
MAg-R_pT_p	-0.67 (-24.77,19.5)	3.61 (-25.62,33.8)	-2.72 (-22.99,13.2)	1.00 (1.00,1.01)	0.235
MAg-T_p	-64.66 (-71.34,-45.44)	-55.82 (-70.28,-12.79)	-67.91 (-72.69,-53.13)	1.02 (1.01,1.03)	0.002
CAg_{max}-T_p	43.1 (29.4,52.0)	45.0 (27.6,74.7)	42.2 (30.7,46.9)	1.01 (1.00,1.02)	0.039
RtoAm-T_p	0.76 (0.57,1.08)	0.81 (0.52,1.22)	0.75 (0.57,0.98)	1.52 (0.93,2.48)	0.368

Dt = Distance, Ps = Position, Ag = Angle, Am = Magnitude, Ar = Area, Rto = Ratio, P = Positive, Positive Pole = PP, N = Negative, NP = Negative Pole, M = Magnetic Field, C = Current, max = Maximum, min = Minimum, sum=Sum of all, std = Standard deviation, δ = Change value, TT= TT segment (the position from one-third of the T max amplitude (T onset) to T max (T peak)), R_p=R peak, T_p=T peak

Supplementary Table 4 Diagnostic model for assessment of myocardial ischemia in borderline coronary artery lesions

Parameters	Diagnostic model			
	B	OR	95%CI	P value
MAg_{max}-TT	0.011	1.011	(1.000-1.021)	0.029
CAg_{max}-TT	0.008	1.008	(0.998-1.018)	[illegible]
δAg_{sum}-C	0.008	1.009	(1.000-1.019)	[illegible]
δPs_{sum}-PP	0.007	1.007	(1.001-1.013)	0.022
δAr_{sum}-N	0.001	1.001	(1.000-1.001)	0.002
$RtoAr_{max}$-PN	17.324	33409.498	(0.694-50738)	0.123

M = Magnetic Field, Ag = Angle, max = Maximum, TT= TT segment (the position from one-third of the T max amplitude (T onset) to T max (T peak)) , sum=Sum of all, C = Current, δ = Change value, PP= Positive Pole, Ps = Position, Ar = Area, N = Negative, Rto = Ratio, P = Positive.

BMJ Open

Development and validation of a clinical diagnostic model for myocardial ischemia in borderline coronary lesions based on optical pumped magnetometer magnetocardiography: a prospective observational cohort study

Journal:	*BMJ Open*
Manuscript ID	bmjopen-2024-086433.R2
Article Type:	Original research
Date Submitted by the Author:	28-Aug-2024
Complete List of Authors:	yang, shuwen; Capital Medical University Affiliated Anzhen Hospital, Department of Cardiology Feng, Lanxin; Capital Medical University Affiliated Anzhen Hospital, Department of Cardiology Zhang, Mingduo; Capital Medical University Affiliated Anzhen Hospital Zhang , Min; Capital Medical University Affiliated Anzhen Hospital Ma, Zhao; Capital Medical University Affiliated Anzhen Hospital, Department of Cardiology Zhang, Huan; Capital Medical University Affiliated Anzhen Hospital, Department of Cardiology Zhang, YaZhe; Capital Medical University Affiliated Anzhen Hospital, Department of Cardiac Surgery Liu, Linqi; Capital Medical University Affiliated Anzhen Hospital, Department of Cardiology Zhou, Shu; Capital Medical University Affiliated Anzhen Hospital, Department of Cardiology Zhao, Xin; Capital Medical University Affiliated Anzhen Hospital, Department of Cardiology Yang, Xue Yao; Capital Medical University Affiliated Anzhen Hospital He, Jiqiang; Capital Medical University Affiliated Anzhen Hospital, Cardiology Ren, Yanlong; Capital Medical University Affiliated Anzhen Hospital Luo, Yawei; Capital Medical University Affiliated Anzhen Hospital Xu, Feng; Capital Medical University Affiliated Anzhen Hospital Tu, Chenchen; Capital Medical University Affiliated Anzhen Hospital, Department of Cardiology song, xiantao; Capital Medical University Affiliated Anzhen Hospital, Department of Cardiology Zhang, Hong-Jia; Capital Medical University Affiliated Anzhen Hospital,
Primary Subject Heading:	Diagnostics
Secondary Subject Heading:	Diagnostics
Keywords:	Diagnostic Imaging, Ischaemic heart disease < CARDIOLOGY, Clinical Trial

SCHOLARONE™
Manuscripts

I, the Submitting Author has the right to grant and does grant on behalf of all authors of the Work (as defined in the below author licence), an exclusive licence and/or a non-exclusive licence for contributions from authors who are: i) UK Crown employees; ii) where BMJ has agreed a CC-BY licence shall apply, and/or iii) in accordance with the terms applicable for US Federal Government officers or employees acting as part of their official duties; on a worldwide, perpetual, irrevocable, royalty-free basis to BMJ Publishing Group Ltd ("BMJ") its licensees and where the relevant Journal is co-owned by BMJ to the co-owners of the Journal, to publish the Work in this journal and any other BMJ products and to exploit all rights, as set out in our licence.

The Submitting Author accepts and understands that any supply made under these terms is made by BMJ to the Submitting Author unless you are acting as an employee on behalf of your employer or a postgraduate student of an affiliated institution which is paying any applicable article publishing charge ("APC") for Open Access articles. Where the Submitting Author wishes to make the Work available on an Open Access basis (and intends to pay the relevant APC), the terms of reuse of such Open Access shall be governed by a Creative Commons licence – details of these licences and which Creative Commons licence will apply to this Work are set out in our licence referred to above.

Other than as permitted in any relevant BMJ Author's Self Archiving Policies, I confirm this Work has not been accepted for publication elsewhere, is not being considered for publication elsewhere and does not duplicate material already published. I confirm all authors consent to publication of this Work and authorise the granting of this licence.

Development and validation of a clinical diagnostic model for myocardial ischemia in borderline coronary lesions based on optical pumped magnetometer magnetocardiography: a prospective observational cohort study

Shuwen Yang1#, Lanxin Feng 1#, Mingduo Zhang1, Min Zhang1, Zhao Ma1, Huan Zhang1, Yazhe Zhang2, Linqi Liu1, Shu Zhou1, Xin Zhao1, Xueyao Yang1, Jiqiang He1, Yanlong Ren1, Yawei Luo1, Feng Xu1, Chenchen Tu1*, Xiantao Song1*, Hongjia Zhang2

#These authors contributed equally to this work.

* These corresponding authors contributed equally to this work.

1Department of Cardiology, Beijing Anzhen Hospital, Capital Medical University, 100029, Beijing, China

2Department of Cardiac Surgery, Beijing Anzhen Hospital, Capital Medical University, 100029, Beijing, China

Corresponding Author:

The first corresponding author：Dr ChenChen Tu

Department of Cardiology, Anzhen Hospital, Capital Medical University, 2 Anzhen Road, Chaoyang District, 100020, Beijing, China E-mail: tcc2033@163.com

Dr Xiantao Song

Department of Cardiology, Anzhen Hospital, Capital Medical University, 2 Anzhen Road, Chaoyang District, 100020, Beijing, China E-mail: song0929@mail.ccmu.edu.cn

Disclosures: The authors have nothing to disclose.

Abstract

Objectives: To develop and validate a clinical diagnostic model based on optical pumped magnetometer magnetocardiography (OPM-MCG) for the detection of myocardial ischemia in patients with borderline coronary lesions prior to invasive coronary angiography (CAG).

Design: Prospective observational cohort study.

Setting: Single center of the China National Clinical Research Center for Cardiovascular Disease (NCCMRC).

Participants: Adults with borderline coronary lesions on CAG (N=141).

Interventions: Underwent OPM-MCG before CAG and fractional flow reserve measurement.

Results: Five parameters were included in the final diagnostic model: MAg_{max}-TT, δDt_{sum}-PN, δAg_{sum}-C, δAr_{sum}-N and δAr_{min}-N. 1000 bootstrap replications showed that the area under the receiver operating characteristic curve (AUC) and 95% confidence interval (CI) of the diagnostic model were 0.864 (0.803-0.925), with sensitivity of 79.4%, specificity of 80.8%, positive predictive value of 79.4%, negative predictive value of 80.8%. 1000 bootstrap replications showed that the model was well-calibrated. Decision curve analysis showed a net benefit from the predictive model when the threshold probability of an ischemic patient was greater than 12%, suggesting the potential utility of the model in the real world.

Conclusions: A nomogram based on five OPM-MCG parameters was developed to assess myocardial ischemia in patients with borderline coronary lesions and has the potential to reduce the need for unnecessary CAG.

Trial registration number: ChiCTR2300072382.

Keywords: borderline coronary lesions; optical pumped magnetometer magnetocardiography; fractional flow reserve; myocardial ischemia

Strengths and limitations of this study

1) As a prospective observational cohort study, this study provides real-world evidence of the diagnostic performance of OPM-MCG for myocardial ischemia, enhancing the generalization of the findings.

2) The study was a single-center study, which may affect its adaptability to different settings.

3) The clinical diagnostic model did not account for myocardial ischemia due to coronary microcirculatory dysfunction and did not include evaluations performed with other MCG devices.

Introduction

Borderline coronary lesions exhibit ranging from 40% to 90% as seen in invasive coronary angiography (CAG). The FAME study [1] found that over 80% of lesions fell into this category, with only 35% of stenoses between 50-70% being hemodynamically significant. Predicting relevance was most accurate when estimating coronary artery diameter over 90%. Therefore, fractional flow reserve (FFR) guided intervention in patients with borderline coronary lesions (40-90% stenosis) has become a recommended treatment strategy in the 2018 ESC Interventional Guidelines [2]. The 2021 ACC/AHA/SCAI Guidelines for Coronary Artery Revascularization [3] also provide clear recommendations for managing borderline coronary lesions: FFR and instantaneous wave-free ratio (iFR) are used to assess the need for percutaneous coronary intervention (PCI) in patients without evidence of ischemia but with angina and other equivalent symptoms (Class I); PCI is not recommended for stable patients with FFR >0.8 or iFR >0.89 (Class III). However, its widespread adoption in coronary catheter laboratories is hindered by its time-consuming nature, resource consumption, and potential adverse effects associated with adenosine application.

Optical pumped magnetometer magnetocardiography (OPM-MCG) measures tiny magnetic fields (10^{-15} Tesla) from the heart using atomic magnetometer technology, without radiation. It is quick, contactless, and suitable for diverse populations. Clinical studies have demonstrated that magnetocardiography (MCG) is superior to electrocardiogram (ECG) in detecting early myocardial ischemia [4,5,6,7] and has similar diagnostic effectiveness as SPECT for coronary artery disease (CAD) [8,9]. MCG was proven to be precise in diagnosing non-ST-segment elevation myocardial infarction, even in individuals who do not exhibit typical angina symptoms. [10,11]. However, the parameters and cut-off values of OPM-MCG that indicate myocardial ischemia in borderline coronary lesion are presently undefined.

Hence, this study aims to investigate the accuracy of OPM-MCG in diagnosing myocardial ischemia in patients with borderline coronary lesions, with invasive FFR examination serving as the reference standard.

Method

Study population

This study was a prospective, single-center, observational, cohort study which was reviewed by the Ethics Committee of Beijing Anzhen Hospital, Capital Medical University, and registered with the China Clinical Trial Registry (ChiCTR2300072382). All participants signed an informed consent. The methods described in this article follow the STARD 2015 guidelines.

Participants aged 18-80 with typical angina symptoms (CCS class II or higher) or 40-90% stenosis on CCTA were scheduled for hospitalization for CAG. Exclusion criteria included: 1) Coronary artery stenosis outside of 40%-90% range on CAG; 2) Acute myocardial infarction; 3) Previous myocardial infarction; 4) Complex arrhythmias; 5) Bundle-branch block; 6) Pacemakers, metallic implants in trunk; 7) Claustrophobia.

This study was based on a prospective cohort design, the sample size of which was calculated by PASS 2021 software using the area under the receiver-operating characteristic (ROC) curve. The significance level (α) was 0.025 and the degree of certainty ($1-\beta$) was 0.90, combining the results of the literature review of related studies as well as the statistics of the small sample in the previous period, and calculating according to the FFR-positive (ischemic)/FFR-negative (non-ischemic) =2:3. The sample size was calculated as 138.

A total of 163 patients from June 30th to November 30th, 2023 were consecutively enrolled, and 22 patients were excluded, of which 11 patients with stenosis >90%, 7 patients underwent direct PCI without FFR testing, and 4 patients with poor quality MCG imaging, and Finally 141 patients with borderline coronary lesions underwent MCG and FFR sequentially (Figure 1). In this study, the cardiologists were not aware of the MCG results at the time of the FFR examination, and the MCG parameters were determined before the FFR examination (Supplementary Figure 1-Graphical Abstract).

CAG and FFR procedures

CAG and FFR measurements were performed on the vessels according to the 2021 ACC/AHA/SCAI Guidelines for Coronary Artery Revascularization and Expert consensus on the clinical pathway for FFR measurement in China. After administration of nitroglycerin, a pressure monitoring guidewire was advanced through the stenosis. Hyperemia was attained by administration of intravenous adenosine (140μg/kg/min). The FFR pressure wire was positioned a minimum of 20 mm distal to the stenosis in vessel segments ≥2 mm. The presence of an FFR ≤0.80 was considered a positive indicator of functional ischemia in patients and was defined as the FFR-positive group.

MCG imaging

The MCG recordings were conducted using a 36-channel OPM-MCG system (Miracle MCG), featuring OPM sensors sourced from Beijing X-Mag Technologies Limited's mature commercial product. The OPM sensor is based on spin-exchange relaxation free (SERF) technology, with alkali metal atoms as the core sensitive element. The OPM sensor has a sensitivity below 30 $fT/Hz^{1/2}$, a recording bandwidth of 1 Hz to 40 Hz, a sampling frequency of 200 Hz, and a noise baseline with not higher than 15 fT. The OPM-MCG residual magnetic field is kept below 1.5 nT, and the data acquisition mode is analog signal acquisition (Supplementary Figure 2). Each subject had a 90-second continuous recording at 36 locations (6×6 grid) above the chest using an arrayed sensor grid.

MCG Signal Analysis and Statistical Analysis

After MCG data acquisition, the software automatically post-processes the signals to generate magnetic field and current density maps and output sixty-five parameters (Supplementary Table 1). The sixty-five parameters we output characterize the stability of the current dipole in the TT segment (the position from one-third of the T max amplitude (T onset) to T max (T peak)) according to the previous studies of Park et al. and Pena et al. (see supplementary material for post-processing steps).

Statistical analysis was performed with SPSS 25.0 and R 4.3.2 (http //www.R-project.org/). Counting data were presented as numbers and percentages, while normally distributed measurement data were shown as mean ± standard deviation. Continuous variables that were not normally distributed were presented using median and quartile values. Statistical significance was determined for all analyses with a P-value less than 0.05. Based on this cohort and the principle of at least 10 events per variable (10 EPV), we considered the rationality of the parameters included in the diagnostic model and evaluated the number of parameters. sixty-five potential predictor variables were evaluated using univariable logistic regression, selecting those with p-values < 0.1. These variables were then subjected to Least Absolute Shrinkage and Selection Operator (LASSO) regression, ultimately identifying the most impactful predictors. Continuous variables representing the amount of change were transformed into ordered categorical variables based on interquartile range. Continuous variables representing absolute values were converted into dichotomous variables by grouping their upper and lower quartile values into extreme categories, while middle-range values were grouped and incorporated into the model. The final model was developed using multivariate logistic regression with a backward selection approach. The model's predictive performance was assessed using the enhanced bootstrap method and clinical benefit was evaluated using decision curve analysis. The MCG-FFR nomogram was used to report scores for assessing myocardial ischemia with OPM-MCG parameters.

Patient and Public Involvement

Patients make more people aware of the clinical use of the OPM-MCG and how it is examined by sharing news and information about clinical studies with others.

Result

Clinical characteristics

The study included 141 patients, mostly male (77.3%) with an average age of 60.64 ± 9.70 years. After MCG scans, all patients underwent CAG and FFR examination, with 48.2% having positive FFR ($FFR \leq 0.8$). A total of 157 vessels were examined, with 47.1% having $FFR \leq 0.8$. Interval between MCG and FFR less than 30 days, median 2 days. Most patients had FFR measurements primarily done on the LAD. See Table 1 for patient clinical characteristics.

Selection of parameters and development of the diagnostic model

Fifty variables that were statistically significant ($P < 0.1$) in univariable logistic regression were included in the LASSO regression (Supplementary Table 2 and Supplementary Figure 3), and 8 variables were selected based on the reasonableness of the parameters selected to reduce the model overfitting and covariance through LASSO regression. By using the backward approach, 5 parameters were included in the final diagnostic model: MAg_{max}-TT, δDt_{sum}-PN,

δAg_{sum}-C, δAr_{sum}-N and δAr_{min}-N (Table 2, Figure 2). The model area under the receiver operating characteristic curve (AUC) obtained from multivariate logistic regression analysis was 0.864, with sensitivity of 79.4%, specificity of 80.8%, positive predictive value of 79.4%, negative predictive value of 80.8%. The nomogram (Figure 3) provides a graphical overview of the diagnostic model using multivariate logistic regression analysis (Supplementary Table 3).

Internal validation and net benefit of the model

The model performance for the diagnosis of myocardial ischemia in borderline coronary lesions of the OPM-MCG was evaluated by bootstrap replications. 1000 bootstrap replications showed that the model AUC and a 95% confidence interval (CI) of 0.864(0.803-0.925) (Figure 4). 1000 bootstrap replications showed that the model was well-calibrated. The mean absolute error was 0.017 (Figure 4). The decision curve analysis (DCA) for the diagnostic model showed that if the threshold probability of patients is greater than 12% (Figure 4), screening strategies based on the OPM-MCG diagnostic model resulted in superior net benefit than screen-none or screen-all strategies.

Discussion

CAD is presently characterized by an epicardial vascular lesion with a stenosis exceeding 50% in the CAG. Frequently, the degree of stenosis indicated by CAG is used as a reference standard for myocardial revascularization. Moreover, FFR can be used to evaluate the existence of myocardial ischemia, with a threshold of 0.8. However, as illustrated in Figure 2, the coronary stenosis identified in CAG may not precisely align with the FFR results. This observation is in line with the conclusions drawn in the 2019 ESC Guidelines for Chronic Coronary Syndromes [12,13], emphasizing that the accuracy of determining CAD solely based on angiographic stenosis was as low as 64% when compared to flow reserve fraction. The positive mismatch rate, where lesions with less than 50% stenosis may demonstrate an FFR ≤ 0.8, was 19%, while the negative mismatch rate, where lesions with over 50% stenosis may result in an FFR value > 0.8, reached up to one-third. Numerous studies [14,15] have consistently demonstrated that FFR-guided stenting leads to superior immediate outcomes and long-term prognosis. Therefore, FFR carries a Class 1a recommendation for guiding revascularization in angiographically borderline coronary stenoses in patients with stable angina. The feasibility of diagnosing myocardial ischemia in patients with borderline coronary lesions using OPM-MCG was shown in our study, when compared to invasive FFR. The collective diagnostic potential of MCG parameters in detecting myocardial ischemia in borderline coronary lesions resulted in an AUC of 0.864 (95% CI 0.803 to 0.925). Due to factors such as time consumption, costs, patient-related discomfort, contraindications, and a lack of reimbursement, the current rate of FFR utilization in catheterization laboratories in China is less than 6% [3]. OPM-MCG allows ischemia assessment in patients with borderline coronary lesions prior to CAG and has a good concordance with FFR.

In comparing our MCG results with those reported by Park JW et al. [16], it is clear that FFR, serving as the reference standard, evaluates ischemia through direct measurement of pressure beyond the coronary lesion. In contrast, the Five parameters of our OPM-MCG, along with the ST-segment fluctuation scores (AUC=0.835) and Bull's eye analysis (AUC=0.914) employed by Park, offer a non-invasive alternative. According to Park JW et al, the TT segment, defined as the interval from T onset to T peak, is a more effective parameter for analyzing MCG signals due to its superior signal-to-noise ratio for reflecting ventricular repolarization electrical activity [17]. In terms of the selected parameters, consistent with earlier literature [18], we focused on assessing the overall homogeneity of the repolarization process, including spatial structural similarity and smoothing of current changes. Park et al. utilized ST-segment fluctuation scores and Bull's eye analysis to evaluate the uniformity of the repolarization process in relation to current variations and spatial distribution variances for ischemia assessment. In our study, we further characterized the images by incorporating the δDt_{sum}-PN, δAg_{sum}-C, δAr_{sum}-N and δAr_{min}-N parameters of the model to analyze changes in currents, pole areas, and distances. Additionally, describing the images using the parameters of the 3 different angular points provided a comprehensive description and response to the images. In terms of image feature discrimination, the ischemia-positive features of the OPM-MCG (pole multipolarization and magnetic field angle deflection) initially are consistent with the FFR (Figure 2). For practical clinical application, Park JW et al. used a 64-channel axial gradiometer system, which offers greater channel capacity and higher sensitivity for positional discrimination. However, this approach required patients to complete two MCG tests—one during stress and one at rest—in a shielded room. Comparatively, OPM-MCG is equipped with a shielding barrel that can effectively diagnose myocardial ischemia caused by borderline coronary lesions at rest, without the need for a specially constructed shielding room. This enhances the practicality and universality of its clinical application.

Non-invasive methods like PET/CT, SPECT and CMR are accurate for assessing myocardial ischemia, but their use is limited due to cost, long wait times and radioactive substances [19]. In a prospective study done by Roel S. et al. [20], which included 189 patients in a head-to-head comparison, it was found that using FFR as the gold standard, the sensitivity of SPECT, PET/CT, and CMR was only 67%, 81%, and 66%, and the specificity was only 61%, 65%, and 62%. The diagnostic accuracy of PET/CT was not statistically different from that of SPECT and CMR. Recently, CT-derived fractional flow reserve (CT-FFR) has emerged as a noninvasive test for detecting myocardial ischemia, with a sensitivity of 89% and specificity of 91% according to a multicenter study [21]. The widespread use of CT-FFR has limitations including the need for good image quality and inability to assess microvascular and diffuse lesions [22]. ECG is widely used in the clinic as the fastest and low-cost test. ECG uses a two-dimensional linear approach to record cardiac radial currents to detect ischemia, but it can be affected by body tissues or fluids and has low spatial resolution. MCG detects and measures weak magnetic fields generated by the electrical activity of the heart, and the waveform of the MCG waveform is similar to that of the ECG signal. However, MCG is less affected by changes in conductivity and does not suffer from skin electrode contact problems. In addition, MCG is more sensitive to magnetic fields generated by tangential currents that are more affected by myocardial ischemia, and MCG detects eddy currents that are not apparent with ECG [23]. Thus, previous studies have demonstrated that MCG has a higher sensitivity to early myocardial ischemia [24,25]. In most studies of MCG detection of myocardial ischemia, researchers have categorized the analysis of MCG into morphological and quantitative data analyses [26]. Morphological analysis often focuses on amplitude, nondipole phenomena, and current or magnetic field angle. Quantitative data analysis is mostly based on changes in the magnetic field during ventricular repolarization, usually at the end of the ST segment (before the T wave) and/or during the T wave, and partially measured during the QT and QRS segment. These parameters describe the poles, the angles of the magnetic and current fields, and the waveform amplitude by extrema, dynamics, and ratios. Current studies analyzing MCG at rest for the detection of myocardial ischemia use a variety of methods, including dichotomous classification methods based on MCG parameters, quantification of abnormal MCG parameters, creation of composite indices using MCG parameters, and the application of machine-learning methods [27].

This is similar to our finding that a positive OPM-MCG scan was demonstrated by one or more abnormalities in the TT segment, including changes in TT segment parameters and the changes in image (non-dipole phenomena and angular deflection of currents or magnetic fields). Different MCG parameters and their combinations can provide more incremental information on cardiovascular disease. In addition, studies have shown that MCG is capable of accurately diagnosing myocardial ischemia resulting from epicardial coronary artery disease as well as effectively detecting myocardial ischemia caused by coronary microvascular dysfunction (CMD). The accuracy of MCG identification of CMD is 94.8%, sensitivity of 100%, and specificity of 93.3% [28]. In our study, we also found a small number of FFR-negative patients with positive MCG scans as described above, and considered the possibility of CMD. In the future, we will summarize the characteristic images of patients with CMD and further explore the incremental information provided by the MCGs for these patients.

The difference between SQUID-based and OPM-based MCG systems lies on their sensor technology. SQUID-based MCGs were developed earlier and offer high sensitivity. But their reliance on liquid helium refrigeration for achieving low-temperature superconductivity, as well as the high maintenance costs associated with them, have hindered their widespread adoption and utilization. In contrast, the OPM-MCG operates at room temperature without liquid helium cooling and offers comparable sensitivity, as it is easier to use and less expensive to operate [29,30]. However, OPM-MCG is also unsuitable for claustrophobic patients. Furthermore, as a result of its late development, there is a lack of established guidelines for analyzing MCG parameters. As such, we intend to conduct further exploratory studies on OPM-MCG in various clinical settings.

Limitation

The study is a single-center registry study with some limitations. We are aware that the current diagnostic model may suffer from potential overfitting and therefore the conclusions of this study require further validation in multicenter studies. In addition, the definition of positive and negative poles we currently use differs from the Rome Biomag Conference in 1981 standard, and there are currently multiple types of MCGs globally, and the current methodology for analyzing myocardial ischemia has not been compared head-to-head with other MCG devices.

Conclusion

MCG shows excellent sensitivity, specificity, and diagnostic accuracy in identifying significant myocardial ischemia when compared to FFR. MCG can provide the evidence of a precise diagnostic strategy in patients with borderline coronary lesions before CAG, reducing unnecessary invasive examination.

Ethics approval and consent to participate

This study was performed in accordance with the principles of the Declaration of Helsinki. This study was approved by the ethics committee of Beijing Anzhen Hospital, Capital Medical University (KS2023008). Written informed consent was required for participation in the study.

Competing interests

The authors declare that they have no conflicts of interest.

Funding statement

This work was supported by Coordinated innovation of scientific and technological in Beijing-Tianjin-Hebei Region (Z231100003923008), Beijing Nova Program (20220484222) , Capital's Funds for Health Improvement and Research (2024-2-2066) , Beijing Hospitals Authority 'sailing' Program (YGLX202323), Beijing Hospitals Authority's Ascent Plan (DFL20220603) ， High-level public health technical talent construction project of Beijing Municipal Health Commission (Leading Talent-02-01) and Project of The Beijing Lab for Cardiovascular Precision Medicine (PXM2018_014226_000013).

Author Contribution Statement

Xiantao Song and Chenchen Tu acted as guarantors. Xiantao Song, Chenchen Tu and Hongjia Zhang helped to conceive the topic and revised the article. Shuwen Yang and Lanxin

Feng wrote the manuscript and finished the statistics, Mingduo Zhang, Min Zhang, Jiqiang He, Yanlong Ren, Yawei Luo and Feng Xu contributed to the data collection. Zhao Ma, Huan Zhang, Yazhe Zhang, Linqi Liu, Shu Zhou, Xin Zhao, and Xueyao Yang helped with data analysis. All authors read and approved the final manuscript.

Acknowledgments

The authors thank Zhechun Zeng, Ming Ding, and Bin Cai for their help in data analysis, and Xin Chen, Jinfan Tian, and Yulong Xue for their help in data collection.

Abbreviations

AUC= area under the receiver operating characteristic curve

CCTA= coronary computed tomography angiography

CI= confidence intervals

FFR= fractional flow reserve

CAG= coronary angiography

OPM-MCG= optical pumped magnetometer magnetocardiography

ROC= receiver-operating characteristic

Availability of data and materials

The data that support the findings of this study are available on request from the corresponding author, Xiantao Song， upon reasonable request.

Reference

[1] van Nunen LX, Zimmermann FM, Tonino PA, et al. Fractional flow reserve versus angiography for guidance of PCI in patients with multivessel coronary artery disease (FAME): 5-year follow-up of a randomised controlled trial. Lancet. 2015;386(10006):1853-1860.

[2]Neumann FJ, Sousa-Uva M, Ahlsson A, et al. 2018 ESC/EACTS Guidelines on myocardial revascularization [published correction appears in Eur Heart J. 2019 Oct 1;40(37):3096]. Eur Heart J. 2019;40(2):87-165.

[3] Writing Committee Members, Lawton JS, Tamis-Holland JE, Bates ER, et al. 2021 ACC/AHA/SCAI Guideline for Coronary Artery Revascularization: Executive Summary: A Report of the American College of Cardiology/American Heart Association Joint Committee on Clinical Practice Guidelines [published correction appears in J Am Coll Cardiol. 2022 Apr 19;79(15):1547]. J Am Coll Cardiol. 2022;79(2):197-215.

[4] Nomura M, Nakaya Y, Fujino K, et al. Magnetocardiographic studies of ventricular repolarization in old inferior myocardial infarction. Eur Heart J. 1989;10(1):8-15.

[5] Brisinda D, Meloni AM, Fenici R. First 36-channel magnetocardiographic study of CAD patients in an unshielded laboratory for interventional and intensive cardiac care. Funct Imaging Model Hear. 2003;LNCS 2674:122-131.

[6] Gapelyuk A, Wessel N, Fischer R, et al. Detection of patients with coronary artery disease using cardiac magnetic field mapping at rest. J Electrocardiol. 2007;40(5):401-407.

[7]Kanzaki H, Nakatani S, Kandori A, et al. A new screening method to diagnose coronary artery disease using multichannel magnetocardiogram and simple exercise. Basic Res Cardiol. 2003;98(2):124-132.

[8] Nakai K, Izumoto H, Kawazoe K, et al. Three-dimensional recovery time dispersion map by 64-channel magnetocardiography may demonstrate the location of a myocardial injury and heterogeneity of repolarization. Int J Cardiovasc Imaging. 2006;22(3-4):573-580. doi:10.1007/s10554-005-9019-x.

[9]Tolstrup, Kirsten, Donatella Brisinda, Am Meloni, et al. Comparison of resting magnetocardiography with stress single photon emission computed tomography in patients with stable and unstable angina. J Am Coll Cardiol 2006;47(4 Suppl 1):176A. Abstract 930-247.

[10] Lim HK, Kwon H, Chung N, et al. Usefulness of magnetocardiogram to detect unstable angina pectoris and non-ST elevation myocardial infarction. Am J Cardiol. 2009;103(4):448-454.

[11] Shin ES, Lam YY, Her AY, et al. Incremental diagnostic value of combined quantitative and qualitative parameters of MCG to detect coronary artery disease. Int J Cardiol. 2017;228:948-952.

[12] Knuuti J, Wijns W, Saraste A, et al. 2019 ESC Guidelines for the diagnosis and management of chronic coronary syndromes [published correction appears in Eur Heart J. 2020 Nov 21;41(44):4242]. Eur Heart J. 2020;41(3):407-477.

[13] Derimay F, Finet G and Rioufol G. Coronary artery stenosis prediction does not mean coronary artery stenosis obstruction. Eur Heart J. 2021;42(42):4401.

[14] Xaplanteris P, Fournier S, Pijls NHJ, et al. Five-Year Outcomes with PCI Guided by Fractional Flow Reserve. N Engl J Med. 2018;379(3):250-259.

[15] Zimmermann FM, Ferrara A, Johnson NP, et al. Deferral vs. performance of percutaneous coronary intervention of functionally non-significant coronary stenosis: 15-year follow-up of the DEFER trial. Eur Heart J. 2015;36(45):3182-3188.

[16] Park JW, Shin ES, Ann SH, et al. Validation of magnetocardiography versus fractional flow reserve for detection of coronary artery disease. Clin Hemorheol Microcirc. 2015;59(3):267-281.

[17]Park J-W, Hill PM, Chung N, Hugenholtz PG, Jung F. Magnetocardiography predicts coronary artery disease in patients with acute chest pain. Ann Noninvasive Electrocardiol. 2005;10(3):312-323.

[18] Chaikovsky I, Hailer B, Sosnytskyy V, et al. Predictive value of the complex magnetocardiographic index in patients with intermediate pretest probability of chronic coronary artery disease: results of a two-center study. Coron Artery Dis. 2014;25(6):474-484.

[19] Working Group of Cardiovascular Imaging of National Center for Medical Quality Control of Cardiovascular Diseases Survey of the Application Status of Cardiovascular Imaging Modalities and Medical Quality Report in China [J]. Chin circ J ,2020,35(7):625-633.

[20] Driessen RS, van Diemen PA, Raijmakers PG, et al. Functional stress imaging to predict abnormal coronary fractional flow reserve: the PACIFIC 2 study. Eur Heart J. 2022;43(33):3118-3128.

[21] Tang CX, Liu CY, Lu MJ, et al. CT FFR for Ischemia-Specific CAD With a New Computational Fluid Dynamics Algorithm: A Chinese Multicenter Study. JACC Cardiovasc Imaging. 2020;13(4):980-990.

[22] Li Y, Yu M, Dai X, et al. Detection of Hemodynamically Significant Coronary Stenosis: CT Myocardial Perfusion versus Machine Learning CT Fractional Flow Reserve. Radiology. 2019;293(2):305-314.

[23]Chaikovsky I, Hailer B, Sosnytskyy V, et al. Predictive value of the complex magnetocardiographic index in patients with intermediate pretest probability of chronic coronary artery disease: results of a two-center study. Coron Artery Dis. 2014;25(6):474-484.

[24]Mace SE, Peacock WF, Stopyra J, et al. American Heart Journal Plus : Cardiology Research and Practice Accelerated magnetocardiography in the evaluation of patients with suspected cardiac ischemia : The MAGNETO trial. Am Hear J Plus Cardiol Res Pract. 2024;40(February):100372.

[25]Tolstrup K, Madsen BE, Ruiz JA, et al. Non-invasive resting magnetocardiographic imaging for the rapid detection of ischemia in subjects presenting with chest pain. Cardiology.

[26]Camm AJ, Henderson R, Brisinda D, et al. Clinical utility of magnetocardiography in cardiology for the detection of myocardial ischemia. J Electrocardiol. 2019;57:10-17.

[27] Rong Tao, Shulin Zhang, Xiao Huang, et al. Magnetocardiography-Based Ischemic Heart Disease Detection and Localization Using Machine Learning Methods. IEEE Trans Biomed Eng. 2019;66(6):1658-1667.

[28] Rong Tao, Shulin Zhang, Xiao Huang, et al. Magnetocardiography-Based Ischemic Heart Disease Detection and Localization Using Machine Learning Methods. IEEE Trans Biomed Eng. 2019;66(6):1658-1667.

[29]Brisinda D, Fenici P, Fenici R. Clinical magnetocardiography: the unshielded bet—past, present, and future. Front Cardiovasc Med. 2023;10(August):1-24.

[30] Pena ME, Pearson CL, Goulet MP, et al. A 90-second magnetocardiogram using a novel analysis system to assess for coronary artery stenosis in Emergency department observation unit chest pain patients. IJC Hear Vasc. 2020;26(100466):1-7.

Table 1 Clinical characteristics (n = 141)

Characteristics	Total(n=141)
Age (yrs)	60.64±9.70
Male, n (%)	109(77.3)
BMI (Kg/m2)	26.15±3.36
Diabetes, n (%)	47(33.3)
Hypercholesterolemia, n (%)	65(46.1)
Hypertension, n (%)	82(58.2)
Stroke, n (%)	9(6.4)
Smoke, n (%)	43(30.5)
Systolic blood pressure, mmHg	128.69±15.54
Diastolic blood pressure, mmHg	75.15±10.79
Heart rate	73.81±10.38
Medication, n(%)	
Aspirin	129(91.5)
Statin	137(97.2)
ACEI/ARB	45(35.6)
SGLT2 inhibitors	22(16.7)

Nicorandil	23(16.3)
Admission lab results	
Low-density lipoprotein cholesterol (mmol/L)	1.82±0.69
hs Tnl(pg/ml)	3.5(2.5,5.8)
Brain natriuretic peptide (pg/ml)	29.00(14.75,48.25)
Blood glucose (mmol/L)	5.52(4.82,7.33)
HbA1c(%)	6.25(5.7,7.1)
ICA and FFR characteristics	
1-vessel disease	50(35.5)
2-vessel disease	43(30.5)
3-vessel disease	48(34.0)
Number of patients with FFR$\leq$0.8	68(48.2)
Number of vessels with FFR	157
Number of vessels with FFR$\leq$0.8	74(47.1)
Left anterior descending artery with FFR	97(68.8)
Left circumflex artery with FFR	25(17.7)
Right coronary artery with FFR	35(24.8)
Interval between MCG and FFR	2(1,7)

Values are n (%) or mean ± SD

BMI= Body Mass Index, ACEI= angiotensin converting enzyme inhibitor, ARB = angiotensin receptor blocker, SGLT2 inhibitors = sodium-glucose cotransporter-2 inhibitors, HbA1c=

glycated hemoglobin, ICA = invasive coronary angiography, FFR = fractional flow reserve.

Table 2 The definitions of the MCG parameters

MCG Parameters	Definitions
MAg_{max}-TT	The maximum magnetic field angle at intervals of a certain time τ within TT segment
δDt_{sum}-PN	The sum of changes in magnetic pole distance at intervals of a certain time τ within TT segment
δAg_{sum}-C	The sum of changes in current angle at intervals of a certain time τ within TT segment
δAr_{sum}-N	The sum of changes in negative pole area at intervals of a certain time τ within TT segment
δAr_{min}-N	The minimum value of changes in negative pole area at intervals of a certain time τ within TT segment

M= Magnetic Field; Ag= Angle; TT= from T onset to T peak; δ= Change value; DT= Distance; PN= Positive Pole to Negative Pole; C=Current; Ar= Area; N= Negative Pole; ; τ= one tenth of the time interval between TT segment.

Figure legend

Figure 1. Flowchart of the study design.

Figure legend: CCTA= coronary computed tomography angiography;

MCG=magnetocardiography; ICA= invasive coronary angiography; FFR=fractional flow reserve; PCI= percutaneous coronary intervention.

Figure 2 Schematic diagram of OPM-MCG scan.

Figure legend: (A) Schematic diagram of MAg_{max}-TT and current angle. In magnetic field distribution maps and current density maps, the definition rule for angle values is based on the horizontal axis, with counterclockwise angles being negative and clockwise angles being positive. MAg_{max}-TT is the maximum angle between the line connecting the maximum positive and negative magnetic poles and the horizontal axis. in the TT segment. δAg_{sum}-C is the sum of changes in current angle at intervals of a certain time τ within TT segment (B)Normal OPM-MCG scan. The OPM-MCG scan showed no evidence of ischemia or obstructive coronary artery disease, as demonstrated by the lack of significant current deviations within the myocardium and absence of angle shift between the positive red pole and negative blue pole between T-onset and T-peak. (C) The OPM-MCG scan of a patient in his 70s showed magnetic field angular deflection, abnormal magnetic field distribution of the positive and multipolarisation of negative poles, suggesting significant myocardial ischemia, and the ECG showed no significant abnormality. The CAG showed two lesions: 60% stenosis of the D1, 50% stenosis of the R-PDA. The FFRs were 0.77 for the R-PDA. (D) The OPM-MCG scan of a patient in his 60s showed no myocardial ischemia, ECG showed no significant abnormalities, echocardiography showed widening of the ascending aorta and aortic sinus. CAG showed 75% stenosis of the LAD, 60% stenosis of the RCA, FFR value of the LAD was 0.88.

MCG= magnetocardiography; FFR= fractional flow reserve; ICA= invasive coronary angiography; D1= Diagonal branches; R-PDA= Posterior descending artery; LAD= Left Anterior descending artery; RCA= right coronary artery.

Figure 3. Nomogram of the diagnostic model.

Figure legend: The nomogram graphically demonstrates the diagnostic model of OPM-MCG. Points for MAg_{max}-TT, δDt_{sum}-PN, δAg_{sum}-C, δAr_{sum}-N and δAr_{min}-N can be obtained using a point caliper and then summed to obtain a total score that can be measured with diagnosing myocardial ischemia in patients with borderline coronary lesions.

Figure 4 Accuracy and internal validation of the diagnostic model.

Figure legend: (A) ROC curves for the diagnostic model. After 1000 bootstrap replications, the area under the curve and 95% confidence interval for receiver operating characteristic is 0.864 (0.803-0.925). (B) Calibration curve for the diagnostic model. Calibration curve for the borderline lesion ischemia diagnostic model was established by comparing the actual and predicted probability of a positive FFR in patients with borderline lesions of the coronary arteries. The smaller the distance of the scatter from the dashed line, the better the calibration. (C) Decision curve analysis (DCA) for diagnostic models of ischemia in borderline coronary lesions. Treat none: net benefit when it is assumed that no patients with borderline lesions of the coronary arteries would have the outcome (FFR-positive). Treat all: net benefit when all patients with borderline coronary lesions are assumed to have an outcome (FFR-positive). Diagnostic model: net benefit of managing borderline coronary lesions with a diagnosis of myocardial ischemia based on the diagnostic model estimate. The strategy with the highest net benefit at any given threshold is the preferred strategy.

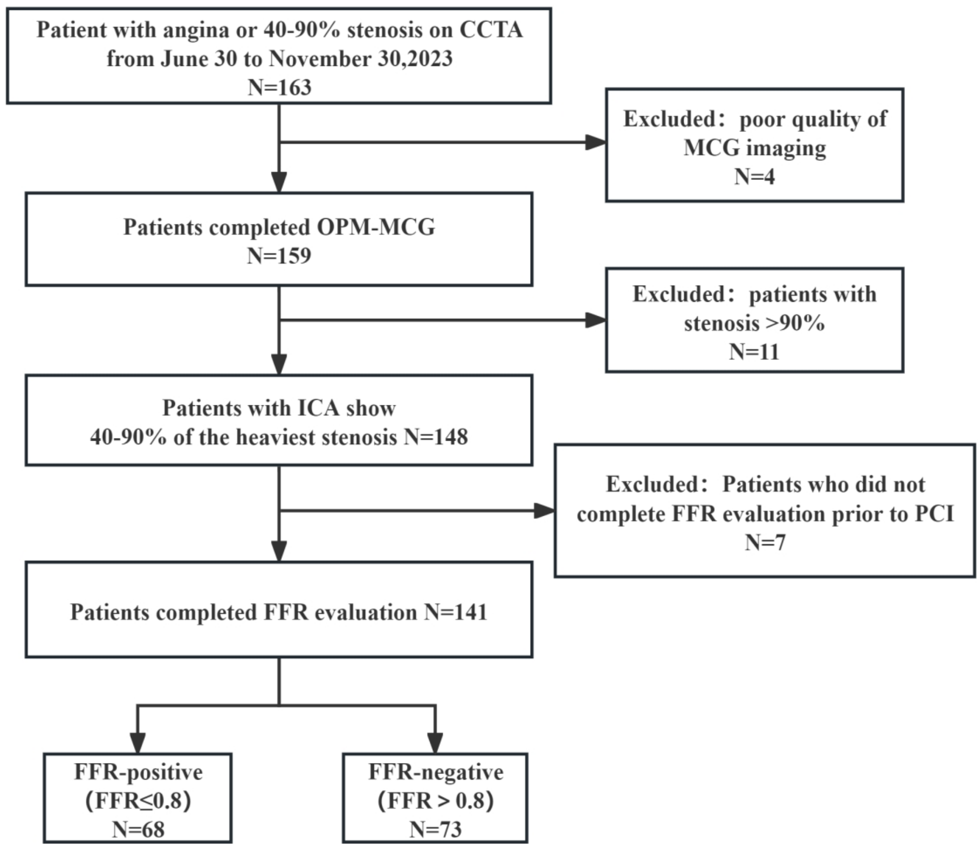

Figure 1. Flowchart of the study design.
Figure legend: CCTA= coronary computed tomography angiography; MCG=magnetocardiography; ICA= invasive coronary angiography; FFR=fractional flow reserve; PCI= percutaneous coronary intervention.

510x441mm (96 x 96 DPI)

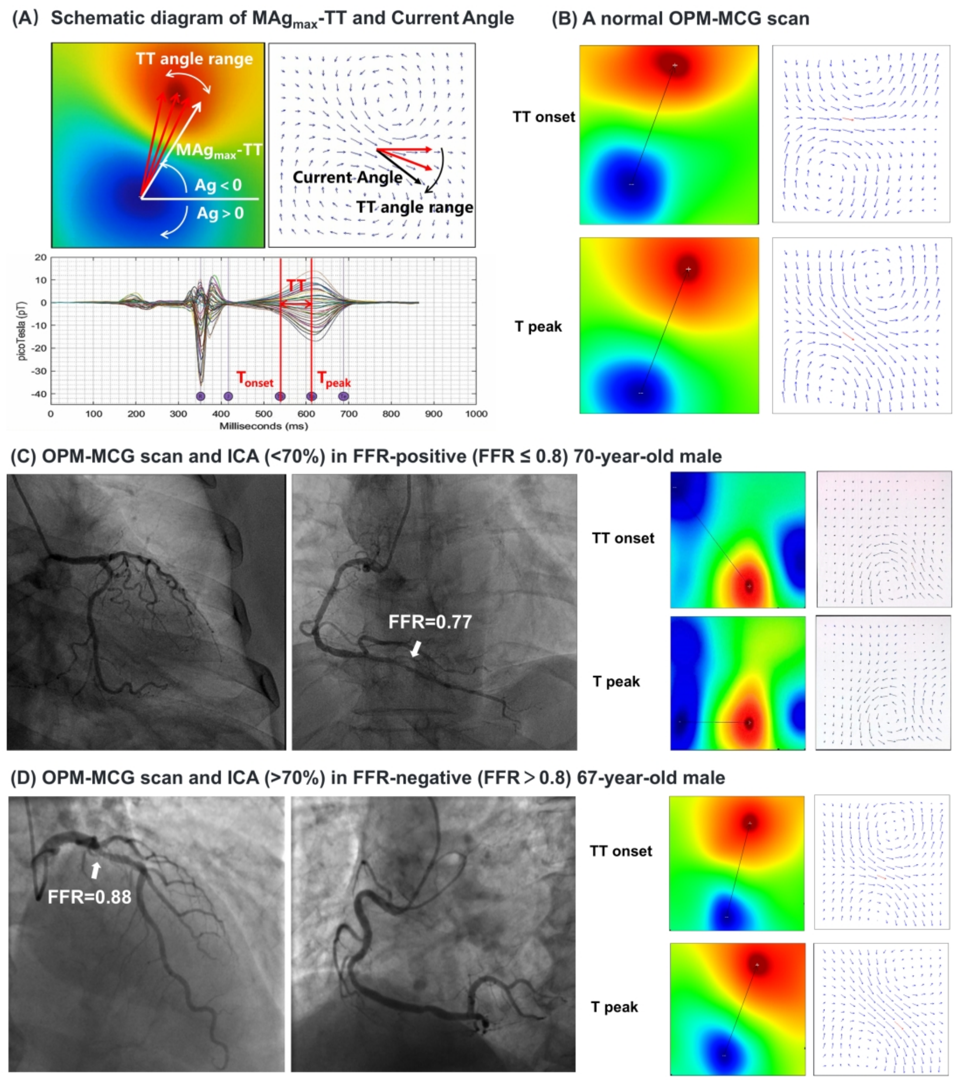

Figure 2 Schematic diagram of OPM-MCG scan.

Figure legend: (A) Schematic diagram of MAgmax-TT and current angle. In magnetic field distribution maps and current density maps, the definition rule for angle values is based on the horizontal axis, with counterclockwise angles being negative and clockwise angles being positive. MAgmax-TT is the maximum angle between the line connecting the maximum positive and negative magnetic poles and the horizontal axis. in the TT segment. δAgsum-C is the sum of changes in current angle at intervals of a certain time τ within TT segment (B)Normal OPM-MCG scan. The OPM-MCG scan showed no evidence of ischemia or obstructive coronary artery disease, as demonstrated by the lack of significant current deviations within the myocardium and absence of angle shift between the positive red pole and negative blue pole between T-onset and T-peak. (C) The OPM-MCG scan of a patient in his 70s showed magnetic field angular deflection, abnormal magnetic field distribution of the positive and multipolarisation of negative poles, suggesting significant myocardial ischemia, and the ECG showed no significant abnormality. The CAG showed two lesions: 60% stenosis of the D1, 50% stenosis of the R-PDA. The FFRs were 0.77 for the R-PDA. (D) The OPM-MCG scan of a patient in his 60s showed no myocardial ischemia, ECG showed no significant abnormalities, echocardiography showed widening of the ascending aorta and aortic sinus. CAG showed 75% stenosis of the LAD, 60% stenosis of the RCA, FFR value of the LAD was 0.88.
MCG= magnetocardiography; FFR= fractional flow reserve; ICA= invasive coronary angiography; D1=

Diagonal branches; R-PDA= Posterior descending artery; LAD= Left Anterior descending artery; RCA= right coronary artery.

1090x1206mm (96 x 96 DPI)

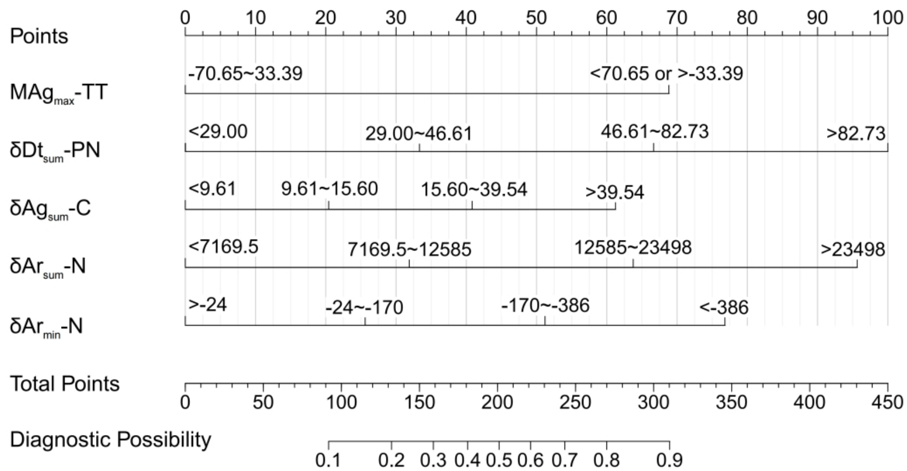

Figure 3. Nomogram of the diagnostic model.

Figure legend: The nomogram graphically demonstrates the diagnostic model of OPM-MCG. Points for MAgmax-TT, δDtsum-PN, δAgsum-C, δArsum-N and δArmin-N can be obtained using a point caliper and then summed to obtain a total score that can be measured with diagnosing myocardial ischemia in patients with borderline coronary lesions.

310x182mm (300 x 300 DPI)

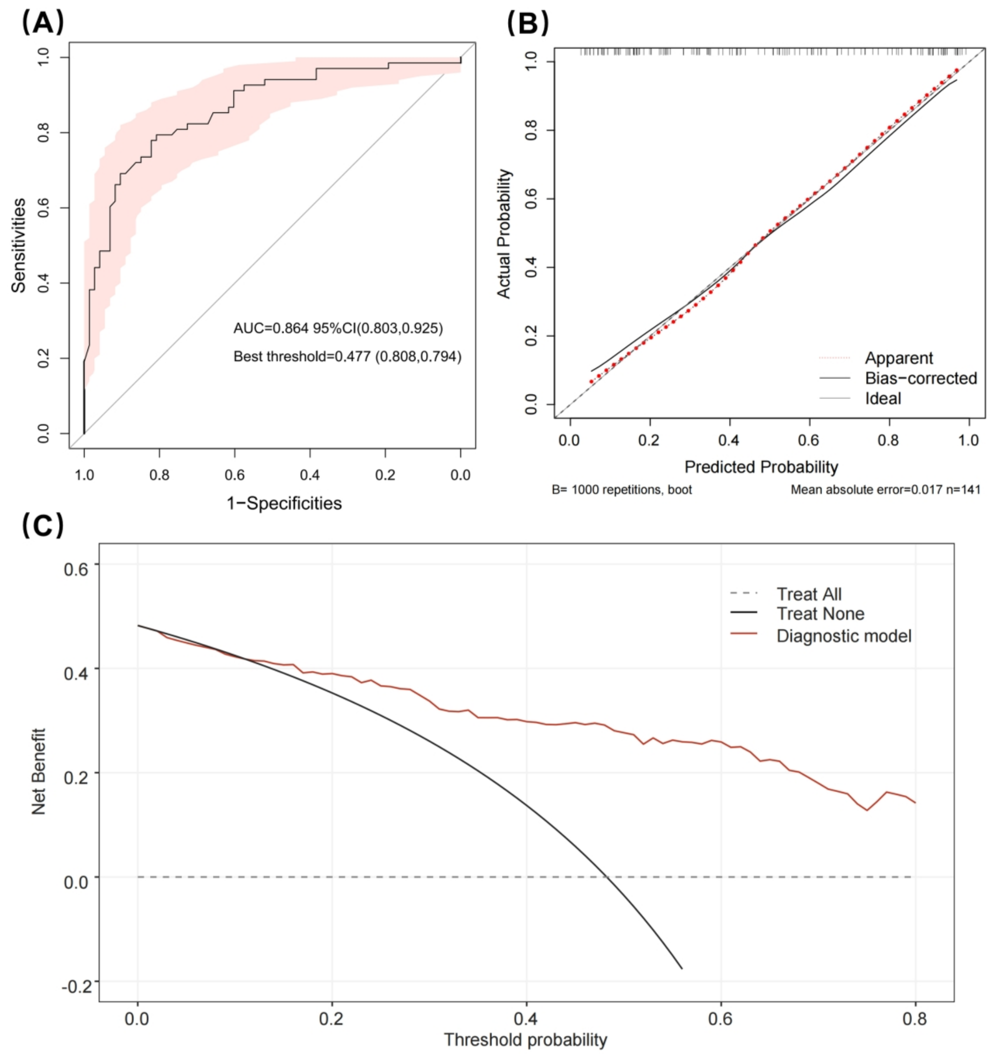

Figure 4 Accuracy and internal validation of the diagnostic model.
Figure legend: (A) ROC curves for the diagnostic model. After 1000 bootstrap replications, the area under the curve and 95% confidence interval for receiver operating characteristic is 0.864 (0.803-0.925). (B) Calibration curve for the diagnostic model. Calibration curve for the borderline lesion ischemia diagnostic model was established by comparing the actual and predicted probability of a positive FFR in patients with borderline lesions of the coronary arteries. The smaller the distance of the scatter from the dashed line, the better the calibration. (C) Decision curve analysis (DCA) for diagnostic models of ischemia in borderline coronary lesions. Treat none: net benefit when it is assumed that no patients with borderline lesions of the coronary arteries would have the outcome (FFR-positive). Treat all: net benefit when all patients with borderline coronary lesions are assumed to have an outcome (FFR-positive). Diagnostic model: net benefit of managing borderline coronary lesions with a diagnosis of myocardial ischemia based on the diagnostic model estimate. The strategy with the highest net benefit at any given threshold is the preferred strategy.

239x257mm (300 x 300 DPI)

Supplementary Material

Development and validation of a clinical diagnostic model for myocardial ischemia in borderline coronary lesions based on optical pumped magnetometer magnetocardiography: a prospective observational cohort study

Contents

OPM-MCG post-processing steps

The post-processing process of MCG signals is as follows. Firstly, a composite gradient magnetometer array is constructed using a separate environmental monitoring channel, and the common mode projection components of the monitoring channel are subtracted from the MCG detection array channels, effectively suppressing environmental magnetic field drift and power frequency interference. Then, notching the 50Hz power frequency and its harmonic components of the data, and performing a 1-40Hz bandpass filter to further remove power frequency interference and limit the bandpass frequency to the main frequency range of the MCG. Finally, the denoised data is subjected to R-peak detection and recognition, with an average heartbeat cycle of 90 seconds as the length of the slice time, and the identified R-peak point is used as the time alignment point to slice the data and overlay it for average

Supplementary Table and Figures

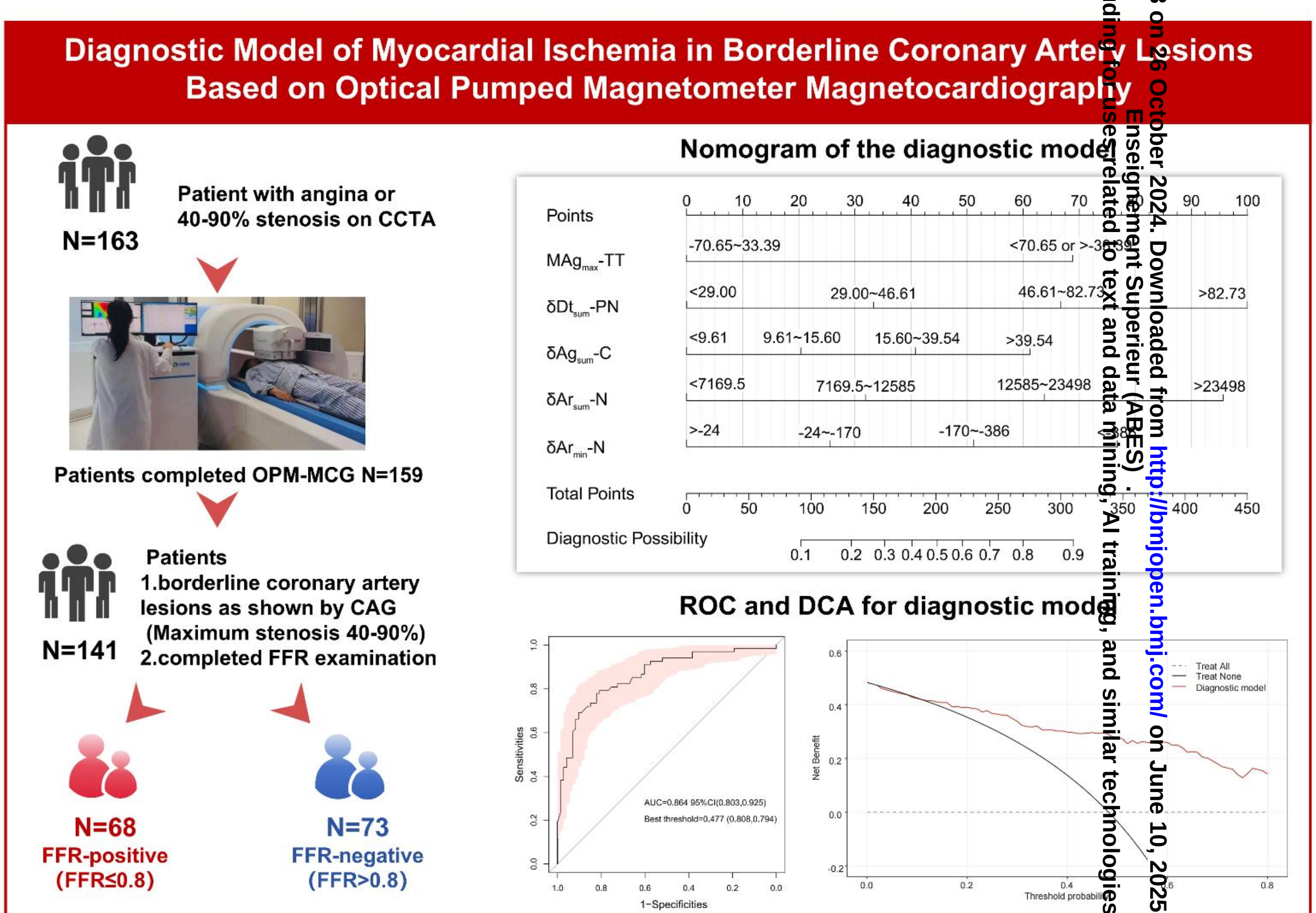

Supplementary Figure 1 Graphical Abstracts: Diagnostic Model of Myocardial Ischemia in Borderline Coronary Artery Lesions Based on Optical Pumped Magnetometer Magnetocardiography

CCTA= coronary computed tomography angiography; MCG=magnetocardiography; CAG= invasive coronary angiography; FFR=fractional flow reserve; PCI= percutaneous coronary intervention.

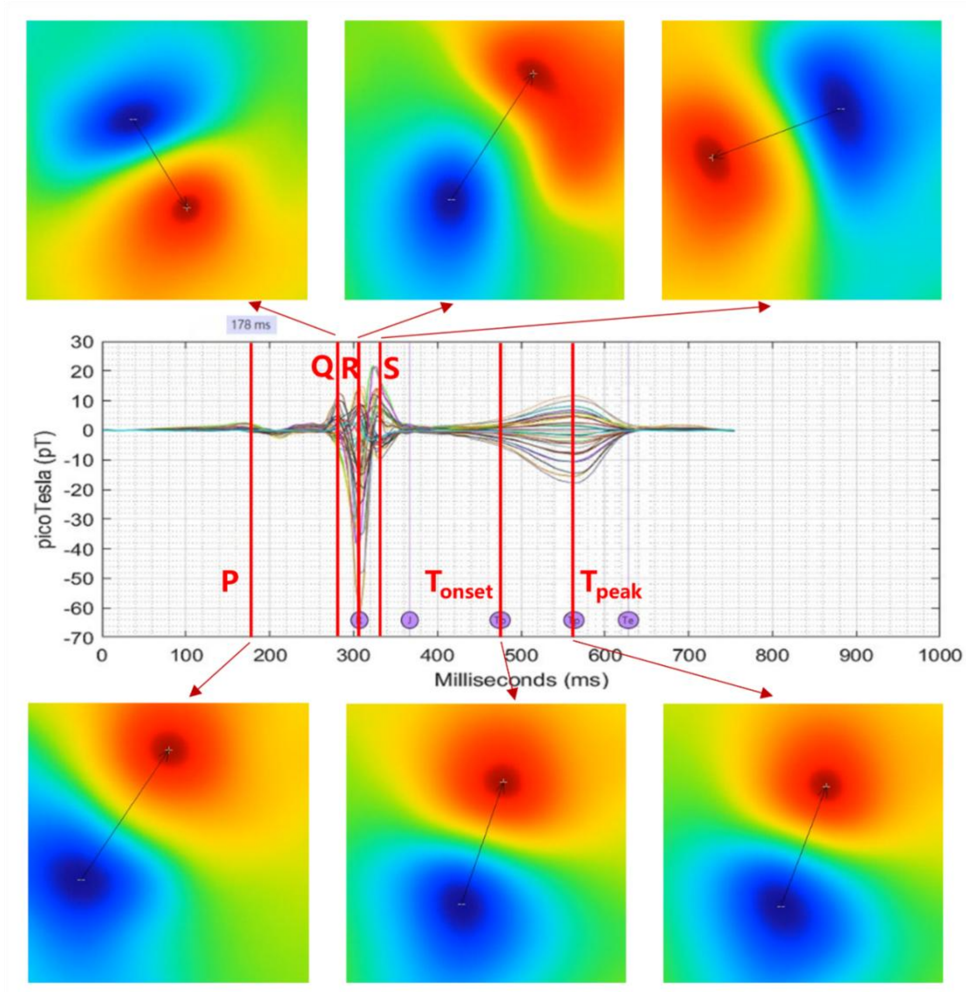

Supplementary Figure 2 The magnetic field distributions (MFDs) of key points (P, QRS, and T onset and T peak) in the cardiac cycle of healthy individuals

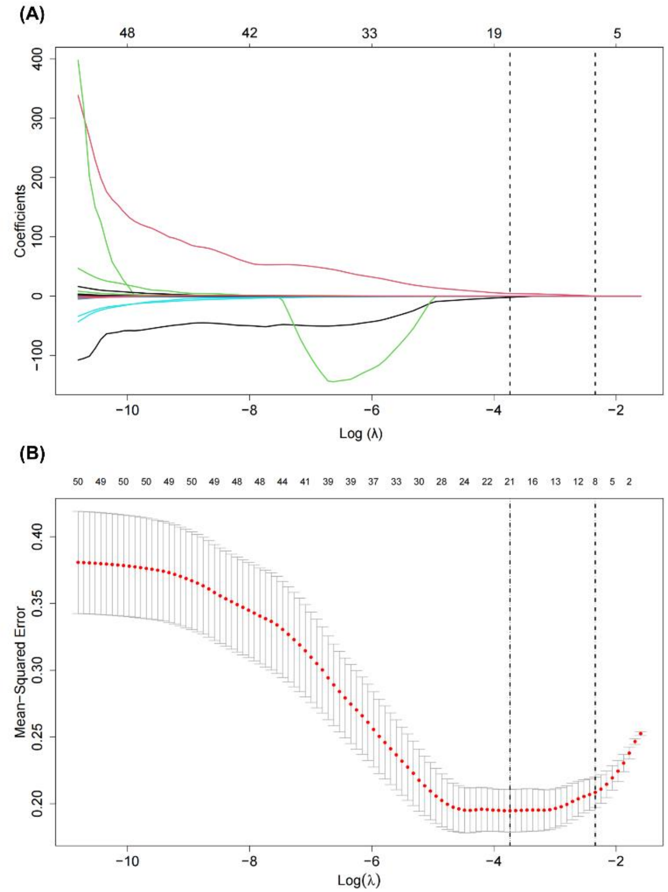

Supplementary Figure 3 Least absolute shrinkage and selection operator (LASSO) regression

Figure legend :(A) LASSO model coefficient profiles of the 50 candidate parameters. As log λ increases, the regression coefficients continue to converge, and there are fewer parameters with non-zero regression coefficients.

(B) Tuning parameter selection by cross-validation in the LASSO model. The solid vertical lines represent the partial likelihood deviance standard error (SE). The red dotted line indicates the cross-validation curve. The vertical dashed lines are drawn at the optimal values on the basis of the minimum criteria and 1-SE criteria. Considering the reasonableness of the variables included in this model, with the λ value of 0.02380779 was chosen.

Supplementary Table 1 OPM-MCG Parameters and Definitions

Parameters	Definition
δ Ag_{max}-M	The maximum value of changes in magnetic field angle at intervals of a certain time τ within TT segment
δ Ag_{min}-M	The minimum value of changes in magnetic field angle at intervals of a certain time τ within TT segment
δ Ag_{std}-M	The standard deviation of changes in magnetic field angle at intervals of a certain time τ within TT segment
δ Ag_{sum}-M	The sum of changes in magnetic field angle at intervals of a certain time τ within TT segment
δ Dt_{max}-PN	The maximum value of changes in magnetic pole distance at intervals of a certain time τ within TT segment
δ Dt_{min}-PN	The minimum value of changes in magnetic pole distance at intervals of a certain time τ within TT segment
δ Dt_{std}-PN	The standard deviation of changes in magnetic pole distance at intervals of a certain time τ within TT segment
δ Dt_{sum}-PN	The sum of changes in magnetic pole distance at intervals of a certain time τ within TT segment
δ Ag_{max}-C	The maximum value of changes in current angle at intervals of a certain time τ within TT segment
δ Ag_{min}-C	The minimum value of changes in current angle at intervals of a certain time τ within TT segment
δ Ag_{std}-C	The standard deviation of changes in current angle at intervals of a certain time τ within TT segment
δ Ag_{sum}-C	The sum of changes in current angle at intervals of a certain time τ within TT segment
δ Ps_{max}-C	The maximum value of changes in the position of the current angle at intervals of a certain time τ within TT segment
δ Ps_{std}-C	The standard deviation of changes in the position of the current angle at intervals of a certain time τ within TT segment
δ Ps_{sum}-C	The sum of changes in the position of the current angle at intervals of a certain time τ within TT segment
δ Ar_{max}-NP	The maximum value of changes in negative pole point area at intervals of a certain time τ within TT segment
δ Ar_{min}-NP	The minimum value of changes in negative pole point area at intervals of a certain time τ within TT segment
δ Ar_{std}-NP	The standard deviation of changes in negative pole point area at intervals of a certain time τ within TT segment
δ Ar_{sum}-NP	The sum of changes in negative pole point area at intervals of a certain time τ within TT segment
δ Ar_{bp}-NP	The change in negative pole point area between T-begin and T-peak
Ar_{max}-NP	The maximum value of the negative pole point area at intervals of a certain time τ within TT segment
Ar_{min}-NP	The minimum value of the negative pole point area at intervals of a certain time τ within TT segment
δ Ps_{max}-NP	The maximum value of changes in the position of the negative pole point at intervals of a certain time τ within TT segment
δ Ps_{std}-NP	The standard deviation of changes in the negative of the positive pole point at intervals of a certain time τ within TT segment
δ Ps_{sum}-NP	The sum of changes in the position of the negative pole point at intervals of a certain time τ within TT segment
δ Ar_{max}-N	The maximum value of changes in negative pole area at intervals of a certain time τ within TT segment

Parameters	Definition
δ Ag_{max}-M	The maximum value of changes in magnetic field angle at intervals of a certain time τ within TT segment
δ Ar_{min}-N	The minimum value of changes in negative pole area at intervals of a certain time τ within TT segment
δ Ar_{std}-N	The standard deviation of changes in negative pole area at intervals of a certain time τ within TT segment
δ Ar_{sum}-N	The sum of changes in negative pole area at intervals of a certain time τ within TT segment
δ Ar_{bp}-N	The change in nagative pole area between T-begin and T-peak
Ar_{max}-N	The maximum value of the negative pole area at intervals of a certain time τ within TT segment
Ar_{min}-N	The minimum value of the negative pole area at intervals of a certain time τ within TT segment
δ $ArRto_{max}$-PN	The maximum value of changes in the ratio of positive and negative pole area at intervals of a certain time τ within TT segment
δ $ArRto_{min}$-PN	The minimum value of changes in the ratio of positive and negative pole area at intervals of a certain time τ within TT segment
δ $ArRto_{std}$-PN	The standard deviation of changes in the ratio of positive and negative pole area at intervals of a certain time τ within TT segment
δ $ArRto_{sum}$-PN	The sum of changes in the ratio of positive and negative pole area at intervals of a certain time τ within TT segment
δ Ar_{max}-PP	The maximum value of changes in positive pole point area at intervals of a certain time τ within TT segment
δ Ar_{min}-PP	The minimum value of changes in positive pole point area at intervals of a certain time τ within TT segment
δ Ar_{std}-PP	The standard deviation of changes in positive pole point area at intervals of a certain time τ within TT segment
δ Ar_{sum}-PP	The sum of changes in positive pole point area at intervals of a certain time τ within TT segment
δ Ar_{bp}-PP	The change in positive pole point area between T-begin and T-peak
Ar_{max}-PP	The maximum value of the positive pole point area at intervals of a certain time τ within TT segment
Ar_{min}-PP	The minimum value of the positive pole point area at intervals of a certain time τ within TT segment
δ Ps_{max}-PP	The maximum value of changes in the position of the positive pole point at intervals of a certain time τ within TT segment
δ Ps_{std}-PP	The standard deviation of changes in the position of the positive pole point at intervals of a certain time τ within TT segment
δ Ps_{sum}-PP	The sum of changes in the position of the positive pole point at intervals of a certain time τ within TT segment
δ Ar_{max}-P	The maximum value of changes in positive pole area at intervals of a certain time τ within TT segment
δ Ar_{min}-P	The minimum value of changes in positive pole area at intervals of a certain time τ within TT segment
δ Ar_{std}-P	The standard deviation of changes in positive pole area at intervals of a certain time τ within TT segment

Parameters	Definition
δ Ag_{max}-M	The maximum value of changes in magnetic field angle at intervals of a certain time τ within TT segment
δ Ar_{sum}-P	The sum of changes in positive pole area at intervals of a certain time τ within TT segment
δ Ar_{bp}-P	The change in positive pole area between T-begin and T-peak
Ar_{ma}x-P	The maximum value of the positive pole area at intervals of a certain time τ within TT segment
Ar_{min}-P	The minimum value of the positive pole area at intervals of a certain time τ within TT segment
MAg_{max}-TT	The maximum magnetic field angle at intervals of a certain time τ within TT segment
CAg_{max}-TT	The maximum current angle at intervals of a certain time τ within TT segment
MAg_{min}-TT	The minimum magnetic field angle at intervals of a certain time τ within TT segment
CAg_{min}-TT	The minimum current angle at intervals of a certain time τ within TT segment
MAg-Rp	The magnetic field angle of the R-peak
RtoAm-R_pT_pN	The ratio of magnetic field amplitude at R-peak and the negative amplitude at T-peak
RtoAm-R_pT_pP	The ratio o magnetic field amplitude at R-peak and the positive amplitude at T-peak
RtoAm-R_pT_p	The ratio of magnetic field amplitudes at R-peak and T-peak
MAg-RpTp	The magnetic field angle between R-peak and T-peak
MAg-Tp	The magnetic field angle of the T-peak
CAg_{max}-Tp	The maximum current angle at T-peak
RtoAm-Tp	The ratio of positive to negative magnetic field amplitude at T-peak
TT	The interval from the beginning of the T-wave to its peak within the cardiac cycle

Dt = Distance, Ps = Position, Ag = Angle, Am = Magnitude, Ar = Area, Rto = Ratio, P = Positive, Positive Pole = PP, N = Negative, NP = Negative Pole, M = Magnetic Field, C = Current, max = Maximum, min = Minimum, sum=Sum of all, std = Standard deviation, δ = Change value, TT= TT segment (the position from one-third of the T max amplitude (T onset) to T max (T peak)), R_p=R peak, T_p=T peak

Supplementary Table 2 OPM-MCG parameters of univariable logistic regression model P < 0.1

Parameters	ALL N=141	FFR-Positive N=68	FFR-Negative N=73	Odds Ratio (95%CI)	P value
δ Ag_{max}-M	0.62 (0.44,1.19)	0.77 (0.47,5.76)	0.54 (0.43,0.72)	1.0[illegible]7(1.023-1.163)	0.021
δ Ag_{min}-M	-0.34 (-0.57,-0.18)	-0.42 (-0.82,-0.28)	-0.26 (-0.42,-0.14)	0.9[illegible]4(0.924-0.992)	0.034
δ Ag_{std}-M	0.16 (0.11,0.68)	0.28 (0.14,2.06)	0.14 (0.10,0.20)	1.5[illegible]4(1.213-2.313)	0.004
δ Ag_{sum}-M	10.6 (6.18,26.2)	20.2 (9.88,45.5)	8.28 (4.55,11.8)	[illegible]64(1.037-1.1)	<0.001
δ Dt_{max}-PN	2.69 (1.97,4.12)	3.51 (2.16,12.9)	2.22 (1.89,3.16)	1.0[illegible]4(1.001-1.032)	0.063
δ Dt_{min}-PN	-2.20 (-3.27,-1.76)	-2.38 (-4.70,-1.91)	-2.00 (-2.80,-1.63)	0.971(0.94-0.991)	0.023
δ Dt_{std}-PN	0.74 (0.55,1.18)	0.82 (0.63,3.45)	0.63 (0.52,0.89)	1.1[illegible]8(1.031-1.332)	0.024
δ Dt_{sum}-PN	46.6 (29.1,80.7)	66.6 (42.0,110)	33.3 (25.7,48.6)	1.026(1.015-1.039)	<0.001
δ Ag_{max}-C	1.70 (1.21,4.83)	1.79 (1.27,9.10)	1.52 (1.16,2.98)	1.009(1-1.022)	0.089
δ Ag_{min}-C	-1.24 (-3.81,0.00)	-1.70 (-8.89,-1.01)	-0.91 (-1.75,0.00)	0.9[illegible]3(0.962-0.997)	0.051
δ Ag_{std}-C	0.54 (0.36,1.32)	0.80 (0.37,3.16)	0.45 (0.34,0.70)	1.117(1.026-1.252)	0.025
δ Ag_{sum}-C	15.6 (9.64,38.6)	29.8 (13.5,71.6)	11.9 (7.79,17.5)	1.0[illegible]4(1.006-1.025)	0.003
δ Ps_{max}-C	33.0 (1.00,48.8)	33.0 (1.41,125)	31.0 (1.00,34.0)	1.0[illegible]8(1.003-1.015)	0.004
δ Ps_{std}-C	3.35 (0.24,6.16)	3.57 (0.29,11.7)	3.20 (0.24,4.86)	1.073(1.019-1.14)	0.013
δ Ps_{sum}-C	39.1 (6.00,86.1)	74.4 (8.31,161)	33.4 (4.00,66.0)	1.01(1.005-1.015)	<0.001
δ Ar_{max}-NP	136 (74.0,220)	182 (102,314)	105 (59.0,180)	1.002 (1.0002,1.003)	0.027
δ Ar_{std}-NP	29.6 (20.0,56.7)	31.7 (23.4,70.1)	25.7 (17.1,41.4)	1.0[illegible]4 (1.000,1.010)	0.067
δ Ar_{sum}-NP	2469 (1443,4286)	3369 (2230,5728)	1672 (1277,2987)	1.00020 (1.00006, 1.00034)	0.005
Ar_{max}-NP	3873 (3001,5765)	4269 (3260,6056)	3828 (2894,5406)	1.000101 (0.999989, 1.000213)	0.077
δ Ps_{sum}-NP	41.7 (22.2,79.9)	59.8 (39.8,104)	26.4 (20.1,51.1)	1.013(1.006-1.021)	0.001
δ Ar_{max}-N	435 (243,750)	539 (269,990)	404 (221,526)	1.001(1-1.002)	0.022
δ Ar_{min}-N	-170.00 (-369.00,-25.00)	-267.00 (-565.25,-108.75)	-79.00 (-224.00,-15.00)	0.998(0.996-0.999)	0.002
δ Ar_{std}-N	125 (80.2,225)	160 (90.5,273)	114 (74.6,158)	1.005(1.002-1.008)	0.003
δ Ar_{sum}-N	12585 (7372,23204)	19058 (10208,29054)	9520 (6202,15009)	1.000084 (1.000046, 1.000122)	<0.001
Ar_{max}-N	53635 (43655,65410)	56546 (44597,77766)	51431 (38201,58878)	1.000014 (1.000002, 1.000026)	0.025
δ $ArRto_{max}$-PN	0.01 (0.00,0.02)	0.01 (0.00,0.03)	0.00 (0.00,0.01)	4.494e+1[illegible](5.890e+2,3.427+29)	0.008

Parameters	ALL N=141	FFR-Positive N=68	FFR-Negative N=73	Odds Ratio (95%CI)	P value
δ $ArRto_{min}$-PN	-0.02 (-0.05,-0.01)	-0.02 (-0.07,-0.01)	-0.02 (-0.04,-0.01)	<0.001 (0,0.062)	0.014
δ $ArRto_{std}$-PN	0.01 (0.00,0.02)	0.01 (0.00,0.02)	0.01 (0.00,0.01)	3.177e+16 (1.758e+3,5.740e+29)	0.015
δ $ArRto_{sum}$-PN	0.63 (0.32,1.72)	0.85 (0.39,2.36)	0.58 (0.29,0.88)	1.5[illegible]9 (1.175,2.117)	0.004
δ Ar_{max}-PP	195 (126,404)	281 (141,704)	153 (111,286)	1.0[illegible]1 (1.001,1.003)	0.001
δ Ar_{min}-PP	-171.00 (-295.00,-106.00)	-196.00 (-563.75,-109.50)	-153.00 (-226.00,-104.00)	0.9[illegible]8 (0.996,0.999)	0.003
δ Ar_{std}-PP	54.3 (33.7,124)	77.3 (35.5,167)	43.7 (32.1,79.7)	1.0[illegible]7 (1.003,1.012)	0.004
δ Ar_{sum}-PP	4689 (2685,8783)	6608 (3410,14024)	3487 (2556,5786)	1.00[illegible]12[illegible] (1.000053, 1.000187)	<0.001
Ar_{min}-PP	5151 (2774,7571)	4626 (2618,6928)	5754 (3719,8258)	0.999[illegible]3 (0.999933, 1.000003)	0.06
δ Ps_{max}-PP	3.16 (2.24,5.00)	3.61 (3.00,100)	3.00 (2.24,3.61)	1.0[illegible]1(1.005-1.019)	0.002
δ Ps_{std}-PP	0.82 (0.60,1.15)	0.98 (0.66,8.50)	0.75 (0.57,0.90)	1.[illegible]17(1.05-1.221)	0.003
δ Ps_{sum}-PP	40.4 (23.1,88.6)	73.8 (29.9,195)	32.8 (21.7,54.2)	1.0[illegible]2(1.006-1.019)	<0.001
δ Ar_{max}-P	244 (90.0,430)	312 (150,692)	172 (70.0,362)	1.001(1-1.002)	0.007
δ Ar_{std}-P	120 (80.2,203)	135 (82.3,267)	109 (75.7,159)	1.002(1-1.005)	0.07
δ Ar_{sum}-P	11899 (6525,19157)	15787 (7938,28576)	9566 (5985,15629)	1.000[illegible]46 (1.000017, 1.000074)	0.001
MAg_{max}-TT	-62.32 (-70.64,-34.61)	-48.00 (-66.89,15.5)	-67.39 (-72.03,-53.13)	1.0[illegible]9(1.009-1.029)	<0.001
CAg_{max}-TT	45.0 (33.3,71.0)	58.2 (39.2,118)	43.1 (32.0,51.1)	1.0[illegible]8(1.009-1.028)	<0.001
MAg_{min}-TT	-70.76 (-76.85,-56.92)	-68.28 (-75.62,-41.24)	-71.98 (-77.61,-64.94)	1.0[illegible]9(1.000-1.018)	0.052
MAg-R_p	-61.41 (-71.15,-42.88)	-53.44 (-70.66,-38.24)	-65.92 (-71.78,-50.54)	1.0[illegible]5(1.003-1.028)	0.017
RtoAm-R_pT_pN	6.49 (4.32,9.57)	7.35 (4.92,10.4)	5.68 (3.71,8.14)	1.0[illegible]5(1.005-1.126)	0.064
RtoAm-R_pT_pP	7.97 (5.88,12.0)	8.66 (6.03,12.9)	7.69 (5.56,11.1)	1.0[illegible](1.004-1.133)	0.061
RtoAm-R_pT_p	3.64 (2.38,4.70)	4.13 (3.08,5.01)	3.28 (2.36,4.50)	1.2[illegible]7(1.047-1.445)	0.016
MAg-T_p	-64.66 (-71.34,-45.44)	-55.82 (-70.28,-12.79)	-67.91 (-72.69,-53.13)	1.0[illegible]5(1.006-1.026)	0.002
CAg_{max}-T_p	43.1 (29.4,52.0)	45.0 (27.6,74.7)	42.2 (30.7,46.9)	1.0[illegible]9(1.001-1.017)	0.037
RtoAm-T_p	0.76 (0.57,1.08)	0.81 (0.52,1.22)	0.75 (0.57,0.98)	1.5[illegible]9(0.978-2.618)	0.095

Dt = Distance, Ps = Position, Ag = Angle, Am = Magnitude, Ar = Area, Rto = Ratio, P = Positive, Positive Pole = PP, N = Negative, NP = Negative Pole, M = Magnetic Field, C = Current, max = Maximum, min = Minimum, sum=Sum of all, std = Standard deviation, δ = Change value, TT= TT segment (the position from one-third of the T max amplitude (T onset) to T max (T peak)), R_p=R peak, T_p=T peak

Supplementary Table 3 Diagnostic model for assessment of myocardial ischemia in borderline coronary artery lesions

Parameters	Diagnostic model			
	B	OR	95%CI	P value
MAg_{max}-TT	1.385	3.995	(1.592-10.023)	0.003
δDt_{sum}-PN	0.671	1.956	(1.270-3.012)	0.002
δAg_{sum}-C	0.411	1.508	(0.989-2.298)	0.056
δAr_{sum}-N	0.641	1.899	(1.251-2.883)	0.003
δAr_{min}-N	0.515	1.674	(1.121-2.500)	0.012

M= Magnetic Field; Ag= Angle; TT= from T onset to T peak; δ= Change value; DT= Distance; PN= Positive Pole to Negative Pole; C=Current; Ar= Area; N= Negative Pole; ; τ= one tenth of the time interval between TT segment.

BMJ Open

Development and validation of a clinical diagnostic model for myocardial ischemia in borderline coronary lesions based on optical pumped magnetometer magnetocardiography: a prospective observational cohort study

Journal:	*BMJ Open*
Manuscript ID	bmjopen-2024-086433.R3
Article Type:	Original research
Date Submitted by the Author:	13-Sep-2024
Complete List of Authors:	yang, shuwen; Capital Medical University Affiliated Anzhen Hospital, Department of Cardiology Feng, Lanxin; Capital Medical University Affiliated Anzhen Hospital, Department of Cardiology Zhang, Mingduo; Capital Medical University Affiliated Anzhen Hospital Zhang , Min; Capital Medical University Affiliated Anzhen Hospital Ma, Zhao; Capital Medical University Affiliated Anzhen Hospital, Department of Cardiology Zhang, Huan; Capital Medical University Affiliated Anzhen Hospital, Department of Cardiology Zhang, YaZhe; Capital Medical University Affiliated Anzhen Hospital, Department of Cardiac Surgery Liu, Linqi; Capital Medical University Affiliated Anzhen Hospital, Department of Cardiology Zhou, Shu; Capital Medical University Affiliated Anzhen Hospital, Department of Cardiology Zhao, Xin; Capital Medical University Affiliated Anzhen Hospital, Department of Cardiology Yang, Xue Yao; Capital Medical University Affiliated Anzhen Hospital He, Jiqiang; Capital Medical University Affiliated Anzhen Hospital, Cardiology Ren, Yanlong; Capital Medical University Affiliated Anzhen Hospital Luo, Yawei; Capital Medical University Affiliated Anzhen Hospital Xu, Feng; Capital Medical University Affiliated Anzhen Hospital Tu, Chenchen; Capital Medical University Affiliated Anzhen Hospital, Department of Cardiology song, xiantao; Capital Medical University Affiliated Anzhen Hospital, Department of Cardiology Zhang, Hong-Jia; Capital Medical University Affiliated Anzhen Hospital,
Primary Subject Heading:	Diagnostics
Secondary Subject Heading:	Diagnostics
Keywords:	Diagnostic Imaging, Ischaemic heart disease < CARDIOLOGY, Clinical Trial

SCHOLARONE™
Manuscripts

I, the Submitting Author has the right to grant and does grant on behalf of all authors of the Work (as defined in the below author licence), an exclusive licence and/or a non-exclusive licence for contributions from authors who are: i) UK Crown employees; ii) where BMJ has agreed a CC-BY licence shall apply, and/or iii) in accordance with the terms applicable for US Federal Government officers or employees acting as part of their official duties; on a worldwide, perpetual, irrevocable, royalty-free basis to BMJ Publishing Group Ltd ("BMJ") its licensees and where the relevant Journal is co-owned by BMJ to the co-owners of the Journal, to publish the Work in this journal and any other BMJ products and to exploit all rights, as set out in our licence.

The Submitting Author accepts and understands that any supply made under these terms is made by BMJ to the Submitting Author unless you are acting as an employee on behalf of your employer or a postgraduate student of an affiliated institution which is paying any applicable article publishing charge ("APC") for Open Access articles. Where the Submitting Author wishes to make the Work available on an Open Access basis (and intends to pay the relevant APC), the terms of reuse of such Open Access shall be governed by a Creative Commons licence – details of these licences and which Creative Commons licence will apply to this Work are set out in our licence referred to above.

Other than as permitted in any relevant BMJ Author's Self Archiving Policies, I confirm this Work has not been accepted for publication elsewhere, is not being considered for publication elsewhere and does not duplicate material already published. I confirm all authors consent to publication of this Work and authorise the granting of this licence.

Development and validation of a clinical diagnostic model for myocardial ischemia in borderline coronary lesions based on optical pumped magnetometer magnetocardiography: a prospective observational cohort study

Shuwen Yang1#, Lanxin Feng 1#, Mingduo Zhang1, Min Zhang1, Zhao Ma1, Huan Zhang1, Yazhe Zhang2, Linqi Liu1, Shu Zhou1, Xin Zhao1, Xueyao Yang1, Jiqiang He1, Yanlong Ren1, Yawei Luo1, Feng Xu1, Chenchen Tu1*, Xiantao Song1*, Hongjia Zhang2

#These authors contributed equally to this work.

* These corresponding authors contributed equally to this work.

1Department of Cardiology, Beijing Anzhen Hospital, Capital Medical University, 100029, Beijing, China

2Department of Cardiac Surgery, Beijing Anzhen Hospital, Capital Medical University, 100029, Beijing, China

Corresponding Author:

The first corresponding author：Dr ChenChen Tu

Department of Cardiology, Anzhen Hospital, Capital Medical University, 2 Anzhen Road, Chaoyang District, 100020, Beijing, China E-mail: tcc2033@163.com

Dr Xiantao Song

Department of Cardiology, Anzhen Hospital, Capital Medical University, 2 Anzhen Road, Chaoyang District, 100020, Beijing, China E-mail: song0929@mail.ccmu.edu.cn

Disclosures: The authors have nothing to disclose.

Abstract

Objectives: To develop and validate a clinical diagnostic model based on optical pumped magnetometer magnetocardiography (OPM-MCG) for the detection of myocardial ischemia in patients with borderline coronary lesions prior to invasive coronary angiography (CAG).

Design: Prospective observational cohort study.

Setting: Single center of the China National Clinical Research Center for Cardiovascular Disease (NCCMRC).

Participants: Adults with borderline coronary lesions on CAG (N=141).

Interventions: Underwent OPM-MCG before CAG and fractional flow reserve (FFR) measurement.

Results: Five parameters were included in the final diagnostic model: MAg_{max}-TT, δDt_{sum}-PN, δAg_{sum}-C, δAr_{sum}-N and δAr_{min}-N. 1000 bootstrap replications showed that the area under the receiver operating characteristic curve (AUC) and 95% confidence interval (CI) of the diagnostic model were 0.864 (0.803-0.925), with sensitivity of 79.4%, specificity of 80.8%, positive predictive value of 79.4%, negative predictive value of 80.8%. Decision curve analysis showed a net benefit from the predictive model when the threshold probability of an ischemic patient was greater than 12%, suggesting the potential utility of the model in the real world.

Conclusions: A nomogram based on five OPM-MCG parameters was developed to assess myocardial ischemia in patients with borderline coronary lesions and has the potential to reduce the need for unnecessary CAG.

Trial registration number: ChiCTR2300072382.

Keywords: borderline coronary lesions; optical pumped magnetometer magnetocardiography; fractional flow reserve; myocardial ischemia

Strengths and limitations of this study

1) As a prospective observational cohort study, this study provides real-world evidence of the diagnostic performance of OPM-MCG for myocardial ischemia, enhancing the generalization of the findings.

2) The study was a single-center study, which may affect its adaptability to different settings.

3) The clinical diagnostic model did not account for myocardial ischemia due to coronary microcirculatory dysfunction and did not include evaluations performed with other magnetocardiography devices.

Introduction

Borderline coronary lesions exhibit ranging from 40% to 90% as seen in invasive coronary angiography (CAG). The FAME study [1] found that over 80% of lesions fell into this category, with only 35% of stenoses between 50-70% being hemodynamically significant. Predicting relevance was most accurate when estimating coronary artery diameter over 90%. Therefore, fractional flow reserve (FFR) guided intervention in patients with borderline coronary lesions (40-90% stenosis) has become a recommended treatment strategy in the 2018 ESC Interventional Guidelines [2]. The 2021 ACC/AHA/SCAI Guidelines for Coronary Artery Revascularization [3] also provide clear recommendations for managing borderline coronary lesions: FFR and instantaneous wave-free ratio (iFR) are used to assess the need for percutaneous coronary intervention (PCI) in patients without evidence of ischemia but with angina and other equivalent symptoms (Class I); PCI is not recommended for stable patients with FFR >0.8 or iFR >0.89 (Class III). However, its widespread adoption in coronary catheter laboratories is hindered by its time-consuming nature, resource consumption, and potential adverse effects associated with adenosine application.

Optical pumped magnetometer magnetocardiography (OPM-MCG) measures tiny magnetic fields (10^{-15} Tesla) from the heart using atomic magnetometer technology, without radiation. It is quick, contactless, and suitable for diverse populations. Clinical studies have demonstrated that magnetocardiography (MCG) is superior to electrocardiogram (ECG) in detecting early myocardial ischemia [4,5,6,7] and has similar diagnostic effectiveness as SPECT for coronary artery disease (CAD) [8,9]. MCG was proven to be precise in diagnosing non-ST-segment elevation myocardial infarction, even in individuals who do not exhibit typical angina symptoms. [10,11]. However, the parameters and cut-off values of OPM-MCG that indicate myocardial ischemia in borderline coronary lesion are presently undefined.

Hence, this study aims to investigate the accuracy of OPM-MCG in diagnosing myocardial ischemia in patients with borderline coronary lesions, with invasive FFR measurement serving as the reference standard.

Method

Study population

This study was a prospective, single-center, observational, cohort study which was reviewed by the Ethics Committee of Beijing Anzhen Hospital, Capital Medical University, and registered with the China Clinical Trial Registry (ChiCTR2300072382). All participants signed an informed consent. The methods described in this article follow the STARD 2015 guidelines.

Participants aged 18-80 with typical angina symptoms (CCS class II or higher) or 40-90% stenosis on CCTA were scheduled for hospitalization for CAG. Exclusion criteria included: 1) Coronary artery stenosis outside of 40%-90% range on CAG; 2) Acute myocardial infarction; 3) Previous myocardial infarction; 4) Complex arrhythmias; 5) Bundle-branch block; 6) Pacemakers, metallic implants in trunk; 7) Claustrophobia.

This study was based on a prospective cohort design, the sample size of which was calculated by PASS 2021 software using the area under the receiver-operating characteristic (ROC) curve. The significance level (α) was 0.025 and the degree of certainty (1-β) was 0.90, combining the results of the literature review of related studies as well as the statistics of the small sample in the previous period, and calculating according to the FFR-positive (ischemic)/FFR-negative (non-ischemic) =2:3. The sample size was calculated as 138.

A total of 163 patients from June 30th to November 30th, 2023 were consecutively enrolled, and 22 patients were excluded, of which 11 patients with stenosis >90%, 7 patients underwent direct PCI without FFR testing, and 4 patients with poor quality MCG imaging, and Finally 141 patients with borderline coronary lesions underwent MCG and FFR sequentially (Figure 1). In this study, the cardiologists were not aware of the MCG results at the time of the FFR examination, and the MCG parameters were determined before the FFR examination (Supplementary Figure 1-Graphical Abstract).

CAG and FFR procedures

CAG and FFR measurements were performed on the vessels according to the 2021 ACC/AHA/SCAI Guidelines for Coronary Artery Revascularization and Expert consensus on the clinical pathway for FFR measurement in China. After administration of nitroglycerin, a pressure monitoring guidewire was advanced through the stenosis. Hyperemia was attained by administration of intravenous adenosine (140μg/kg/min). The FFR pressure wire was positioned a minimum of 20 mm distal to the stenosis in vessel segments ≥2 mm. The presence of an FFR ≤0.80 was considered a positive indicator of functional ischemia in patients and was defined as the FFR-positive group.

MCG imaging

The MCG recordings were conducted using a 36-channel OPM-MCG system (Miracle MCG), featuring OPM sensors sourced from Beijing X-Mag Technologies Limited's mature commercial product. The OPM sensor is based on spin-exchange relaxation free (SERF) technology, with alkali metal atoms as the core sensitive element. The OPM sensor has a sensitivity below 30 $fT/Hz^{1/2}$, a recording bandwidth of 1 Hz to 40 Hz, a sampling frequency of 200 Hz, and a noise baseline with not higher than 15 fT. The OPM-MCG residual magnetic field is kept below 1.5 nT, and the data acquisition mode is analog signal acquisition (Supplementary Figure 2). Each subject had a 90-second continuous recording at 36 locations (6×6 grid) above the chest using an arrayed sensor grid.

MCG Signal Analysis and Statistical Analysis

After MCG data acquisition, the software automatically post-processes the signals to generate magnetic field and current density maps and output sixty-five parameters (Supplementary Table 1). The sixty-five parameters we output characterize the stability of the current dipole in the TT segment (the position from one-third of the T max amplitude (T onset) to T max (T peak)) according to the previous studies of Park et al. and Pena et al. (see supplementary material for post-processing steps).

Statistical analysis was performed with SPSS 25.0 and R 4.3.2 (http //www.R-project.org/). Counting data were presented as numbers and percentages, while normally distributed measurement data were shown as mean ± standard deviation. Continuous variables that were not normally distributed were presented using median and quartile values. Statistical significance was determined for all analyses with a P-value less than 0.05. Based on this cohort and the principle of at least 10 events per variable (10 EPV), we considered the rationality of the parameters included in the diagnostic model and evaluated the number of parameters. sixty-five potential predictor variables were evaluated using univariable logistic regression, selecting those with p-values < 0.1. These variables were then subjected to Least Absolute Shrinkage and Selection Operator (LASSO) regression, ultimately identifying the most impactful predictors. Continuous variables representing the amount of change were transformed into ordered categorical variables based on interquartile range. Continuous variables representing absolute values were converted into dichotomous variables by grouping their upper and lower quartile values into extreme categories, while middle-range values were grouped and incorporated into the model. The final model was developed using multivariate logistic regression with a backward selection approach. The model's predictive performance was assessed using the enhanced bootstrap method and clinical benefit was evaluated using decision curve analysis. The nomogram was used to report scores for assessing myocardial ischemia with OPM-MCG parameters.

Patient and Public Involvement

Patients make more people aware of the clinical use of the OPM-MCG and how it is examined by sharing news and information about clinical studies with others.

Result

Clinical characteristics

The study included 141 patients, mostly male (77.3%) with an average age of 60.64 ± 9.70 years. After MCG scans, all patients underwent CAG and FFR examination, with 48.2% having positive FFR (FFR ≤ 0.8). A total of 157 vessels were examined, with 47.1% having FFR ≤ 0.8. Interval between MCG and FFR less than 30 days, median 2 days. Most patients had FFR measurements primarily done on the left anterior descending artery. See Table 1 for patient clinical characteristics.

Selection of parameters and development of the diagnostic model

Fifty variables that were statistically significant (P < 0.1) in univariable logistic regression were included in the LASSO regression (Supplementary Table 2 and Supplementary Figure 3), and 8 variables were selected based on the reasonableness of the parameters selected to reduce the model overfitting and covariance through LASSO regression. By using the backward approach, 5 parameters were included in the final diagnostic model: MAg_{max}-TT, δDt_{sum}-PN, δAg_{sum}-C, δAr_{sum}-N and δAr_{min}-N (Table 2, Figure 2). The model area under the receiver operating characteristic curve (AUC) obtained from multivariate logistic regression analysis was 0.864, with sensitivity of 79.4%, specificity of 80.8%, positive predictive value of 79.4%, negative predictive value of 80.8% (See Supplementary Figure 4 for the confusion matrix of the diagnostic model). The nomogram (Figure 3) provides a graphical overview of the diagnostic model using multivariate logistic regression analysis (Supplementary Table 3).

Internal validation and net benefit of the model

The model performance for the diagnosis of myocardial ischemia in borderline coronary lesions of the OPM-MCG was evaluated by bootstrap replications. 1000 bootstrap replications showed that the model AUC and a 95% confidence interval (CI) of 0.864(0.803-0.925) (Figure 4). 1000 bootstrap replications showed that the mean absolute error was 0.017 (Figure 4). The decision curve analysis (DCA) for the diagnostic model showed that if the threshold probability of patients is greater than 12% (Figure 4), screening strategies based on the OPM-MCG diagnostic model resulted in superior net benefit than screen-none or screen-all strategies.

Discussion

CAD is presently characterized by an epicardial vascular lesion with a stenosis exceeding 50% in the CAG. Frequently, the degree of stenosis indicated by CAG is used as a reference standard for myocardial revascularization. Moreover, FFR can be used to evaluate the existence of myocardial ischemia, with a threshold of 0.8. However, as illustrated in Figure 2, the coronary stenosis identified in CAG may not precisely align with the FFR results. This observation is in line with the conclusions drawn in the 2019 ESC Guidelines for Chronic Coronary Syndromes [12,13], emphasizing that the accuracy of determining CAD solely based on angiographic stenosis was as low as 64% when compared to flow reserve fraction. The positive mismatch rate, where lesions with less than 50% stenosis may demonstrate an FFR ≤ 0.8, was 19%, while the negative mismatch rate, where lesions with over 50% stenosis may result in an FFR value > 0.8, reached up to one-third. Numerous studies [14,15] have consistently demonstrated that FFR-guided stenting leads to superior immediate outcomes and long-term prognosis. Therefore, FFR carries a Class 1a recommendation for guiding revascularization in angiographically borderline coronary stenoses in patients with stable angina. The feasibility of diagnosing myocardial ischemia in patients with borderline coronary lesions using OPM-MCG was shown in our study, when compared to invasive FFR. The collective diagnostic potential of MCG parameters in detecting myocardial ischemia in borderline coronary lesions resulted in an AUC of 0.864 (95% CI 0.803 to 0.925). Due to factors such as time consumption, costs, patient-related discomfort, contraindications, and a lack of reimbursement, the current rate of FFR utilization in catheterization laboratories in China is less than 6% [3]. OPM-MCG allows ischemia assessment in patients with borderline coronary lesions prior to CAG and has a good concordance with FFR.

In comparing our MCG results with those reported by Park JW et al. [16], it is clear that FFR, serving as the reference standard, evaluates ischemia through direct measurement of pressure beyond the coronary lesion. In contrast, the Five parameters of our OPM-MCG, along with the ST-segment fluctuation scores (AUC=0.835) and Bull's eye analysis (AUC=0.914) employed by Park, offer a non-invasive alternative. According to Park JW et al, the TT segment, defined as the interval from T onset to T peak, is a more effective parameter for analyzing MCG signals due to its superior signal-to-noise ratio for reflecting ventricular repolarization electrical activity [17]. In terms of the selected parameters, consistent with earlier literature [18], we focused on assessing the overall homogeneity of the repolarization process, including spatial structural similarity and smoothing of current changes. Park et al. utilized ST-segment fluctuation scores and Bull's eye analysis to evaluate the uniformity of the repolarization process in relation to current variations and spatial distribution variances for ischemia assessment. In our study, we further characterized the images by incorporating the δDt_{sum}-PN, δAg_{sum}-C, δAr_{sum}-N and δAr_{min}-N parameters of the model to analyze changes in currents, pole areas, and distances. Additionally, describing the images using the parameters of the 3 different angular points provided a comprehensive description and response to the images. In terms of image feature discrimination, the ischemia-positive features of the OPM-MCG (pole multipolarization and magnetic field angle deflection) initially are consistent with the FFR (Figure 2). For practical clinical application, Park JW et al. used a 64-channel axial gradiometer system, which offers greater channel capacity and higher sensitivity for positional discrimination. However, this approach required patients to complete two MCG tests—one during stress and one at rest—in a shielded room. Comparatively, OPM-MCG is equipped with a shielding barrel that can effectively diagnose myocardial ischemia caused by borderline coronary lesions at rest, without the need for a specially constructed shielding room. This enhances the practicality and universality of its clinical application.

Non-invasive methods like positron emission tomography / computed tomography

(PET/CT), single-photon emission computed tomography (SPECT) and cardiovascular magnetic resonance (CMR) are accurate for assessing myocardial ischemia, but their use is limited due to cost, long wait times and radioactive substances [19]. In a prospective study done by Roel S. et al. [20], which included 189 patients in a head-to-head comparison, it was found that using FFR as the gold standard, the sensitivity of SPECT, PET/CT, and CMR was only 67%, 81%, and 66%, and the specificity was only 61%, 65%, and 62%. The diagnostic accuracy of PET/CT was not statistically different from that of SPECT and CMR. Recently, CT-derived fractional flow reserve (CT-FFR) has emerged as a noninvasive test for detecting myocardial ischemia, with a sensitivity of 89% and specificity of 91% according to a multicenter study [21]. The widespread use of CT-FFR has limitations including the need for good image quality and inability to assess microvascular and diffuse lesions [22]. ECG is widely used in the clinic as the fastest and low-cost test. ECG uses a two-dimensional linear approach to record cardiac radial currents to detect ischemia, but it can be affected by body tissues or fluids and has low spatial resolution. MCG detects and measures weak magnetic fields generated by the electrical activity of the heart, and the waveform of the MCG waveform is similar to that of the ECG signal. However, MCG is less affected by changes in conductivity and does not suffer from skin electrode contact problems. In addition, MCG is more sensitive to magnetic fields generated by tangential currents that are more affected by myocardial ischemia, and MCG detects eddy currents that are not apparent with ECG [23]. Thus, previous studies have demonstrated that MCG has a higher sensitivity to early myocardial ischemia [24,25]. In most studies of MCG detection of myocardial ischemia, researchers have categorized the analysis of MCG into morphological and quantitative data analyses [26]. Morphological analysis often focuses on amplitude, nondipole phenomena, and current or magnetic field angle. Quantitative data analysis is mostly based on changes in the magnetic field during ventricular repolarization, usually at the end of the ST segment (before the T wave) and/or during the T wave, and partially measured during the QT and QRS segment. These parameters describe the poles, the angles of the magnetic and current fields, and the waveform amplitude by extrema, dynamics, and ratios. Current studies analyzing MCG at rest for the detection of myocardial ischemia use a variety of methods, including dichotomous classification methods based on MCG parameters, quantification of abnormal MCG parameters, creation of composite indices using MCG parameters, and the application of machine-learning methods [27].

This is similar to our finding that a positive OPM-MCG scan was demonstrated by one or more abnormalities in the TT segment, including changes in TT segment parameters and the changes in image (non-dipole phenomena and angular deflection of currents or magnetic fields). Different MCG parameters and their combinations can provide more incremental information on cardiovascular disease. In addition, studies have shown that MCG is capable of accurately diagnosing myocardial ischemia resulting from epicardial coronary artery disease as well as effectively detecting myocardial ischemia caused by coronary microvascular dysfunction (CMD). The accuracy of MCG identification of CMD is 94.8%, sensitivity of 100%, and specificity of 93.3% [28]. In our study, we also found a small number of FFR-negative patients with positive MCG scans as described above, and considered the possibility of CMD. In the future, we will summarize the characteristic images of patients with CMD and further explore the incremental information provided by the MCGs for these patients.

The difference between SQUID-based and OPM-based MCG systems lies on their sensor technology. SQUID-based MCGs were developed earlier and offer high sensitivity. But their reliance on liquid helium refrigeration for achieving low-temperature superconductivity, as well as the high maintenance costs associated with them, have hindered their widespread adoption and utilization. In contrast, the OPM-MCG operates at room temperature without liquid helium cooling and offers comparable sensitivity, as it is easier to use and less expensive to operate [29,30]. However, OPM-MCG is also unsuitable for claustrophobic patients. Furthermore, as a result of its late development, there is a lack of established guidelines for analyzing MCG parameters. As such, we intend to conduct further exploratory studies on OPM-MCG in various clinical settings.

Limitation

The study is a single-center registry study with some limitations. We are aware that the current diagnostic model may suffer from potential overfitting and therefore the conclusions of this study require further validation in multicenter studies. In addition, the definition of positive and negative poles we currently use differs from the Rome Biomag Conference in 1981 standard, and there are currently multiple types of MCGs globally, and the current methodology for analyzing myocardial ischemia has not been compared head-to-head with other MCG devices.

Conclusion

MCG shows excellent sensitivity, specificity, and diagnostic accuracy in identifying significant myocardial ischemia when compared to FFR. MCG can provide the evidence of a precise diagnostic strategy in patients with borderline coronary lesions before CAG, reducing unnecessary invasive examination.

Ethics approval and consent to participate

This study was performed in accordance with the principles of the Declaration of Helsinki. This study was approved by the ethics committee of Beijing Anzhen Hospital, Capital Medical University (KS2023008). Written informed consent was required for participation in the study.

Competing interests

The authors declare that they have no conflicts of interest.

Funding statement

This work was supported by Coordinated innovation of scientific and technological in Beijing-Tianjin-Hebei Region (Z231100003923008), Beijing Nova Program (20220484222) , Capital's Funds for Health Improvement and Research (2024-2-2066) , Beijing Hospitals Authority 'sailing' Program (YGLX202323), Beijing Hospitals Authority's Ascent Plan (DFL20220603) , High-level public health technical talent construction project of Beijing Municipal Health Commission (Leading Talent-02-01) and Project of The Beijing Lab for Cardiovascular Precision Medicine (PXM2018_014226_000013).

Author Contribution Statement

Xiantao Song and Chenchen Tu acted as guarantors. Xiantao Song, Chenchen Tu and

Hongjia Zhang helped to conceive the topic and revised the article. Shuwen Yang and Lanxin Feng wrote the manuscript and finished the statistics, Mingduo Zhang, Min Zhang, Jiqiang He, Yanlong Ren, Yawei Luo and Feng Xu contributed to the data collection. Zhao Ma, Huan Zhang, Yazhe Zhang, Linqi Liu, Shu Zhou, Xin Zhao, and Xueyao Yang helped with data analysis. All authors read and approved the final manuscript.

Acknowledgments

The authors thank Zhechun Zeng, Ming Ding, and Bin Cai for their help in data analysis, and Xin Chen, Jinfan Tian, and Yulong Xue for their help in data collection.

Abbreviations

AUC= area under the receiver operating characteristic curve

CAD= coronary artery disease

CAG= coronary angiography

CCTA= coronary computed tomography angiography

CI= confidence intervals

CMR= cardiovascular magnetic resonance

CT-FFR= CT-derived fractional flow reserve

ECG= electrocardiogram

FFR= fractional flow reserve

iFR=instantaneous wave-free ratio

LASSO= Least Absolute Shrinkage and Selection Operator

MCG= magnetocardiography

OPM-MCG= optical pumped magnetometer magnetocardiography

PCI= percutaneous coronary intervention

PET/CT= positron emission tomography / computed tomography

ROC= receiver-operating characteristic

SPECT= single-photon emission computed tomography

Availability of data and materials

The data that support the findings of this study are available on request from the corresponding author, Xiantao Song， upon reasonable request.

Reference

[1] van Nunen LX, Zimmermann FM, Tonino PA, et al. Fractional flow reserve versus angiography for guidance of PCI in patients with multivessel coronary artery disease (FAME): 5-year follow-up of a randomised controlled trial. Lancet. 2015;386(10006):1853-1860.

[2]Neumann FJ, Sousa-Uva M, Ahlsson A, et al. 2018 ESC/EACTS Guidelines on myocardial revascularization [published correction appears in Eur Heart J. 2019 Oct 1;40(37):3096]. Eur Heart J. 2019;40(2):87-165.

[3] Writing Committee Members, Lawton JS, Tamis-Holland JE, Bates ER, et al. 2021 ACC/AHA/SCAI Guideline for Coronary Artery Revascularization: Executive Summary: A Report of the American College of Cardiology/American Heart Association Joint Committee on Clinical Practice Guidelines [published correction appears in J Am Coll Cardiol. 2022 Apr 19;79(15):1547]. J Am Coll Cardiol. 2022;79(2):197-215.

[4] Nomura M, Nakaya Y, Fujino K, et al. Magnetocardiographic studies of ventricular

repolarization in old inferior myocardial infarction. Eur Heart J. 1989;10(1):8-15.

[5] Brisinda D, Meloni AM, Fenici R. First 36-channel magnetocardiographic study of CAD patients in an unshielded laboratory for interventional and intensive cardiac care. Funct Imaging Model Hear. 2003;LNCS 2674:122-131.

[6] Gapelyuk A, Wessel N, Fischer R, et al. Detection of patients with coronary artery disease using cardiac magnetic field mapping at rest. J Electrocardiol. 2007;40(5):401-407.

[7]Kanzaki H, Nakatani S, Kandori A, et al. A new screening method to diagnose coronary artery disease using multichannel magnetocardiogram and simple exercise. Basic Res Cardiol. 2003;98(2):124-132.

[8] Nakai K, Izumoto H, Kawazoe K, et al. Three-dimensional recovery time dispersion map by 64-channel magnetocardiography may demonstrate the location of a myocardial injury and heterogeneity of repolarization. Int J Cardiovasc Imaging. 2006;22(3-4):573-580. doi:10.1007/s10554-005-9019-x.

[9]Tolstrup, Kirsten, Donatella Brisinda, Am Meloni, et al. Comparison of resting magnetocardiography with stress single photon emission computed tomography in patients with stable and unstable angina. J Am Coll Cardiol 2006;47(4 Suppl 1):176A. Abstract 930-247.

[10] Lim HK, Kwon H, Chung N, et al. Usefulness of magnetocardiogram to detect unstable angina pectoris and non-ST elevation myocardial infarction. Am J Cardiol. 2009;103(4):448-454.

[11] Shin ES, Lam YY, Her AY, et al. Incremental diagnostic value of combined quantitative and qualitative parameters of MCG to detect coronary artery disease. Int J Cardiol. 2017;228:948-952.

[12] Knuuti J, Wijns W, Saraste A, et al. 2019 ESC Guidelines for the diagnosis and management of chronic coronary syndromes [published correction appears in Eur Heart J. 2020 Nov 21;41(44):4242]. Eur Heart J. 2020;41(3):407-477.

[13] Derimay F, Finet G and Rioufol G. Coronary artery stenosis prediction does not mean coronary artery stenosis obstruction. Eur Heart J. 2021;42(42):4401.

[14] Xaplanteris P, Fournier S, Pijls NHJ, et al. Five-Year Outcomes with PCI Guided by Fractional Flow Reserve. N Engl J Med. 2018;379(3):250-259.

[15] Zimmermann FM, Ferrara A, Johnson NP, et al. Deferral vs. performance of percutaneous

coronary intervention of functionally non-significant coronary stenosis: 15-year follow-up of the DEFER trial. Eur Heart J. 2015;36(45):3182-3188.

[16] Park JW, Shin ES, Ann SH, et al. Validation of magnetocardiography versus fractional flow reserve for detection of coronary artery disease. Clin Hemorheol Microcirc. 2015;59(3):267-281.

[17]Park J-W, Hill PM, Chung N, Hugenholtz PG, Jung F. Magnetocardiography predicts coronary artery disease in patients with acute chest pain. Ann Noninvasive Electrocardiol. 2005;10(3):312-323.

[18] Chaikovsky I, Hailer B, Sosnytskyy V, et al. Predictive value of the complex magnetocardiographic index in patients with intermediate pretest probability of chronic coronary artery disease: results of a two-center study. Coron Artery Dis. 2014;25(6):474-484.

[19] Working Group of Cardiovascular Imaging of National Center for Medical Quality Control of Cardiovascular Diseases Survey of the Application Status of Cardiovascular Imaging Modalities and Medical Quality Report in China [J]. Chin circ J ,2020,35(7):625-633.

[20] Driessen RS, van Diemen PA, Raijmakers PG, et al. Functional stress imaging to predict abnormal coronary fractional flow reserve: the PACIFIC 2 study. Eur Heart J. 2022;43(33):3118-3128.

[21] Tang CX, Liu CY, Lu MJ, et al. CT FFR for Ischemia-Specific CAD With a New Computational Fluid Dynamics Algorithm: A Chinese Multicenter Study. JACC Cardiovasc Imaging. 2020;13(4):980-990.

[22] Li Y, Yu M, Dai X, et al. Detection of Hemodynamically Significant Coronary Stenosis: CT Myocardial Perfusion versus Machine Learning CT Fractional Flow Reserve. Radiology. 2019;293(2):305-314.

[23]Chaikovsky I, Hailer B, Sosnytskyy V, et al. Predictive value of the complex magnetocardiographic index in patients with intermediate pretest probability of chronic coronary artery disease: results of a two-center study. Coron Artery Dis. 2014;25(6):474-484.

[24]Mace SE, Peacock WF, Stopyra J, et al. American Heart Journal Plus : Cardiology Research and Practice Accelerated magnetocardiography in the evaluation of patients with suspected cardiac ischemia : The MAGNETO trial. Am Hear J Plus Cardiol Res Pract.

2024;40(February):100372.

[25]Tolstrup K, Madsen BE, Ruiz JA, et al. Non-invasive resting magnetocardiographic imaging for the rapid detection of ischemia in subjects presenting with chest pain. Cardiology.

[26]Camm AJ, Henderson R, Brisinda D, et al. Clinical utility of magnetocardiography in cardiology for the detection of myocardial ischemia. J Electrocardiol. 2019;57:10-17.

[27] Rong Tao, Shulin Zhang, Xiao Huang, et al. Magnetocardiography-Based Ischemic Heart Disease Detection and Localization Using Machine Learning Methods. IEEE Trans Biomed Eng. 2019;66(6):1658-1667.

[28] Rong Tao, Shulin Zhang, Xiao Huang, et al. Magnetocardiography-Based Ischemic Heart Disease Detection and Localization Using Machine Learning Methods. IEEE Trans Biomed Eng. 2019;66(6):1658-1667.

[29]Brisinda D, Fenici P, Fenici R. Clinical magnetocardiography: the unshielded bet—past, present, and future. Front Cardiovasc Med. 2023;10(August):1-24.

[30] Pena ME, Pearson CL, Goulet MP, et al. A 90-second magnetocardiogram using a novel analysis system to assess for coronary artery stenosis in Emergency department observation unit chest pain patients. IJC Hear Vasc. 2020;26(100466):1-7.

Table 1 Clinical characteristics (n = 141)

Characteristics	Total(n=141)
Age (yrs)	60.64±9.70
Male, n (%)	109(77.3)
BMI (Kg/m2)	26.15±3.36
Diabetes, n (%)	47(33.3)
Hypercholesterolemia, n (%)	65(46.1)
Hypertension, n (%)	82(58.2)

Stroke, n (%)	9(6.4)
Smoke, n (%)	43(30.5)
Systolic blood pressure, mmHg	128.69±15.54
Diastolic blood pressure, mmHg	75.15±10.79
Heart rate	73.81±10.38
Medication, n(%)	
Aspirin	129(91.5)
Statin	137(97.2)
ACEI/ARB	45(35.6)
SGLT2 inhibitors	22(16.7)
Nicorandil	23(16.3)
Admission lab results	
Low-density lipoprotein cholesterol (mmol/L)	1.82±0.69
hs Tnl(pg/ml)	3.5(2.5,5.8)
Brain natriuretic peptide (pg/ml)	29.00(14.75,48.25)
Blood glucose (mmol/L)	5.52(4.82,7.33)
HbA1c(%)	6.25(5.7,7.1)
ICA and FFR characteristics	
1-vessel disease	50(35.5)
2-vessel disease	43(30.5)
3-vessel disease	48(34.0)

Number of patients with FFR⩽0.8	68(48.2)
Number of vessels with FFR	157
Number of vessels with FFR⩽0.8	74(47.1)
Left anterior descending artery with FFR	97(68.8)
Left circumflex artery with FFR	25(17.7)
Right coronary artery with FFR	35(24.8)
Interval between MCG and FFR	2(1,7)

Values are n (%) or mean ± SD

BMI= Body Mass Index, ACEI= angiotensin converting enzyme inhibitor, ARB = angiotensin receptor blocker, SGLT2 inhibitors = sodium-glucose cotransporter-2 inhibitors, HbA1c= glycated hemoglobin, ICA = invasive coronary angiography, FFR = fractional flow reserve.

Table 2 The definitions of the MCG parameters

MCG Parameters	Definitions
MAg_{max}-TT	The maximum magnetic field angle at intervals of a certain time τ within TT segment
δDt_{sum}-PN	The sum of changes in magnetic pole distance at intervals of a certain time τ within TT segment
δAg_{sum}-C	The sum of changes in current angle at intervals of a certain time τ within TT segment
δAr_{sum}-N	The sum of changes in negative pole area at intervals of a certain

	time τ within TT segment
δAr_{min}-N	The minimum value of changes in negative pole area at intervals of a certain time τ within TT segment

M= Magnetic Field; Ag= Angle; TT= from T onset to T peak; δ= Change value; DT= Distance; PN= Positive Pole to Negative Pole; C=Current; Ar= Area; N= Negative Pole; ; τ= one tenth of the time interval between TT segment.

Figure legend

Figure 1. Flowchart of the study design.

Figure legend: CCTA= coronary computed tomography angiography; MCG=magnetocardiography; ICA= invasive coronary angiography; FFR=fractional flow reserve; PCI= percutaneous coronary intervention.

Figure 2 Schematic diagram of OPM-MCG scan.

Figure legend: (A) Schematic diagram of MAg_{max}-TT and current angle. In magnetic field distribution maps and current density maps, the definition rule for angle values is based on the horizontal axis, with counterclockwise angles being negative and clockwise angles being positive. MAg_{max}-TT is the maximum angle between the line connecting the maximum positive and negative magnetic poles and the horizontal axis. in the TT segment. δAg_{sum}-C is the sum of changes in current angle at intervals of a certain time τ within TT segment (B)Normal OPM-MCG scan. The OPM-MCG scan showed no evidence of ischemia or obstructive coronary artery disease, as demonstrated by the lack of significant current deviations within the myocardium and absence of angle shift between the positive red pole and negative blue pole between T-onset and T-peak. (C) The OPM-MCG scan of a patient in his 70s showed magnetic field angular deflection, abnormal magnetic field distribution of the positive and multipolarisation of negative poles, suggesting significant myocardial ischemia, and the ECG showed no significant abnormality. The CAG showed two lesions: 60% stenosis of the D1, 50% stenosis of the R-PDA. The FFRs were 0.77 for the R-PDA. (D) The OPM-MCG scan of a patient in his 60s showed no myocardial ischemia, ECG showed no significant abnormalities, echocardiography showed widening of the ascending aorta and aortic sinus. CAG showed 75% stenosis of the LAD, 60% stenosis of the RCA, FFR value of the LAD was 0.88.

MCG= magnetocardiography; FFR= fractional flow reserve; ICA= invasive coronary angiography; D1= diagonal branches; R-PDA= posterior descending artery; LAD= left anterior descending artery; RCA= right coronary artery.

Figure 3. Nomogram of the diagnostic model.

Figure legend: The nomogram graphically demonstrates the diagnostic model of OPM-MCG. Points for MAg_{max}-TT, δDt_{sum}-PN, δAg_{sum}-C, δAr_{sum}-N and δAr_{min}-N can be obtained using a point caliper and then summed to obtain a total score that can be measured with diagnosing myocardial ischemia in patients with borderline coronary lesions.

Figure 4 Accuracy and internal validation of the diagnostic model.

Figure legend: (A) ROC curves for the diagnostic model. After 1000 bootstrap replications, the area under the curve and 95% confidence interval for receiver operating characteristic is 0.864 (0.803-0.925). (B) Calibration curve for the diagnostic model. Calibration curve for the borderline lesion ischemia diagnostic model was established by comparing the actual and predicted probability of a positive FFR in patients with borderline lesions of the coronary arteries. The smaller the distance of the scatter from the dashed line, the better the calibration. (C) Decision curve analysis (DCA) for diagnostic models of ischemia in borderline coronary lesions. Treat none: net benefit when it is assumed that no patients with borderline lesions of the coronary arteries would have the outcome (FFR-positive). Treat all: net benefit when all patients with borderline coronary lesions are assumed to have an outcome (FFR-positive). Diagnostic model: net benefit of managing borderline coronary lesions with a diagnosis of myocardial ischemia based on the diagnostic model estimate. The strategy with the highest net benefit at any given threshold is the preferred strategy.

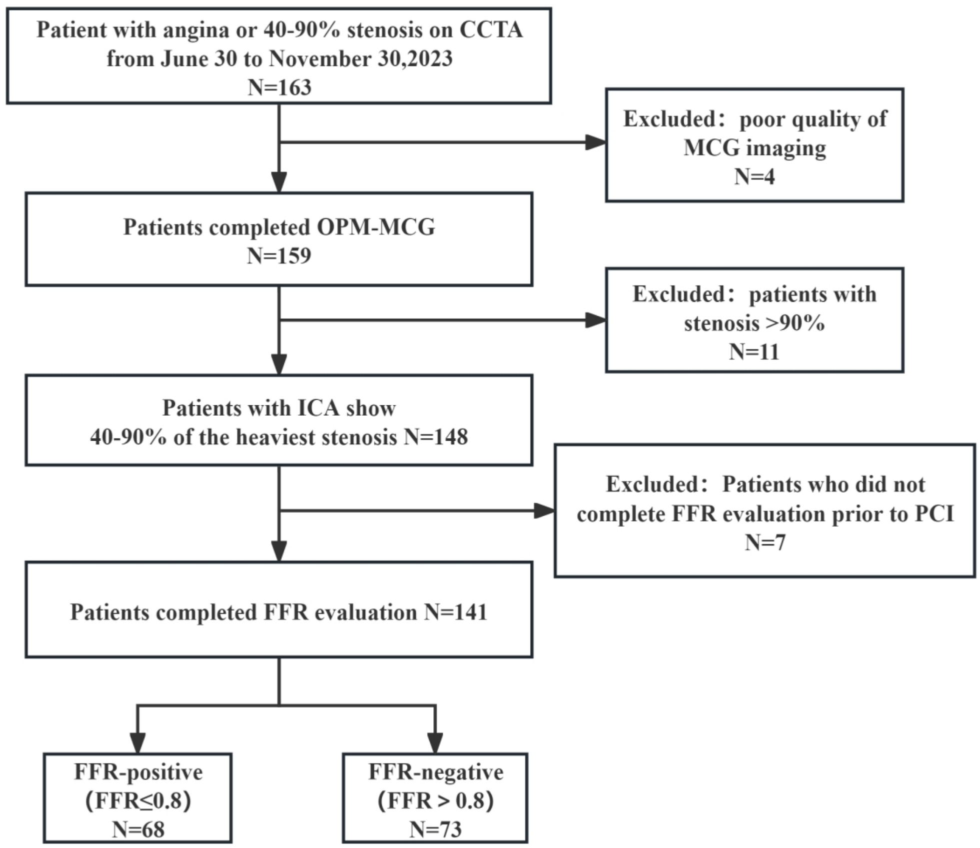

Figure 1. Flowchart of the study design.
Figure legend: CCTA= coronary computed tomography angiography; MCG=magnetocardiography; ICA= invasive coronary angiography; FFR=fractional flow reserve; PCI= percutaneous coronary intervention.

510x441mm (96 x 96 DPI)

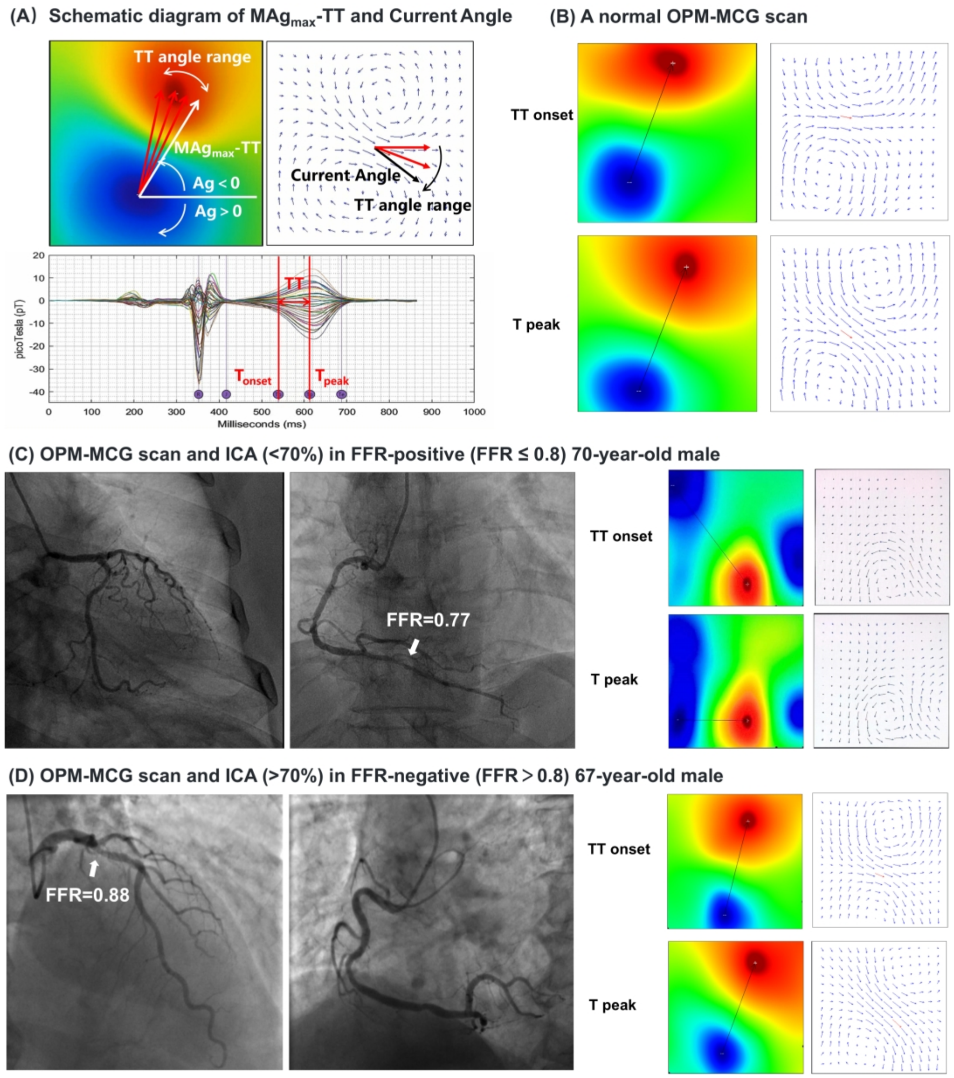

Figure 2 Schematic diagram of OPM-MCG scan.

Figure legend: (A) Schematic diagram of MAgmax-TT and current angle. In magnetic field distribution maps and current density maps, the definition rule for angle values is based on the horizontal axis, with counterclockwise angles being negative and clockwise angles being positive. MAgmax-TT is the maximum angle between the line connecting the maximum positive and negative magnetic poles and the horizontal axis. in the TT segment. δAgsum-C is the sum of changes in current angle at intervals of a certain time τ within TT segment (B)Normal OPM-MCG scan. The OPM-MCG scan showed no evidence of ischemia or obstructive coronary artery disease, as demonstrated by the lack of significant current deviations within the myocardium and absence of angle shift between the positive red pole and negative blue pole between T-onset and T-peak. (C) The OPM-MCG scan of a patient in his 70s showed magnetic field angular deflection, abnormal magnetic field distribution of the positive and multipolarisation of negative poles, suggesting significant myocardial ischemia, and the ECG showed no significant abnormality. The CAG showed two lesions: 60% stenosis of the D1, 50% stenosis of the R-PDA. The FFRs were 0.77 for the R-PDA. (D) The OPM-MCG scan of a patient in his 60s showed no myocardial ischemia, ECG showed no significant abnormalities, echocardiography showed widening of the ascending aorta and aortic sinus. CAG showed 75% stenosis of the LAD, 60% stenosis of the RCA, FFR value of the LAD was 0.88.
MCG= magnetocardiography; FFR= fractional flow reserve; ICA= invasive coronary angiography; D1=

Diagonal branches; R-PDA= Posterior descending artery; LAD= Left Anterior descending artery; RCA= right coronary artery.

1090x1206mm (96 x 96 DPI)

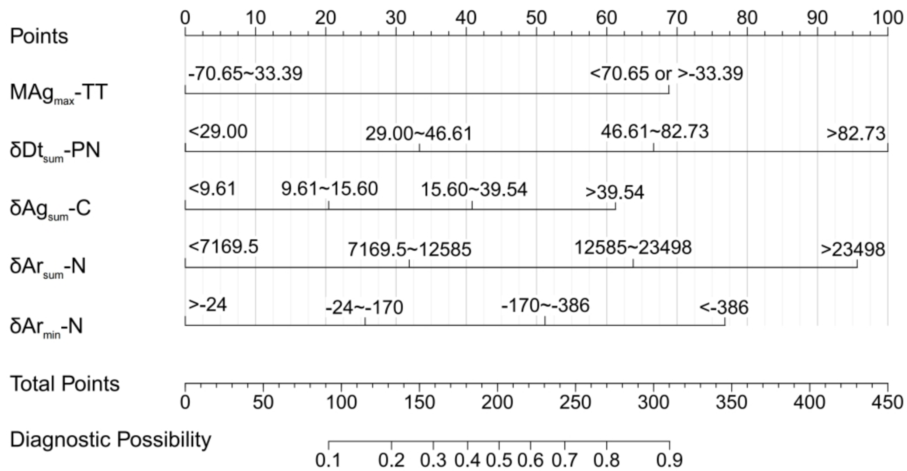

Figure 3. Nomogram of the diagnostic model.

Figure legend: The nomogram graphically demonstrates the diagnostic model of OPM-MCG. Points for MAgmax-TT, δDtsum-PN, δAgsum-C, δArsum-N and δArmin-N can be obtained using a point caliper and then summed to obtain a total score that can be measured with diagnosing myocardial ischemia in patients with borderline coronary lesions.

310x182mm (300 x 300 DPI)

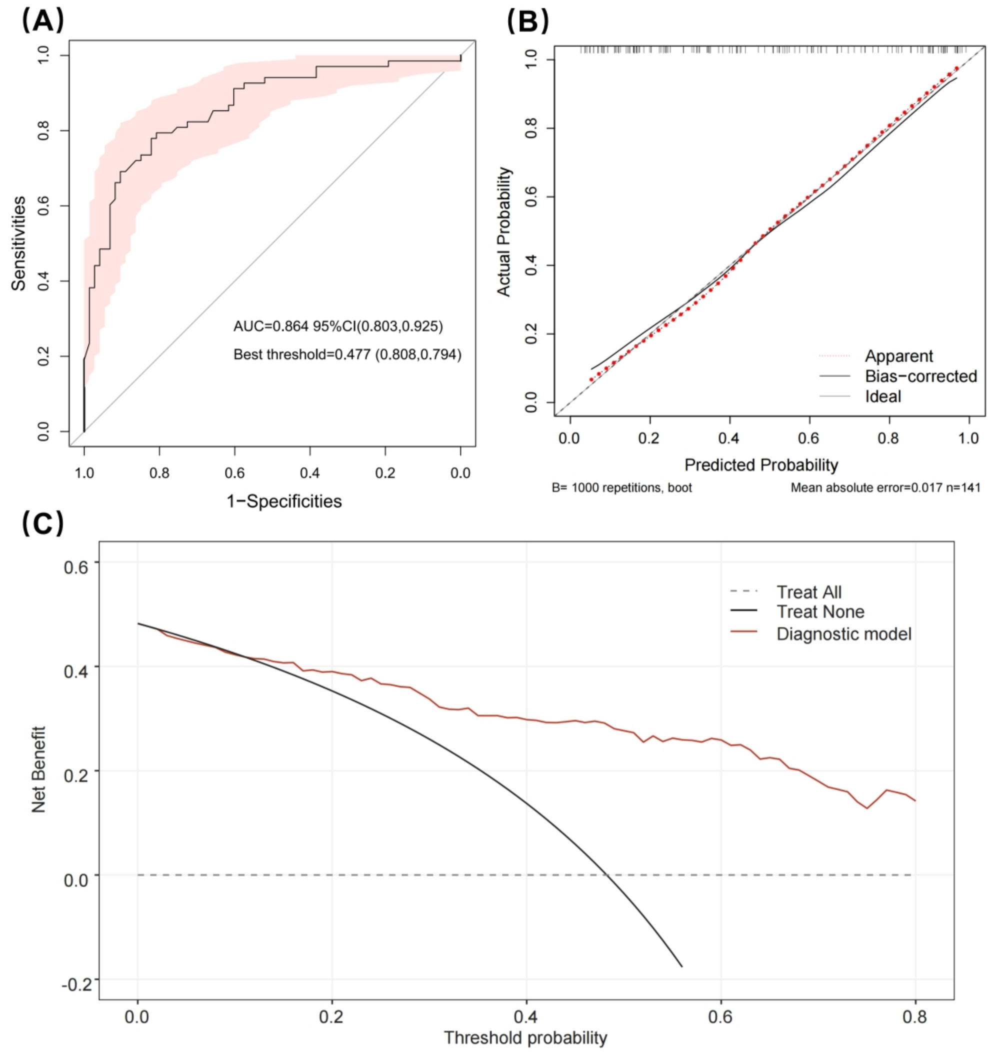

Figure 4 Accuracy and internal validation of the diagnostic model.
Figure legend: (A) ROC curves for the diagnostic model. After 1000 bootstrap replications, the area under the curve and 95% confidence interval for receiver operating characteristic is 0.864 (0.803-0.925). (B) Calibration curve for the diagnostic model. Calibration curve for the borderline lesion ischemia diagnostic model was established by comparing the actual and predicted probability of a positive FFR in patients with borderline lesions of the coronary arteries. The smaller the distance of the scatter from the dashed line, the better the calibration. (C) Decision curve analysis (DCA) for diagnostic models of ischemia in borderline coronary lesions. Treat none: net benefit when it is assumed that no patients with borderline lesions of the coronary arteries would have the outcome (FFR-positive). Treat all: net benefit when all patients with borderline coronary lesions are assumed to have an outcome (FFR-positive). Diagnostic model: net benefit of managing borderline coronary lesions with a diagnosis of myocardial ischemia based on the diagnostic model estimate. The strategy with the highest net benefit at any given threshold is the preferred strategy.

239x257mm (375 x 375 DPI)

Supplementary Material

Development and validation of a clinical diagnostic model for myocardial ischemia in borderline coronary lesions based on optical pumped magnetometer magnetocardiography: a prospective observational cohort study

Contents

Optical pumped magnetometer magnetocardiography (OPM-MCG) post-processing steps

The post-processing process of OPM-MCG signals is as follows. Firstly, a composite gradient magnetometer array is constructed using a separate environmental monitoring channel, and the common mode projection components of the monitoring channel are subtracted from the OPM-MCG detection array channels, effectively suppressing environmental magnetic field drift and power frequency interference. Then, notching the 50Hz power frequency and its harmonic components of the data, and performing a 1-40Hz bandpass filter to further remove power frequency interference and limit the bandpass frequency to the main frequency range of the MCG. Finally, the denoised data is subjected to R-peak detection and recognition, with an average heartbeat cycle of 90 seconds as the length of the slice time, and the identified R-peak point is used as the time alignment point to slice the data and overlay it for average

Supplementary Table and Figures

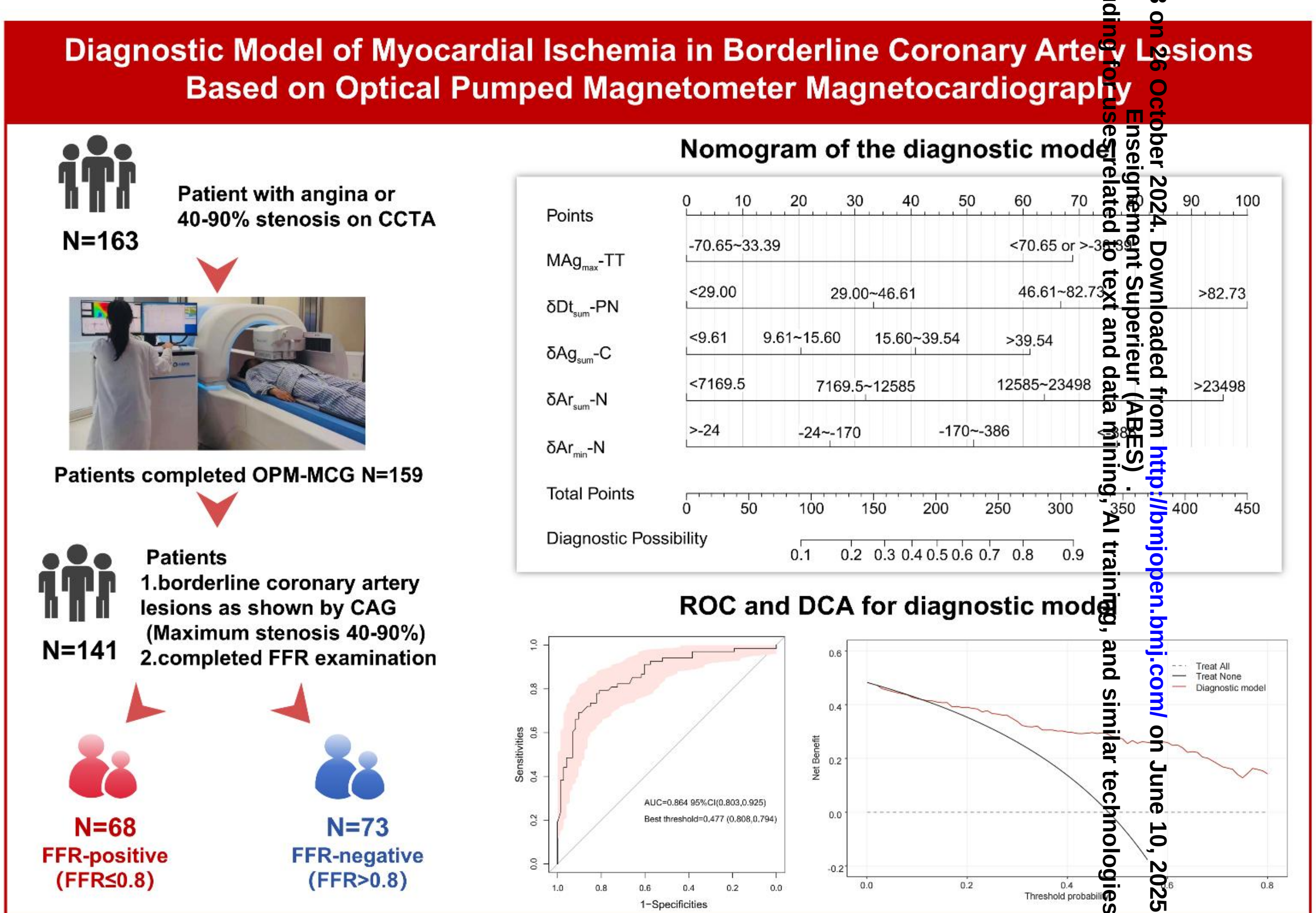

Supplementary Figure 1 Graphical Abstracts: Diagnostic Model of Myocardial Ischemia in Borderline Coronary Artery Lesions Based on OPM-MCG

CCTA= coronary computed tomography angiography; OPM-MCG=optical pumped magnetometer magnetocardiography; CAG= invasive coronary angiography; FFR=fractional flow reserve; PCI= percutaneous coronary intervention; DCA=decision curve analysis.

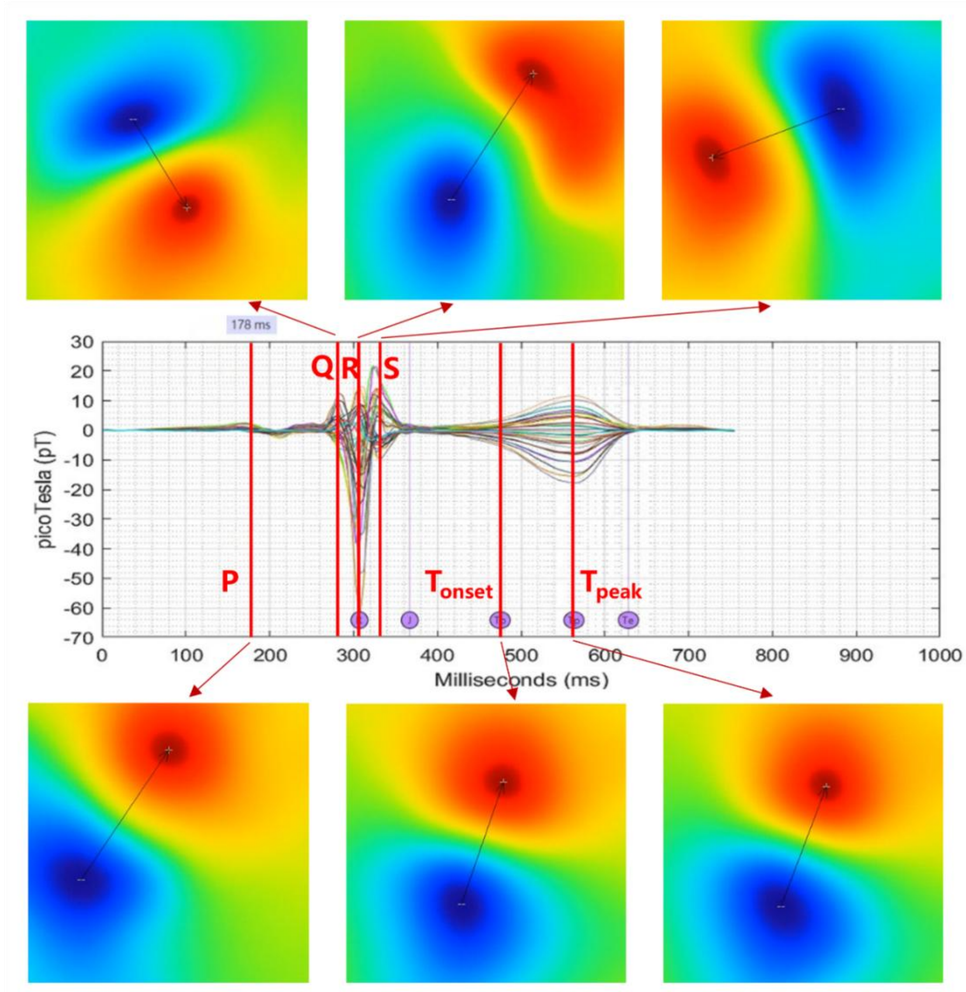

Supplementary Figure 2 The Magnetic Field Distributions (MFDs) of Key Points (P, QRS, and T onset and T peak) in the Cardiac Cycle of Healthy Individuals

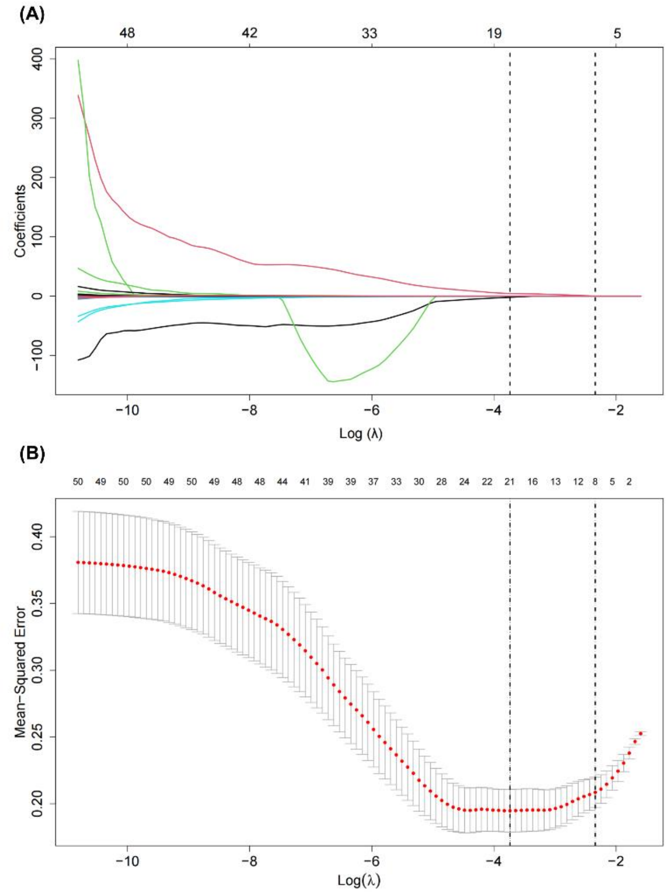

Supplementary Figure 3 Least Absolute Shrinkage and Selection Operator (LASSO) Regression

Figure legend :(A) LASSO model coefficient profiles of the 50 candidate parameters. As log λ increases, the regression coefficients continue to converge, and there are fewer parameters with non-zero regression coefficients.(B) Tuning parameter selection by cross-validation in the LASSO model. The solid vertical lines represent the partial likelihood deviance standard error (SE). The red dotted line indicates the cross-validation curve. The vertical dashed lines are drawn at the optimal values on the basis of the minimum criteria and 1-SE criteria. Considering the reasonableness of the variables included in this model, with the λ value of 0.02380779 was chosen.

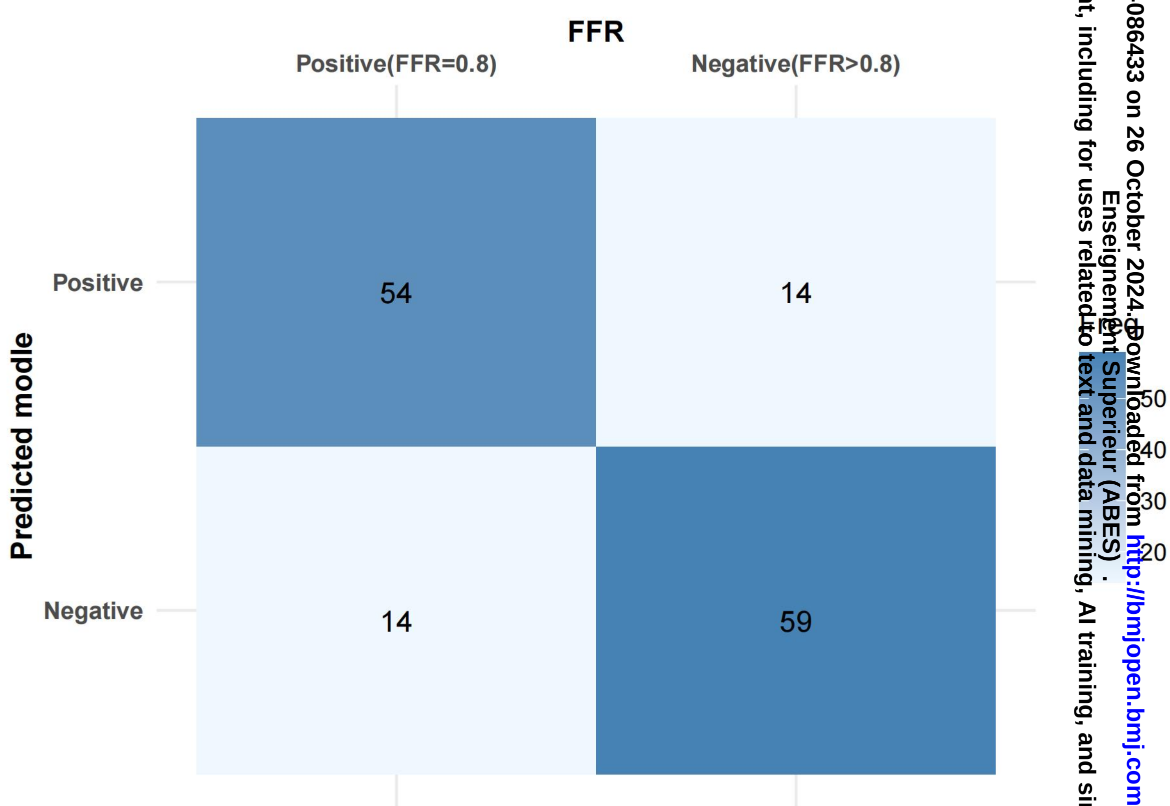

Supplementary Figure 4 Confusion Matrix for the Diagnostic Model

Figure Legend: The confusion matrix compares the FFR diagnostic results with those from the predictive model. The color intensity represents the frequency of occurrences, with darker shades indicating higher frequencies.

Supplementary Table 1 OPM-MCG Parameters and Definitions

Parameters	Definition
δ Ag_{max}-M	The maximum value of changes in magnetic field angle at intervals of a certain time τ within TT segment
δ Ag_{min}-M	The minimum value of changes in magnetic field angle at intervals of a certain time τ within TT segment
δ Ag_{std}-M	The standard deviation of changes in magnetic field angle at intervals of a certain time τ within TT segment
δ Ag_{sum}-M	The sum of changes in magnetic field angle at intervals of a certain time τ within TT segment
δ Dt_{max}-PN	The maximum value of changes in magnetic pole distance at intervals of a certain time τ within TT segment
δ Dt_{min}-PN	The minimum value of changes in magnetic pole distance at intervals of a certain time τ within TT segment
δ Dt_{std}-PN	The standard deviation of changes in magnetic pole distance at intervals of a certain time τ within TT segment
δ Dt_{sum}-PN	The sum of changes in magnetic pole distance at intervals of a certain time τ within TT segment
δ Ag_{max}-C	The maximum value of changes in current angle at intervals of a certain time τ within TT segment
δ Ag_{min}-C	The minimum value of changes in current angle at intervals of a certain time τ within TT segment
δ Ag_{std}-C	The standard deviation of changes in current angle at intervals of a certain time τ within TT segment
δ Ag_{sum}-C	The sum of changes in current angle at intervals of a certain time τ within TT segment
δ Ps_{max}-C	The maximum value of changes in the position of the current angle at intervals of a certain time τ within TT segment
δ Ps_{std}-C	The standard deviation of changes in the position of the current angle at intervals of a certain time τ within TT segment
δ Ps_{sum}-C	The sum of changes in the position of the current angle at intervals of a certain time τ within TT segment
δ Ar_{max}-NP	The maximum value of changes in negative pole point area at intervals of a certain time τ within TT segment
δ Ar_{min}-NP	The minimum value of changes in negative pole point area at intervals of a certain time τ within TT segment
δ Ar_{std}-NP	The standard deviation of changes in negative pole point area at intervals of a certain time τ within TT segment
δ Ar_{sum}-NP	The sum of changes in negative pole point area at intervals of a certain time τ within TT segment
δ Ar_{bp}-NP	The change in negative pole point area between T-begin and T-peak
Ar_{max}-NP	The maximum value of the negative pole point area at intervals of a certain time τ within TT segment
Ar_{min}-NP	The minimum value of the negative pole point area at intervals of a certain time τ within TT segment
δ Ps_{max}-NP	The maximum value of changes in the position of the negative pole point at intervals of a certain time τ within TT segment
δ Ps_{std}-NP	The standard deviation of changes in the negative of the positive pole point at intervals of a certain time τ within TT segment
δ Ps_{sum}-NP	The sum of changes in the position of the negative pole point at intervals of a certain time τ within TT segment
δ Ar_{max}-N	The maximum value of changes in negative pole area at intervals of a certain time τ within TT segment

Parameters	Definition
δ Ag_{max}-M	The maximum value of changes in magnetic field angle at intervals of a certain time τ within TT segment
δ Ar_{min}-N	The minimum value of changes in negative pole area at intervals of a certain time τ within TT segment
δ Ar_{std}-N	The standard deviation of changes in negative pole area at intervals of a certain time τ within TT segment
δ Ar_{sum}-N	The sum of changes in negative pole area at intervals of a certain time τ within TT segment
δ Ar_{bp}-N	The change in nagative pole area between T-begin and T-peak
Ar_{max}-N	The maximum value of the negative pole area at intervals of a certain time τ within TT segment
Ar_{min}-N	The minimum value of the negative pole area at intervals of a certain time τ within TT segment
δ $ArRto_{max}$-PN	The maximum value of changes in the ratio of positive and negative pole area at intervals of a certain time τ within TT segment
δ $ArRto_{min}$-PN	The minimum value of changes in the ratio of positive and negative pole area at intervals of a certain time τ within TT segment
δ $ArRto_{std}$-PN	The standard deviation of changes in the ratio of positive and negative pole area at intervals of a certain time τ within TT segment
δ $ArRto_{sum}$-PN	The sum of changes in the ratio of positive and negative pole area at intervals of a certain time τ within TT segment
δ Ar_{max}-PP	The maximum value of changes in positive pole point area at intervals of a certain time τ within TT segment
δ Ar_{min}-PP	The minimum value of changes in positive pole point area at intervals of a certain time τ within TT segment
δ Ar_{std}-PP	The standard deviation of changes in positive pole point area at intervals of a certain time τ within TT segment
δ Ar_{sum}-PP	The sum of changes in positive pole point area at intervals of a certain time τ within TT segment
δ Ar_{bp}-PP	The change in positive pole point area between T-begin and T-peak
Ar_{max}-PP	The maximum value of the positive pole point area at intervals of a certain time τ within TT segment
Ar_{min}-PP	The minimum value of the positive pole point area at intervals of a certain time τ within TT segment
δ Ps_{max}-PP	The maximum value of changes in the position of the positive pole point at intervals of a certain time τ within TT segment
δ Ps_{std}-PP	The standard deviation of changes in the position of the positive pole point at intervals of a certain time τ within TT segment
δ Ps_{sum}-PP	The sum of changes in the position of the positive pole point at intervals of a certain time τ within TT segment
δ Ar_{max}-P	The maximum value of changes in positive pole area at intervals of a certain time τ within TT segment
δ Ar_{min}-P	The minimum value of changes in positive pole area at intervals of a certain time τ within TT segment
δ Ar_{std}-P	The standard deviation of changes in positive pole area at intervals of a certain time τ within TT segment

Parameters	Definition
$\delta\ Ag_{max}$-M	The maximum value of changes in magnetic field angle at intervals of a certain time τ within TT segment
$\delta\ Ar_{sum}$-P	The sum of changes in positive pole area at intervals of a certain time τ within TT segment
$\delta\ Ar_{bp}$-P	The change in positive pole area between T-begin and T-peak
$Ar_{ma}x$-P	The maximum value of the positive pole area at intervals of a certain time τ within TT segment
Ar_{min}-P	The minimum value of the positive pole area at intervals of a certain time τ within TT segment
MAg_{max}-TT	The maximum magnetic field angle at intervals of a certain time τ within TT segment
CAg_{max}-TT	The maximum current angle at intervals of a certain time τ within TT segment
MAg_{min}-TT	The minimum magnetic field angle at intervals of a certain time τ within TT segment
CAg_{min}-TT	The minimum current angle at intervals of a certain time τ within TT segment
MAg-Rp	The magnetic field angle of the R-peak
RtoAm-R_pT_pN	The ratio of magnetic field amplitude at R-peak and the negative amplitude at T-peak
RtoAm-R_pT_pP	The ratio o magnetic field amplitude at R-peak and the positive amplitude at T-peak
RtoAm-R_pT_p	The ratio of magnetic field amplitudes at R-peak and T-peak
MAg-RpTp	The magnetic field angle between R-peak and T-peak
MAg-Tp	The magnetic field angle of the T-peak
CAg_{max}-Tp	The maximum current angle at T-peak
RtoAm-Tp	The ratio of positive to negative magnetic field amplitude at T-peak
TT	The interval from the beginning of the T-wave to its peak within the cardiac cycle

Dt = Distance, Ps = Position, Ag = Angle, Am = Magnitude, Ar = Area, Rto = Ratio, P = Positive, Positive Pole = PP, N = Negative, NP = Negative Pole, M = Magnetic Field, C = Current, max = Maximum, min = Minimum, sum=Sum of all, std = Standard deviation, δ = Change value, TT= TT segment (the position from one-third of the T max amplitude (T onset) to T max (T peak)), R_p=R peak, T_p=T peak

Supplementary Table 2 OPM-MCG Parameters of Univariable Logistic Regression Model P < 0.1

Parameters	ALL N=141	FFR-Positive N=68	FFR-Negative N=73	Odds Ratio (95%CI)	P value
δ Ag_{max}-M	0.62 (0.44,1.19)	0.77 (0.47,5.76)	0.54 (0.43,0.72)	1.0[illegible]7(1.023-1.163)	0.021
δ Ag_{min}-M	-0.34 (-0.57,-0.18)	-0.42 (-0.82,-0.28)	-0.26 (-0.42,-0.14)	0.9[illegible]4(0.924-0.992)	0.034
δ Ag_{std}-M	0.16 (0.11,0.68)	0.28 (0.14,2.06)	0.14 (0.10,0.20)	1.5[illegible]4(1.213-2.313)	0.004
δ Ag_{sum}-M	10.6 (6.18,26.2)	20.2 (9.88,45.5)	8.28 (4.55,11.8)	1.064(1.037-1.1)	<0.001
δ Dt_{max}-PN	2.69 (1.97,4.12)	3.51 (2.16,12.9)	2.22 (1.89,3.16)	1.014(1.001-1.032)	0.063
δ Dt_{min}-PN	-2.20 (-3.27,-1.76)	-2.38 (-4.70,-1.91)	-2.00 (-2.80,-1.63)	0.971(0.94-0.991)	0.023
δ Dt_{std}-PN	0.74 (0.55,1.18)	0.82 (0.63,3.45)	0.63 (0.52,0.89)	1.1[illegible]8(1.031-1.332)	0.024
δ Dt_{sum}-PN	46.6 (29.1,80.7)	66.6 (42.0,110)	33.3 (25.7,48.6)	1.026(1.015-1.039)	<0.001
δ Ag_{max}-C	1.70 (1.21,4.83)	1.79 (1.27,9.10)	1.52 (1.16,2.98)	1.009(1-1.022)	0.089
δ Ag_{min}-C	-1.24 (-3.81,0.00)	-1.70 (-8.89,-1.01)	-0.91 (-1.75,0.00)	0.9[illegible]3(0.962-0.997)	0.051
δ Ag_{std}-C	0.54 (0.36,1.32)	0.80 (0.37,3.16)	0.45 (0.34,0.70)	1.1[illegible]7(1.026-1.252)	0.025
δ Ag_{sum}-C	15.6 (9.64,38.6)	29.8 (13.5,71.6)	11.9 (7.79,17.5)	1.014(1.006-1.025)	0.003
δ Ps_{max}-C	33.0 (1.00,48.8)	33.0 (1.41,125)	31.0 (1.00,34.0)	1.008(1.003-1.015)	0.004
δ Ps_{std}-C	3.35 (0.24,6.16)	3.57 (0.29,11.7)	3.20 (0.24,4.86)	1.073(1.019-1.14)	0.013
δ Ps_{sum}-C	39.1 (6.00,86.1)	74.4 (8.31,161)	33.4 (4.00,66.0)	1.01(1.005-1.015)	<0.001
δ Ar_{max}-NP	136 (74.0,220)	182 (102,314)	105 (59.0,180)	1.002 (1.0002,1.003)	0.027
δ Ar_{std}-NP	29.6 (20.0,56.7)	31.7 (23.4,70.1)	25.7 (17.1,41.4)	1.004 (1.000,1.010)	0.067
δ Ar_{sum}-NP	2469 (1443,4286)	3369 (2230,5728)	1672 (1277,2987)	1.00020 (1.00006, 1.00034)	0.005
Ar_{max}-NP	3873 (3001,5765)	4269 (3260,6056)	3828 (2894,5406)	1.000101 (0.999989, 1.000213)	0.077
δ Ps_{sum}-NP	41.7 (22.2,79.9)	59.8 (39.8,104)	26.4 (20.1,51.1)	1.013(1.006-1.021)	0.001
δ Ar_{max}-N	435 (243,750)	539 (269,990)	404 (221,526)	1.001(1-1.002)	0.022
δ Ar_{min}-N	-170.00 (-369.00,-25.00)	-267.00 (-565.25,-108.75)	-79.00 (-224.00,-15.00)	0.998(0.996-0.999)	0.002
δ Ar_{std}-N	125 (80.2,225)	160 (90.5,273)	114 (74.6,158)	1.005(1.002-1.008)	0.003
δ Ar_{sum}-N	12585 (7372,23204)	19058 (10208,29054)	9520 (6202,15009)	1.000084 (1.000046, 1.000122)	<0.001
Ar_{max}-N	53635 (43655,65410)	56546 (44597,77766)	51431 (38201,58878)	1.000014 (1.000002, 1.000026)	0.025
δ $ArRto_{max}$-PN	0.01 (0.00,0.02)	0.01 (0.00,0.03)	0.00 (0.00,0.01)	4.494e+1[illegible](5.890e+2,3.427+29)	0.008

Parameters	ALL N=141	FFR-Positive N=68	FFR-Negative N=73	Odds Ratio (95%CI)	P value
δ $ArRto_{min}$-PN	-0.02 (-0.05,-0.01)	-0.02 (-0.07,-0.01)	-0.02 (-0.04,-0.01)	<0.001 (0,0.062)	0.014
δ $ArRto_{std}$-PN	0.01 (0.00,0.02)	0.01 (0.00,0.02)	0.01 (0.00,0.01)	3.177e+16 (1.758e+3,5.740e+29)	0.015
δ $ArRto_{sum}$-PN	0.63 (0.32,1.72)	0.85 (0.39,2.36)	0.58 (0.29,0.88)	1.5[illegible]9 (1.175,2.117)	0.004
δ Ar_{max}-PP	195 (126,404)	281 (141,704)	153 (111,286)	1.0[illegible]1 (1.001,1.003)	0.001
δ Ar_{min}-PP	-171.00 (-295.00,-106.00)	-196.00 (-563.75,-109.50)	-153.00 (-226.00,-104.00)	0.9[illegible]8 (0.996,0.999)	0.003
δ Ar_{std}-PP	54.3 (33.7,124)	77.3 (35.5,167)	43.7 (32.1,79.7)	1.0[illegible]7 (1.003,1.012)	0.004
δ Ar_{sum}-PP	4689 (2685,8783)	6608 (3410,14024)	3487 (2556,5786)	1.00[illegible]12[illegible] (1.000053, 1.000187)	<0.001
Ar_{min}-PP	5151 (2774,7571)	4626 (2618,6928)	5754 (3719,8258)	0.99[illegible]3 (0.999933, 1.000003)	0.06
δ Ps_{max}-PP	3.16 (2.24,5.00)	3.61 (3.00,100)	3.00 (2.24,3.61)	1.0[illegible]1(1.005-1.019)	0.002
δ Ps_{std}-PP	0.82 (0.60,1.15)	0.98 (0.66,8.50)	0.75 (0.57,0.90)	1.[illegible]17(1.05-1.221)	0.003
δ Ps_{sum}-PP	40.4 (23.1,88.6)	73.8 (29.9,195)	32.8 (21.7,54.2)	1.0[illegible]2(1.006-1.019)	<0.001
δ Ar_{max}-P	244 (90.0,430)	312 (150,692)	172 (70.0,362)	1.001(1-1.002)	0.007
δ Ar_{std}-P	120 (80.2,203)	135 (82.3,267)	109 (75.7,159)	1.002(1-1.005)	0.07
δ Ar_{sum}-P	11899 (6525,19157)	15787 (7938,28576)	9566 (5985,15629)	1.000046 (1.000017, 1.000074)	0.001
MAg_{max}-TT	-62.32 (-70.64,-34.61)	-48.00 (-66.89,15.5)	-67.39 (-72.03,-53.13)	1.0[illegible]9(1.009-1.029)	<0.001
CAg_{max}-TT	45.0 (33.3,71.0)	58.2 (39.2,118)	43.1 (32.0,51.1)	1.0[illegible]8(1.009-1.028)	<0.001
MAg_{min}-TT	-70.76 (-76.85,-56.92)	-68.28 (-75.62,-41.24)	-71.98 (-77.61,-64.94)	1.0[illegible]9(1.000-1.018)	0.052
MAg-R_p	-61.41 (-71.15,-42.88)	-53.44 (-70.66,-38.24)	-65.92 (-71.78,-50.54)	1.0[illegible]5(1.003-1.028)	0.017
RtoAm-R_pT_pN	6.49 (4.32,9.57)	7.35 (4.92,10.4)	5.68 (3.71,8.14)	1.0[illegible]5(1.005-1.126)	0.064
RtoAm-R_pT_pP	7.97 (5.88,12.0)	8.66 (6.03,12.9)	7.69 (5.56,11.1)	1.0[illegible](1.004-1.133)	0.061
RtoAm-R_pT_p	3.64 (2.38,4.70)	4.13 (3.08,5.01)	3.28 (2.36,4.50)	1.2[illegible]7(1.047-1.445)	0.016
MAg-T_p	-64.66 (-71.34,-45.44)	-55.82 (-70.28,-12.79)	-67.91 (-72.69,-53.13)	1.0[illegible]5(1.006-1.026)	0.002
CAg_{max}-T_p	43.1 (29.4,52.0)	45.0 (27.6,74.7)	42.2 (30.7,46.9)	1.0[illegible]9(1.001-1.017)	0.037
RtoAm-T_p	0.76 (0.57,1.08)	0.81 (0.52,1.22)	0.75 (0.57,0.98)	1.5[illegible]9(0.978-2.618)	0.095

Dt = Distance, Ps = Position, Ag = Angle, Am = Magnitude, Ar = Area, Rto = Ratio, P = Positive, Positive Pole = PP, N = Negative, NP = Negative Pole, M = Magnetic Field, C = Current, max = Maximum, min = Minimum, sum=Sum of all, std = Standard deviation, δ = Change value, TT= TT segment (the position from one-third of the T max amplitude (T onset) to T max (T peak)), R_p=R peak, T_p=T peak

Supplementary Table 3 Diagnostic Model for Assessment of Myocardial Ischemia in Borderline Coronary Artery Lesions

Parameters	Diagnostic model			
	B	OR	95%CI	P value
MAg_{max}-TT	1.385	3.995	(1.592-10.023)	0.003
δDt_{sum}-PN	0.671	1.956	(1.270-3.012)	0.002
δAg_{sum}-C	0.411	1.508	(0.989-2.298)	0.056
δAr_{sum}-N	0.641	1.899	(1.251-2.883)	0.002
δAr_{min}-N	0.515	1.674	(1.121-2.500)	0.012

M= Magnetic Field; Ag= Angle; TT= from T onset to T peak; δ= Change value; DT= Distance; PN= Positive Pole to Negative Pole; C=Current; Ar= Area; N= Negative Pole; ; τ= one tenth of the time interval between TT segment.